CHEMICAL COMPOSTION OF ICE SURFACES: IMPLICATIONS FOR SPRINGTIME BROMINE CHEMISTRY

By

Laura Alvarez-Avilés

RECOMMENDED: Richard J Stolzberg

Catherine F Cahill

Advisory Committee Chair

Chair, Department of Chemistry and Biochemistry

APPROVED:

Dean, College of Natural Science and Mathematics

Lawrence K Duffy

Dean of the Graduate School

August 1, 2008

Date

CHEMICAL COMPOSITION OF ICE SURFACES: IMPLICATIONS FOR SPRINGTIME BROMINE CHEMISTRY

A

THESIS

Presented to the Faculty

of the University of Alaska Fairbanks

in Partial Fulfillment of the Requirements

for the Degree of

DOCTOR OF PHILOSOPHY

By

Laura Alvarez-Avilés, B.S.

Fairbanks, Alaska

August 2008

UMI Number: 3337638

INFORMATION TO USERS

The quality of this reproduction is dependent upon the quality of the copy submitted. Broken or indistinct print, colored or poor quality illustrations and photographs, print bleed-through, substandard margins, and improper alignment can adversely affect reproduction.

In the unlikely event that the author did not send a complete manuscript and there are missing pages, these will be noted. Also, if unauthorized copyright material had to be removed, a note will indicate the deletion.

UMI®

UMI Microform 3337638

ProQuest LLC
789 E. Eisenhower Parkway
PO Box 1346
Ann Arbor, MI 48106-1346

Abstract

Reactive bromine chemistry is responsible for events of almost total tropospheric O_3 destruction and the deposition of mercury during the Arctic spring. The source of the majority of the atmospheric bromine loading is salts from seawater, but many questions remain on the mechanism by which salts are transported and chemically activated to reactive species. Specifically, the role of snow and ice surfaces in exchanging bromine with the atmosphere needed investigation. Therefore, we undertook a detailed study of the ionic composition of selected ice surfaces near Barrow, Alaska and tracked modifications with respect to Cl^- and Na^+ (sea-salt tracers) in approximately 1,400 samples. We developed data analysis tools to observe modifications and related these methods to the traditional enrichment factor and the non-sea-salt abundance methods. Surface snow was highly modified in Br^- composition by atmospheric exchanges that both add and remove bromine, providing evidence for snow's involvement in reactive bromine chemistry. Calcium was enriched by dust input. Sulfate in surface snow was fractionated at the source by mirabilite ($Na_2SO_4 \bullet 6H_2O$) precipitation and enriched by Arctic haze inputs. Frost flowers are vapor-grown ice crystals that wick brine and may be involved in sea-salt aerosol production and production of reactive halogen species. Detailed examination of frost flower growth and chemical composition shows that they are sites of mirabilite precipitation and separation, which can lead to sulfate-depleted aerosol particles, but show no sign of direct reactive bromine production. By simultaneously studying snow, ice, aerosol particles, and gas-phase bromine species, we made a mass balance of bromine in various reservoirs. This mass balance points away from frost flowers and towards snow as the dominant source of reactive bromine. This work develops a mechanistic picture of how reactive bromine chemistry depends upon snow and sea ice that is needed to make meaningful predictions of how the recent changes to the Arctic sea ice cover will affect air pollution chemistry.

Table of Contents

Page

Page

Page

List of Figures

Page

List of Tables

List of Other Materials

Acknowledgments

I would like to thank Prof. William Simpson for his help, advice and guidance throughout all my years at the University of Alaska Fairbanks. I admire his vast knowledge and skills in areas such as writing, public speaking, and ethics. I would also like to voice my gratitude to the other members of my committee, Prof. Cathy Cahill, Prof. Tom Trainor, and Prof. Richard Stolzberg and co-authors Dr. Tom Douglas, Dr. Matthew Sturm, Dr. Florent Domine, and Dr. Alex Laskin. Their comments and assistance made this thesis a better product. Also, I would like to thank my lab mates, Randy Apodaca, Dan Carlson, Deanna Donohoue, and Dea Huff for many hours of help, good times, and venting. A very special thanks goes out to Dr. Jeff Gaffney, without whose motivation and encouragement I would not have considered a graduate career at UAF in chemistry research.

I would like to thank my family (Melba, Pepe, and Olga) for their support throughout my entire life and my recently "gained" family for their unconditional support. A unique thanks goes to my husband and best friend, Dave, whose love, encouragement, and computer knowledge made the culmination of this thesis possible. There is no doubt that my sanity remains because of Dave; thanks for listening and just being there.

Finally, I would like to recognize that this research would not have been possible without the financial assistance of NSF grant ATM-0103775, ATM-0420205, and OPP-0435922, the logistic support of the Barrow Arctic Science Consortium, and also the DOE/Graduate Research Environmental Fellowship that provided my stipend, school registration, and most importantly access to top notch research facilities and their people.

Chapter 1. Introduction

The Arctic is characterized by unique chemistry that affects the deposition of pollutants in the region. This unique chemistry arises from a combination of the harsh climate and the physical and chemical properties of the pollutants and reactive species. During the winter, the lack of sunlight suppresses many chemical reactions, which in turn allows some trace chemical species to build to high concentrations. As spring arrives, these accumulated species undergo photochemical reactions and produce new reactive species. To better understand the fate of pollutants in the Arctic region, we need to study the chemically accessible surfaces that hold pollutants and precursors to reactive species that are involved in pollutant deposition. The goal of this thesis is to study the chemical composition of snow, sea ice forms, and atmospheric gases and particles so as to understand better the way these surfaces transform and control the fate of pollutants, specifically mercury and tropospheric ozone. Mercury is a pollutant of great concern in the Arctic because it is deposited through unique springtime atmospheric chemistry and is found in high levels in high-trophic level subsistence food and Arctic people [AMAP, 2005].

Mercury poisoning in mammals is characterized by neurological impairment, compromised immune response, and damage to the central nervous system, liver and kidney [WHO 1989, 1990, 1991]. The polar bear is an example of high-trophic level mammal with high levels of mercury concentrations. The primary source of mercury in polar bears is from their diet of seals, which implies that seals also have high levels of mercury as well. Higher trophic level organisms intake, store and build up the mercury concentrations from their prey, this process is know as biomagnification. Woshner et al. [2001] measured mercury concentrations (among other elements) present in ringed seals and polar bears in the Alaskan Arctic. In liver of ringed seals and polar bears from the Alaskan Arctic, total mercury was present at concentrations that would be considered high or even toxic. The total mercury concentration found in polar bears was 14,220 μg/kg and in ringed seals was 3,520 μg/kg. Alaskan Natives generally consume much more fish than the national average, thus the importance of monitoring mercury levels in their food source. Jewett and Duffy [2007] measured levels of toxic mercury in a significant number of freshwater fish and anadromous and marine fish species. Overall, most fish had muscle mercury concentrations of </=100 μg/kg (wet weight.), within the United States Food and Drug Administration's (USFDA) Action Level and Alaska's guideline for safe concentrations of toxic mercury in edible fish, 1000 μg/kg. Only pike from the Yukon River had total mercury concentrations that exceeded the USFDA action level for human consumption of edible fish (1000 μg/kg) [Jewett et al., 2003].

The inorganic mercury (GEM) that arrives to the Arctic goes through a series of reactions that transforms it to methylmercury (organic mercury), a more toxic chemical species than inorganic mercury, and more readily accumulated. As GEM arrives to the Arctic, photoactive bromine species contribute to its oxidation to a reactive species (RGM, reactive gaseous mercury), which can be scavenged by surfaces like snow. Once in the snow, biological processes transform reactive mercury to organic mercury. We are currently working with colleagues to study mercury and ion composition in snow and ice forms, but many questions remain on how much of the deposited mercury its transformed to organic mercury and assimilated by organisms. Our focus is on the ionic composition of snow and ice forms to be able to understand how sea salts cause mercury deposition.

Halogens such as chlorine, bromine and iodine, are key catalysts in the mercury deposition process, thus the focus of this thesis is to study these halogens in the snow, ice and atmosphere. The oxidation state of these halogens dictates their participation in atmospheric mercury chemistry. As halogens originate from sea salt, they are in oxidation state -1 (e.g., Cl^-, Br^-, and I^-), which are essentially chemically inert. The term halide refers to these halogen anions. During the Arctic spring, halogens are oxidized to their neutral oxidation state, where they are radical atoms (e.g., Cl, Br, and I atoms). It is in this form that halogens participate in mercury deposition and affect other species, like ozone. Reactive halogen chemistry is responsible for the depletion of boundary-layer ozone, which alters the overall oxidation chemistry of the atmosphere.

In this introductory chapter to the thesis, we begin by discussing impacts of halogen chemistry (section 1.1), then review past work on chemical mechanisms for halogen activation (section 1.2). In section 1.3, we explore the participation of various halogens (e.g. Cl, Br, I) in reactive halogen chemistry. In section 1.4, we discuss historical and recent ideas regarding bromine sources, and in section 1.5, we discuss surfaces that may be involved in bromine activation. This introductory material motivates and provides background for our extensive investigation of halides and other ionic components of various ice surfaces in the Arctic system.

Chapter 2 describes a study of all major ions present in the snow pack; it contains data from three years of sampling in the vicinity of Barrow, Alaska, and an the Applied Physics Laboratory Ice Station (APLIS) ice camp in 2007. Close to 1000 surface snow samples are examined in this data set. The main goal of these measurements was to examine snow-air interactions by observing modifications to the ionic composition with respect to the concentration of Na^+, a sea salt tracer.

Chapter 3 is a study of frost flower chemical composition, and the role of frost flowers in bromine chemistry and aerosol formation. Frost flowers are ice forms that grow on newly freezing sea ice and wick concentrated salt solutions (brine) to become highly saline. Some in the community believe that frost flowers are key players in halogen chemistry, thus our measurements were used to address this question.

Chapter 4 presents Br^- and Cl^- measurements of surface snow, freshly deposited snow, vertically integrated snow pack, and aerosol particles along with gas-phase bromine monoxide (BrO), which is an important reactive bromine gas. These measurements explore how bromine reacts and moves between various snow/ice/aerosol surfaces. Mass balance calculations based upon the measurements provide important constraints as to the roles of various types of surfaces in bromine activation chemistry.

Each of these chapters was written as a manuscript for publication in the peer-reviewed literature, so there is a slight degree of repetition between introductions in each chapter and this introductory chapter. Chapter 3 has been accepted to the Journal of Geophysical Research, Atmospheres. Chapter 2 is being reviewed by co-authors, and chapter 4 will soon be sent out to co-authors for review. The references for each publication can be found at the end of each chapter, while the references for this introduction and the conclusions are after the conclusions, chapter 5. Overall, this thesis describes the largest and most comprehensive view of the chemical composition of snow, sea-ice forms and atmospheric gases and particles to better understand the way these surfaces transform and control the fate of pollutants.

1.1 Impacts and history of Arctic springtime bromine chemistry

Observations of surface ozone in the late 1980s showed that unique chemistry was occurring in this environment during springtime. Surface (tropospheric) ozone is a pollutant that can damage living tissue and breakdown certain materials. In the spring, when this chemistry is active, ozone concentrations in the Arctic planetary boundary layer are often observed to decrease suddenly from about 40 parts per billion by volume (ppbv) to below the detection limit (≈ 0.5 ppbv) [Barrie et al., 1988]. These events have been termed Ozone Depletion Events (ODEs). While it is possible that dry deposition could drive an ODEs [Hopper et al., 1998], dry deposition as the main loss mechanism of ozone does not explain why low ozone concentrations are not observed during the dark winter [Barrie et al., 1988]. Rather, the necessity for sunlight indicated that a photochemical mechanism was more likely. Ozone depletion events have been associated with high concentrations of filterable bromine, which appears to originate from the Arctic Ocean [Barrie et al., 1988; Langerndörfer et al., 1999]. Filterable bromine corresponds to all bromine species that are captured in a cellulose filter and is likely to include aerosol Br^- and reactive bromine gases. Figure 1.1 shows the anticorrelation between filterable bromine and ozone during the month of April in 1986. The sudden loss of ozone occurs at the same time as an increase in filterable bromine.

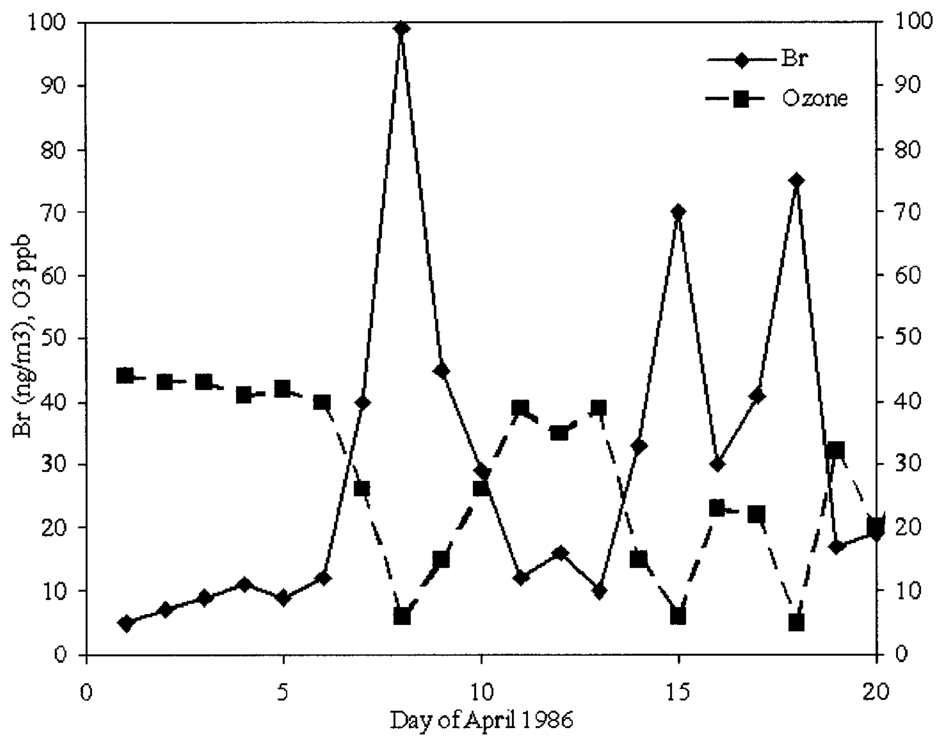

Figure 1.1 Anticorrelation between ozone mixing ratios and filterable bromine in time adapted from Barrie et al. [1988].

Schröeder et al. [1998] discovered that gas-phase mercury depletion was observed concurrently with an ODE. Subsequent work showed that the mercury lost from the gas phase was converted to particulate mercury that rapidly deposited to the snow pack [Lindberg et al., 2002]. Figure 1.2 shows a high correlation between ozone concentration variations and those of gaseous elemental mercury. The correlation between ozone and mercury depletions suggested that the same chemistry involved in depleting ozone (reactive bromine chemistry) could be responsible for mercury deposition. Mercury is a toxic bioaccumulative pollutant that can exist in three oxidation states: 0, +1 and +2. Oxidation state +1 is a rare and very unstable species that is expected to undergo rapid oxidation to the stable +2 state or be reduced back to the elemental form in the gas phase. Mercury is a unique element that has properties that make it different from other metals like a low melting point and a high vapor pressure. Gaseous atmospheric mercury exists predominantly as Hg(0) [Schröeder and Munthe, 1998]. Hg(0) is relatively unreactive and is insoluble in water; therefore the global atmospheric residence time is roughly 6 months to a year [Lin and Pehkonen, 1999]. This long lifetime allows sufficient time for long-range transport, making mercury a global pollutant. Springtime reactive halogen chemistry results in oxidized inorganic Hg(II) species that can be assimilated by polar ecosystems, thus transferring potentially toxic Hg to flora and fauna just as they commence replenishing energy reserves depleted during the long dark polar winter.

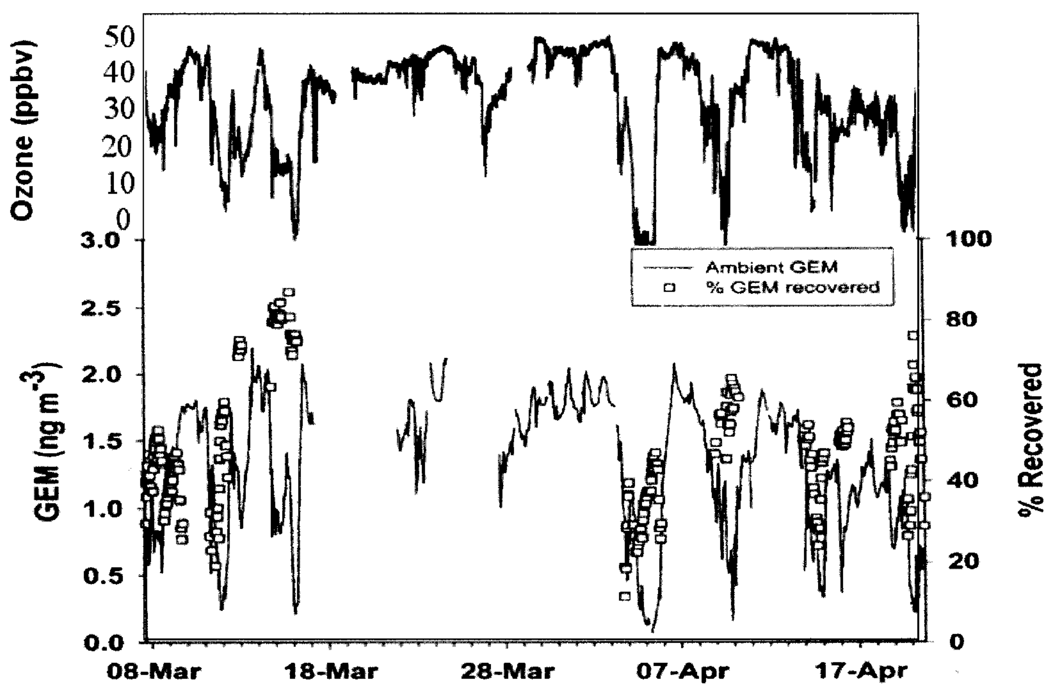

Figure 1.2 Ozone and mercury depletion correlation. Figure adapted from Steffen et al. [2002] (mercury plot) and Bottenheim et al. [2002] (ozone plot).

Mercury is released into the atmosphere from natural and anthropogenic sources. In addition, mercury is known to undergo recycling where deposited mercury has the capacity to be re-emitted from environmental surfaces. Current estimates indicate that about half the global burden of Hg(0) is natural and the other half is due to anthropogenic emissions, but after the considering re-emission the total global Hg(0) budget becomes more complicated and it is difficult to simply characterize an emission as natural or anthropogenic [Schröeder and Munthe, 1998]. Natural sources of mercury to the atmosphere include outgasing from mantle and crustal materials, release from wind-blown dust, emission from surfaces (soils, water bodies, and vegetation), volcanic eruptions and wildfires. Anthropogenic sources include: fossil fuel combustion of fuels containing mercury (e.g. coal), waste incineration, biomass burning, and the release of mercury from industrial applications such as fluorescent light bulbs, fungicides, pesticides, paints, batteries and catalysts. Additionally, metal mining and smelting, as well as chlor-alkali plants, can be sources of atmospheric mercury [Schröeder and Munthe, 1998]. Anthropogenic mercury emissions from 27 countries in Europe in 1987 and 1988 equaled 726 tons of mercury per year. In 1990 the anthropogenic mercury emission for the United States and Canada were 154.1 and 38.8 tons of mercury per year, respectively [Schröeder and Munthe, 1998].

Once mercury is released into the environment, it can be transported and undergo atmospheric oxidation to form Hg(II) species, which can then be rapidly deposited to surfaces or partition to particulate matter due to the increased water solubility and decreased vapor pressure of the Hg(II). Lu et al. [2001] proposed BrO and Br atoms as oxidants capable of transforming Hg(0) to Hg(II). The mechanism for the atmospheric oxidation of mercury is still unclear; however, Br and BrO are still the most likely oxidants [Ariya et al., 2002; 2004]. Once Hg(0) is oxidized to Hg(II), it can deposit to surfaces where organisms can further transform Hg(II) to methyl-Hg, a bioavailable and bioaccumulative species. Bioavailable refers to methyl-Hg being readily assimilated by living organisms and bioaccumulation refers to methyl-Hg concentration increasing as the trophic levels increase [Dehn et al., 2006]. However, there are still many questions on how much of the deposited mercury actually is oxidized to more toxic species and how much of the oxidized mercury is assimilated by living organisms. This thesis explores the role of snow and ice forms in springtime bromine chemistry, which could in turn provide a starting point to find a relation between ions and Hg in snow and other ice surfaces.

A good first step to link ice forms and Hg concentrations was taken by Douglas et al. [2008] when they studied the relationship between snow and ice crystal formation and mercury deposition. The authors found that crystals growing from the vapor phase yield mercury concentrations that are typically 2-10 times higher than reported for snow deposited during atmospheric mercury depletion events (AMDEs) [Douglas et al., 2005; 2008].

In the future, bromine chemistry and its implications may be affected by climate change through sea ice changes that alter the availability of sea-salt bromide, which is a feedstock of reactive halogen production (see section 1.2). To determine how climate change may affect reactive halogen production, it is critical to understand what types of sea ice structures are responsible for reactive halogen production. Kaleschke et al., [2004] found a correlation between satellite-derived reactive bromine (in the form of BrO) and potential production of frost flowers, indicating that frost flowers might be a source of reactive halogens. However, Simpson et al., [2007b] found that airmass contact with first year sea ice was better correlated with BrO observed at Barrow, Alaska than was potential frost flower contact. Because each of these sea ice forms is expected to experience significant changes as the sea ice changes, we expect to see significant changes in halogen activation amounts. The summer sea ice extent was the smallest in historical record in autumn 2007 [NSIDC, 2007], continuing a long declining trend that modelers expect to continue into the near future [Holland et al. 2006]. Because reactive halogen chemistry occurs in springtime, after a winter season that is still expected to go well below freezing, decreasing summer sea ice extent leads to increased fractions of thinner springtime first-year sea ice. Only through a mechanistic understanding of which types of snow/ice/aerosol particles are responsible for halogen activation can we make meaningful predictions as to how this climate change will affect deposition of toxic metals like mercury to the sensitive Arctic ecosystem.

1.2 Bromine activation chemical mechanism overview

There are multiple studies that propose mechanisms attempting to explain the rapid depletion of O_3 during ODEs. The primary ozone depletion reactions follow the sequence:

$$2x\ [\ Br + O_3 \rightarrow BrO + O_2\ ] \qquad (R1.1)$$

$$BrO + BrO \rightarrow 2Br + O_2 \text{ -or- } Br_2 + O_2 \qquad (R1.2)$$

$$\underline{Br_2 + h\nu \rightarrow 2Br \qquad (R1.3)}$$

$$2O_3 \rightarrow 3O_2 \qquad \text{net reaction}$$

Here, bromine is a catalyst that cycles between Br and BrO, destroying ozone in the process. In the case that reaction R1.2 produces Br_2, sunlight, represented by hυ, reforms the reactive bromine atoms. It is in this and other steps that springtime (*i.e.* sunlit) conditions are required for ODEs.

While this mechanism for ozone depletion is well accepted, it is less clear how large levels of Br atoms needed to drive reaction R1.1 are produced. A number of mechanisms have been proposed, most of which share the autocatalytic cycle described below. These mechanisms have been tested primarily by model simulations [Fan and Jacob, 1992; McConnell et al., 1992; Tang and McConnell, 1996; Vogt et al., 1996]. A key reaction is the heterogeneous (gas-surface) reaction, R1.4 that liberates Br^- from condensed phases, producing molecular bromine.

$$HOBr_{(aq)} + Br^-_{(aq)} + H^+_{(aq)} \rightarrow Br_2 + H_2O \qquad (R1.4)$$

$$Br_2 + h\nu \rightarrow 2Br \qquad (R1.3)$$

$$Br + O_3 \rightarrow BrO + O_2 \qquad (R1.1)$$

$$\underline{BrO + HO_2 \rightarrow HOBr + O_2 \qquad (R1.5)}$$

$$Br^-_{(aq)} + H^+_{(aq)} + O_3 + HO_2 + h\nu \rightarrow Br + H_2O + 2\ O_2 \qquad \text{net reaction}$$

In the net reaction, we can see that HO_2 and H^+ are consumed to oxidize Br^- to Br atoms. These Br atoms then speed reactions R1.1 and R1.5, catalyzing further reaction. In this sense, the product of the reaction is a catalyst to further reaction, which we call autocatalysis. Explosions are autocatalytic reactions, and thus, Wennberg [1999] penned the term "the bromine explosion" for this chemical sequence.

The bromine chemistry continues until the O_3 concentration is completely depleted. However, whether the condensed phase in reaction R1.4 is snow, aerosol, frost flowers, or some other ice is not currently known. Evidence for the involvement of snow and ice comes from the fact that ODEs occur while the ground is still covered with snow, but once the snow pack melts, ODEs and bromine explosions cease [Wagner et al., 2001].

Fan and Jacob [1992] proposed a mechanism (see Figure 1.3) based on known aqueous phase chemistry that rapidly converts HBr, HOBr and $BrNO_3$ back to Br and BrO radicals. They also showed that the mechanism is efficient in the presence of high concentrations of sulfuric acid aerosols observed during ODEs, a theory that was later reinforced in Iraci et al. [2005]. To match the proposed mechanism with measurements taken in Alert, Canada, the authors concluded that the uptake of inactive species by aerosols and other condensed phases needed to be fast. If the uptake is slow and inefficient, the conversion of inactive halogen species to reactive halogen species would be too slow to maintain the autocatalytic cycle, resulting in O_3 concentrations that are higher than observed in the environment.

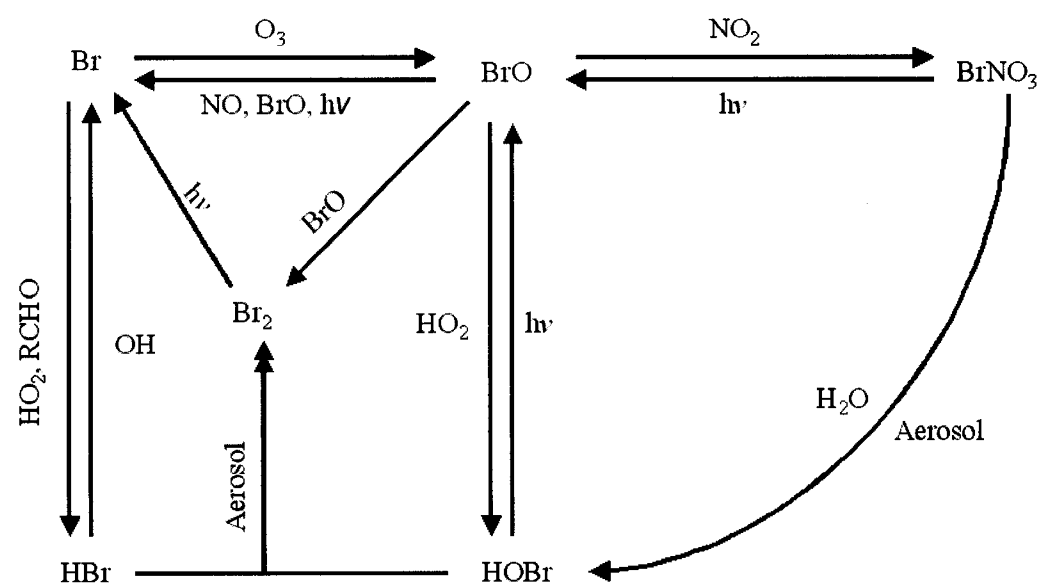

Figure 1.3 Autocatalytic mechanism for ozone destruction by active bromine chemistry. Adapted from Fan and Jacob [1992].

Reactive bromine species (BrO and Br atoms) can be lost by reaction with volatile organic compounds (VOC) and HO_2 to yield HBr. The reaction between bromine atoms and organic compounds (e.g. formaldehyde) is rather effective and would result in a rapid decrease of bromine atoms. The loss of bromine atoms through reaction with formaldehyde would terminate the ozone depletion chemistry. Therefore, rapid and efficient bromine recycling from HBr (unreactive) is necessary to obtain complete ozone loss. McConnell et al. [1992] proposed that HBr and brominated organic compounds can be scavenged by ambient aerosols and ice crystals, and that heterogeneous reactions on these surfaces then release Br_2 back to the atmosphere. Figure 1.4 shows a mechanism summarizing the main pathways to activate bromine, destroy ozone, and de-activate reactive bromine, extracted from the mechanisms proposed by Fan and Jacob [1992] and McConnell et al. [1992].

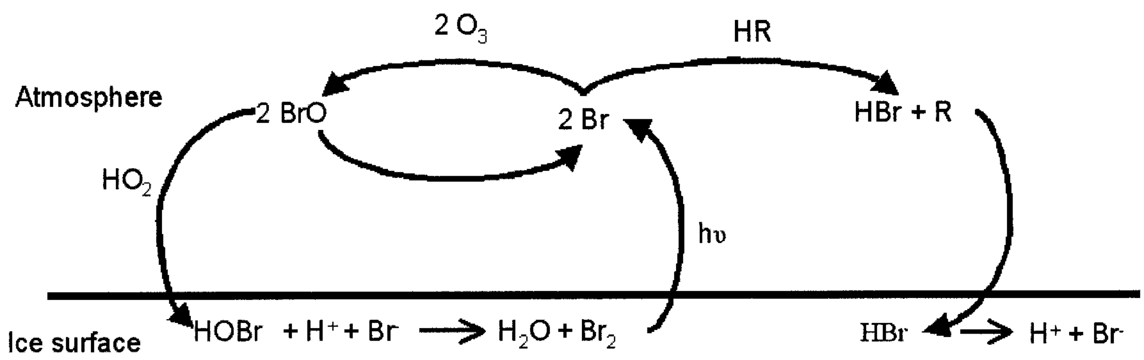

Figure 1.4 Bromine activation chemistry and the termination of the gas-phase chemistry. Key reactions for ozone destruction and bromine activation.

1.3 Role of chloride and iodide in bromine activation

Bromine atoms have been determined to be the most effective halogens for destroying ozone and being recycled, but other halogens may contribute to tropospheric ODEs and help maintain the bromine cycle. Because of the greater reactivity of chlorine with organic compounds, most activated chlorine rapidly reacts with VOC, limiting the ozone depletion from chlorine chemistry [Simpson et al., 2007a]. Evidence of chlorine activation appears in the observation of rapid oxidation of hydrocarbons by Jacobson et al. [1994]. In-situ observations of ClO that indicate that ClO concentrations are too low to maintain an effective ozone destruction cycle [Perner et al., 1999].

Figure 1.5 shows the participation of $Cl^-_{(aq)}$ in bromine activation via BrCl formation. Because Cl^- is usually orders of magnitude more concentrated in condensed phases as compared to Br^-, the initial reaction of HOBr is most often with Cl^-, leading to $BrCl_{(aq)}$. BrCl in the aqueous phase may then either volatilize, or go through further aqueous reactions. In the case that BrCl goes to the gas phase, one Br and one Cl atom are formed after photolysis, leading to formation of both reactive bromine and chlorine. On the other hand, when BrCl remains for some time in the aqueous phase, it may react with Br^- to form Br_2Cl^-, which can re-arrange to $Br_{2(aq)}$ and Cl^-. When $Br_{2(aq)}$ is formed, and it goes to the gas phase and is photolysed, two reactive bromine atoms are produced, which leads to a bromine explosion. However, BrCl formation only produces one reactive bromine atom and thus just sustains the reactive bromine pool and does not cause a bromine explosion. Many of the key reactions in this chemical mechanism have been proven to proceed in laboratory experiments [Fickert et al., 1999, Adams et al., 2002, Huff and Abbatt, 2000; 2002].

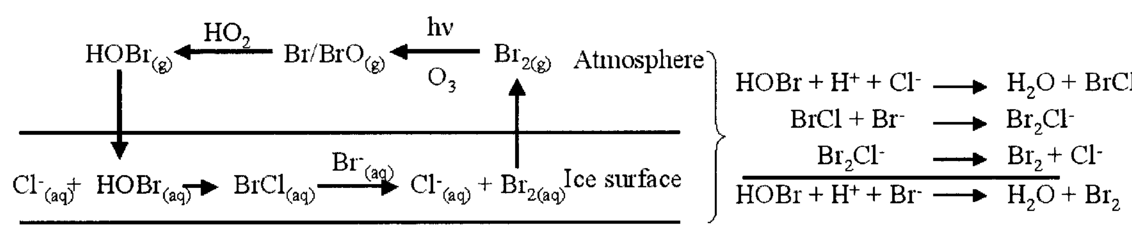

Figure 1.5 Bromine activation via BrCl formation.

In contrast to chlorine, iodine can participate in the destruction of ozone more efficiently than bromine [Vogt et al., 1999] because it is less reactive to organic molecules. But because there is very little of I^- in seawater, it is likely that I^- alone cannot maintain ODEs. Similar to Cl^-, its role in the chemical mechanism of bromine activation and ODEs depends on the reactions between more than one halogen. Iodine activation could serve as a trigger of ODE chemistry or another pathway for the rapid destruction of O_3 [Saiz-Lopez et al., 2006], or could catalyze the oxidation of Br^- and Cl^- to yield IBr_2^- and ICl_2^- to release Br_2 and Cl_2 [Enami et al., 2007].

In short, the efficient heterogeneous reactions between aqueous and gas phase species are needed for the production and recycling of reactive halogens. These heterogeneous reactions depend upon halides (e.g. bromide) being present in condensed phases (i.e. ice, snow, and aerosol particles). Therefore, this thesis focuses on observations of various condensed phases to determine which are most important for halogen activation.

1.4 Reactive bromine sources

A critical question for reactive halogen chemistry is: "Which surfaces and reactive species source reactive bromine?" Early in the history of ODEs, $CHBr_3$ was proposed as the main reactive bromine source [Barrie et al., 1988; Carpenter and Liss, 2000]. However, photo-dissociation of $CHBr_3$ ($J_{CHBr3} \sim 10^{-6}s^{-1}$) is too slow and observed $CHBr_3$ mixing ratios are insufficiently high to explain observed reactive bromine levels. Tang et al. [1996] proposed that the source of the bromine at polar sunrise is the snow pack on the ice covering the Arctic Ocean and that it is released auto-catalytically (see Figure 1.2). Finlayson-Pitts [2003] suggested that N_2O_5 reactions on air-borne sea salt could be the source of Br. However, using the annual average atmospheric Na^+ mixing ratio of $\sim 10^3$ ng m^{-3} and $[Br^-/Na^+]_{bulk\ seawater} \sim 6.2 \times 10^{-3}$ by mass, Tang et al. [1996] estimated that the atmospheric bromine atom content in newly-formed sea salt particles is ~ 2 pptv, which is insufficient to maintain ODEs. Sea salt Br^- residing in the snow pack can be rapidly accessed by atmospheric air as the specific surface area (200 – 600 cm^2/g [Dominé et al., 2004]) and porosity (~ 10^7 cm^2 cm^{-3}) [Tang et al., 1996] for snow is high. Assuming that the penetration of air is limited by molecular diffusion, atmospheric air can diffuse ~ 18 cm into snow pack in ~ 1 hr [Tang et al., 1996]. Lehrer et al. [2004] used a one-dimensional model of the mechanism of halogen liberation and the vertical transport in the polar troposphere to explore the effect of sea ice surfaces on the availability of sea salt Br^-. They successfully reproduced ozone depletions due to rapid bromine catalysis and suggested that the major source of reactive bromine appears to be snow pack covering sea ice. The authors suggested that the sea salt aerosol alone is not sufficient to yield the high levels of reactive bromine, but that aerosols could efficiently recycle bromine through a less reactive species, like HBr.

The strong anticorrelation between ozone and filterable bromine is due to meteorological modulation that alternately brings the depleted ozone and bromine-enriched air masses to the sampling site [Botthenheim et al., 1990; Hopper et al., 1998]. Tracing air mass trajectories, researchers found a good correlation between low ozone and trajectories that originated on the sea ice [Sander et al., 1997; Hopper et al., 1998]. Later these air masses were thought to be correlated to frost flower exposures [Kaleschke et al., 2004] or first-year sea ice contact [Simpson et al., 2007b]. Kaleschke et al. [2004] used a model that yields a maximum percentage area covered by frost flowers for a given surface air temperature to determine a frost flower exposure; this was defined as the potential frost flower (PFF) model. Simpson et al. [2007b] used back trajectories and ice contact times for air masses arriving at Barrow, Alaska to determine the potential effects of contact with first-year sea ice on Br^-.

Because of the inadequate abundance of organobromine precursors (e.g. $CHBr_3$) and low aerosol bromide abundance, modeling studies generally now conclude that the main source of reactive bromine is sea-salt Br^- stored in different ice surfaces. Dominé et al. [2004] proposed that the main sources of sea salt into the Arctic atmosphere are brine, sea spray, frost flowers, and blowing snow. How much reactive bromine each of these ice surfaces contribute to the atmosphere is still in debate and is the main focus of this project.

1.5 Bromine species in the gas and condensed phases

1.5.1 Gas-phase bromine

From the reactions above, we see that Br, BrO, Br_2, and HOBr are the primary reactive bromine species in the gas phase. During the day and when at least a little ozone is present in airmasses (>1ppbv), the main reactive bromine species is BrO. BrO possesses a strong, structured, UV spectrum, allowing it to be detected by spectroscopic remote sensing. Satellite observations from the Global Ozone Monitoring Experiment (GOME) show that tropospheric air masses enriched in BrO are usually situated close to sea ice and typically extend over 300-2000 km [Wagner and Platt, 1998; Wagner et al., 2001]. These observations support the mechanism, where Br^- from the ocean is the source of Br atoms and BrO, so the ozone depletion is initiated in marine regions. The horizontal and temporal extent of large BrO enhancements in the Arctic troposphere has been thoroughly studied, but the vertical distribution of the BrO is uncertain. McElroy et al. [1999] suggested that the BrO could be transported from the lower chemically-active troposphere (PBL) into the free troposphere through convection over large ice leads (openings in the sea ice). The transport of BrO from the PBL into the free troposphere supports the idea that ODEs and bromine activation chemistry can continue at high altitude in the atmosphere, presumably indicating recycling of bromine on aerosol particles. Because satellites cannot distinguish between PBL, free tropospheric, and stratospheric BrO, it is important to use ground-based measurements. Measurements of ozone [Hopper et al., 1998; Ridley et al., 2003] and BrO [Hönninger and Platt, 2002] from different locations in the Arctic confirmed that ozone was depleted more frequently in a site on the sea ice than at coastal or inland sites [Frieβ et al., 2004]. Therefore, ground-based measurements of halogens provide the direct link between snow and other ice surfaces and bromine chemistry [Rankin and Wolff, 2002; Hara et al., 2002; Toom-Sauntry and Barrie, 2002; Kaleschke et al., 2004; Newberg et al., 2005 Simpson et al., 2005; Simpson et al., 2007b].

1.5.2 Bromide in snow

Bromide and other seawater ions are present in the snow pack over the ice-covered ocean during winter. Chloride and Na^+ are the main constituents of seawater and are considered good sea salt tracers. Ionic species ratios are used to trace specific compounds and to observe patterns of distribution over an area. The Br^-/Cl^- ratio can be used to indicate how enriched or depleted in Br^- the snow is compared to sea-salt Cl^-. Deviations from the standard seawater ratio are known as modifications. Br^-/Cl^- ratios show strong variability, changing from low levels of enrichment in the dark to large enrichments after polar sunrise. The observed enrichment in Br^- in snow is believed to be due to a net scavenging by aerosols and snow of gaseous bromine compounds like HBr, HOBr, and Br_2 [Toom-Sauntry and Barrie, 2002]. Simpson et al. [2005] observed Br^- depletions and enrichments in coastal snow suggesting Br^- loss to the gas phase by bromine activation chemistry in some samples and Br^- gain due to the scavenging of HBr from the gas phase to the snow pack in other samples. A detailed understanding of the chemical composition of snowfall is crucial for a better understanding of this chemistry [Toom-Sauntry and Barrie, 2002; de Caritat et al., 2005; Simpson et al., 2005].

Enrichment factors are commonly used to identify modifications with respect to seawater standard ratios. Sea salt enrichment factor (EF_{SS}) were calculated in Toom-Sauntry and Barrie [2002] using the standard definition:

$$EF_{SS} = \frac{\left(\frac{[X]}{[Na^+]}\right)_{Snow}}{\left(\frac{[X]}{[Na^+]}\right)_{Seawater}}. \tag{1.1}$$

where [X] is the concentration of a certain ion in snow or standard seawater and $[Na^+]$ is the concentration of sodium in snow or standard seawater. Toom-Sauntry and Barrie [2002] found Cl^- to be slightly enriched with respect to Na^+ and seawater ($EF_{SS}(Cl^-)$ = 1.4) in snowfall and snow pack during the winter, and more highly enriched during the spring. Chloride and Br^- were enriched with respect to Na^+ and seawater in both snow and aerosol during the dark period, November-February ($EF_{SS}(Br^-)$ = 1.5-5). During the period March-May after polar sunrise, the observations resulted in EF_{SS} (Br^-) = 20-72, which means that Br^- was significantly modified from sea salt Br^-. Bromide was more enriched in snowfall than in aerosol by about a factor of 1.5 in the dark winter and 2 in the sunlight. Bromide enrichment is probably due to the scavenging of HBr from the termination step of the gas-phase bromine chemistry; while enrichments in Cl^- are mostly due to acid displacement reactions, such as reactions R1.6 and R1.7.

$$NaCl_{(P)} + H_2SO_{4(g)} \rightarrow Na_2SO_{4(P)} + HCl_{(g)} \tag{R1.6}$$

$$NaCl_{(P)} + HNO_{3(g)} \rightarrow NaNO_{3(P)} + HCl_{(g)} \tag{R1.7}$$

Relative to SO_4^{2-}, NO_3^- is more abundant in snowfall than in aerosol. This difference is likely due to the scavenging of gaseous nitrate compounds from the atmosphere by snow.

Studies on how chemical species fluctuate between the snow and the atmosphere aim to track anthropogenic pollution or identify chemical seasonal patterns in the Arctic [Davidson et al., 1989; Joranger and Semb, 1989; Jones et al., 1993]. Nitrate in the snow pack is photolyzed to release NO_x. The photolysis of nitrate also leads to the production of OH and HONO. Then the OH in the snow pack can react with organic acids to produce HCHO, acetaldehyde and acetone [Dominé and Shepson, 2002]. Reactions of HCHO are an important sink of reactive bromine, which produce HBr [McConnell et al., 1992].

Sulfate can participate in the oxidation of halide ions in sea salt and the production of gas-phase reactive halogens (Finlayson-Pitts, 2003). The uptake of HOBr by ice surfaces is favored when sulfuric acid is added to solution [Iraci et al., 2005]. Iraci et al. [2005] suggested that the solubility of HOBr is comparable to that of HBr, indicating that upper tropospheric aerosols should contain equilibrium concentrations of HOBr that equal or exceed those of HBr. The acidification of the ice surface favors the efficient release of Br^- [Fan and Jacob, 1992; Huff and Abbatt, 2002]. Calcium carbonate precipitation from sea salts may be responsible for reducing the buffering capacity of sea salt aerosols, and thus facilitates its acidification. The modeling study of Sander et al. [2006] showed that as condensed phase acidity increases, Br^- is more efficiently activated and ozone is more efficiently destroyed [Sander et al., 2006].

1.5.3 Bromide on aerosol particles

Aerosol particles are considered likely surfaces for atmospheric chemical reactions and also transport chemical species. Aerosol chemistry plays a unique role in the overall bromine activation mechanism [Sirois and Barrie, 1999]. These particles can liberate Br^- by reacting with HOBr to yield bromine atoms or can accumulate Br^- by scavenging HBr from the reaction of VOC and bromine atoms. The release of Br^- from aerosol particles would result in Br^- depleted aerosols, while addition of HBr would result in Br^- enriched aerosols. Bromide enrichments in aerosol particles was reported by Ianniello et al. [2002] and confirmed by laboratory experiments by Hess et al. [2007]. Observations of depletions in Br^- in liquid aerosol particles [Newberg et al., 2005] confirmed that aerosols have a highly dynamic role in the bromine activation chemistry. Hara et al. [2002] reported that Br^- liberation occurred in the coarse particles (>2.0 μm) and accumulation occurred in the fine particles (0.2 – 2.0μm). The findings of Hara et al. [2002] and Newberg et al. [2005] suggested that aerosols of different sizes have different roles in the bromine chemistry. Larger aerosols can scavenge acid species and trigger halogen activation [Hara et al., 2004; and 2005]. For example, Cl^- can be removed from the aerosol particle by NO_3^- or SO_4^{2-} acids, as shown in R1.6, R1.7 and R1.8 [Tang and McConnell, 1996; Jourdain and Legrand, 2002].

$$BrONO_{2(aq)} + H_2O \rightarrow HOBr_{(aq)} + HNO_{3(aq)} \qquad \text{(R1.8)}$$

In summary, past studies of aerosol particle chemical composition suggest that aerosols play a dynamic role in the bromine activation chemistry as a source of Br atoms and as a receptor of HBr. Although the chemical composition of aerosols has been intensively studied to assess information on the aerosol particles' role in bromine chemistry, there is need to trace aerosol, snow and gas phase Br^- content simultaneously to explore the actual contribution and role of these Br^- ice surfaces in halogen activation.

1.5.4 Bromide in frost flowers

Rankin and Wolff [2002] first proposed that frost flowers, due to their high salinity and presumed high specific surface areas were important sources of reactive bromine to the atmosphere. Frost flowers are vapor-grown ice crystals that form on new sea ice and wick brine, becoming highly saline in the process. Frost flowers were proposed as a source of reactive bromine to the polar lower atmosphere [Rankin and Wolff, 2002; Kaleschke et al., 2004; Jones et al., 2006]. There are only a few studies on frost flower chemical composition [Rankin et al., 2000; Rankin and Wolff, 2002, and 2003; Simpson et al., 2005; Douglas et al., 2005; Kalnajs and Avallone, 2006], microstructure [Domine et al., 2005], and formation [Martin et al., 1995; and 1996].

Thus, the role of these frost flowers in the bromine activation chemistry is not fully understood and is still in debate. Rankin et al. [2000] and Rankin and Wolff [2002] suggested that 60% of the total sea salt in an inland site in Antarctica was from brine and frost flowers on the sea ice surface rather than open water. The strong temperature gradient observed between the atmosphere and sea-ice surface controls the growth and precipitation of certain salts at different temperatures. At -8°C Na^+ and SO_4^{2-} are thermodynamically favorable to precipitate as $Na_2SO_4 \bullet 6H_2O$ (mirabilite). Precipitation of mirabilite from the sea-ice surface brine and frost flower crystals results in SO_4^{2-} depletion of the brine. The aerosol that originates from either the sea-ice surface brine or the frost flowers would also be depleted in SO_4^{2-}. The sulfate-depleted aerosol suggestion is consistent with the observations of sulfate-depleted aerosol reported by Rankin and Wolff [2003].

Although is believed by few in the community that frost flowers have an active role in bromine activation chemistry [Rankin and Wolff, 2002; Kaleschke et al., 2004] there are some studies that cannot find conclusive evidence of frost flowers as a source of reactive bromine. Simpson et al. [2007b] found a good correlation between first year sea ice and air masses containing enhanced BrO, but a negative correlation between Kaleschke et al.'s [2004] potential frost flower model. Because there was a considerable need to determine the overall role of frost flowers as source of reactive halogens to the atmosphere, we undertook a detailed study of frost flowers (Chapter 3). Our contribution to the frost flower debate was to report the chemical composition of frost flowers and brine during different growth stages and to explore the role of frost flowers and brine in aerosol production and bromine chemistry.

Chapter 2. Chemical composition of Arctic surface snow[1]

2.1 Abstract

From a three-year (2004, 2005, and 2007) snow sampling campaign in the Arctic springtime, surface snow samples were collected in environments that span most Arctic terrains. The environments sampled are land, thin and thick first-year sea ice, and multi-year sea ice. The snow samples were analyzed for Br^-, Cl^-, SO_4^{2-}, NO_3^-, NH_4^+, Na^+, K^+, Mg^{2+} and Ca^{2+}. Our main goal was to examine modifications to ion composition as compared to Na^+ (sea-salt tracer) concentrations. Source fractionation processes and atmospheric influences are important modification mechanisms that influence the shape of the modification pattern for each ion. We find that Cl^-, K^+ and Mg^{2+} are primarily sourced by unfractionated sea salt and only show deviations from sea salt composition at low Na^+ concentration. Bromide and Ca^{2+} are highly influenced by atmospheric processes that are evident at low sea-salt tracer concentrations. Calcium enrichments are due to the addition of non-sea-salt (nss) Ca^{2+} from dust. Bromide enrichments are due to the addition of nss-Br^- and depletions are due to the bromine activation to the gas phase. Sulfate is affected by source fractionation, which is evident at high Na^+ concentrations and atmospheric addition, which is observed at low Na^+ concentrations. Nitrate and NH_4^+ are not correlated with sea salt and show less variability in concentrations than sea salt ions. Modifications can be related to time-integrated air-snow exchange fluxes for Br^-, SO_4^{2-} and Ca^{2+} and are in good agreement with observations of gas-phase species, reinforcing the interpretation of their modifications as being due to atmospheric exchange.

2.2 Introduction

Snow is an important scavenger of pollutants, sea salt, acids and other chemical species in the Arctic. Snow can store the scavenged species, facilitating the accumulation of chemical species, and it can later liberate the accumulated species into the atmosphere.

---

[1] Alvarez-Avilés, L., W. R. Simpson, D. Carlson, T. A. Douglas, M. Sturm, F. Domine (2008), Chemical composition of Arctic surface snow, prepared for submission in Atmospheric Chemistry and Physics.

An example of snow composition influencing Arctic atmosphere chemistry is halogen activation chemistry, which causes ozone destruction. Tropospheric ozone can be destroyed by gas-phase reactive bromine, which is sourced from sea salts stored in snow and other ice surfaces [Barrie et al., 1988; Bottenheim et al., 1990; Fan and Jacob, 1992; McConnell et al., 1992; Vogt et al., 1996; Rankin and Wolff, 2002; Simpson et al., 2007a]. The same halogens involved in ozone destruction are believed to participate in the oxidation of gaseous elemental mercury to gaseous reactive gaseous, which is then added to the ecosystem [Schröeder and Munthe, 1998; Lindberg et al., 2002; Khalizov et al., 2003; Wang and Pehkonen, 2004]. In summary, the snow pack serves as a surface where reactions occur, and as a source and sink of chemical species. Thus, a detailed understanding of the chemical composition of the snow pack is crucial for a better understanding of the Arctic atmosphere's composition.

Two common sources of ions to the snow in polar regions are sea salts and acid gases [Toom-Sauntry and Barrie, 2002; Dominé et al., 2004]. Typical sea-salt ions are Na^+, Cl^- and some SO_4^{2-}, Ca^{2+}, K^+, Mg^{2+}, Br^-, and the acid gases normally exchange H^+, Cl^-, Br^-, SO_4^{2-}, NH_4^+ and NO_3^-. The majority of papers that address composition of the snow pack study interactions between snow and atmosphere by tracking modifications to the components in either snow or atmosphere [Joranger and Semb, 1989; Davidson et al., 1989; Udisti et al., 1999; Aristarain and Delmas., 2002; Gragnani et al., 2002; Toom-Sauntry and Barrie, 2002; Dominé and Shepson, 2002; Nikus, 2003; de Caritat et al., 2005; Benassai et al., 2005; Yalcin et al., 2006]. Enrichment factors, correlation coefficients, ternary plots and non-sea salt abundances are common tools to track modifications to snow composition. But these tools do not normally consider the sea-salt tracer concentration range (low or high) where the modification occurs. In this paper we propose that correlation plots are an effective method to study the chemical composition of snow. The correlation plots consider the modifications to sea salt in context of the sea-salt tracer concentration and can show important details in enrichment or depletions patterns [Udisti et al., 1999; de Caritat et al., 2005; Simpson et al., 2005]. These modification patterns may adopt shapes that could serve to identify specific processes that alter the chemical composition of snow.

There are two significant modification mechanisms that alter the ionic content of snow: source fractionation and atmospheric exchange. Source fractionation is a separation process in which ions separate before formation of aerosol or brine that is later incorporated into snow. An example of source fractionation is the precipitation of sea salts. These precipitation processes become thermodynamically favorable at certain temperatures. At -2°C calcium carbonate precipitates ($CaCO_3$) [Sander and Kaleschke, 2006], at -8°C sulfate and sodium can precipitate as mirabilite ($Na_2SO_4 \bullet 10\ H_2O$) [Rankin and Wolff, 2002], at -22°C hydrohalite ($NaCl \bullet 2\ H_2O$) can crystallize, and below -34°C, $MgCl_2 \bullet 6\ H_2O$ and $KCl \bullet 6\ H_2O$ can precipitate [Rankin et al., 2000]. When precipitation occurs, the precipitated crystal and residual solution may physically separate and as aerosol particles form from the residual solution, the precipitate crystal remains on the sea ice surface. Aerosol particles that form from the residual solution are now fractionated in the ion of interest [Rankin and Wolff, 2003; Alvarez-Aviles et. al., 2008, in press, Chapter 3].

Atmospheric exchange describes the process of removing or adding ions via incorporation of aerosols and acids (addition) or heterogeneous reactions (removal). An example of atmospheric removal is halogen activation, which results in depleted Br^- in the snow pack [Simpson et al., 2005]. In halogen activation Br^- is removed from the snow pack when it reacts with HOBr and yields photoactive bromine species [Fan and Jacob, 1992; McConnell et al., 1992; Vogt et al., 1996]. The termination step of the gas-phase bromine chemistry occurs when bromine reacts with hydrocarbons to form HBr, which can add Br^- to surface snow. This termination step can also happen with Cl^-, but because sea salt Cl^- is more abundant the resulting enrichments are relatively smaller. Acids stronger than HCl can displace Cl^- from aerosol particles or snow through the reaction [Finlayson-Pitts, 2003]

$$2Cl^-_{(aq)} + H_2SO_{4(aq)} \rightarrow 2HCl_{(g)} + SO_4^{2-}{}_{(aq)} \qquad \text{(R2.1)}$$

Removal of Cl^- as HCl would result in depletions [Yalcin et al., 2006], but snow or aerosols can scavenge HCl and add it to the sea-salt Cl^- resulting in enrichments [Toom-Sauntry and Barrie, 2002; de Caritat et al., 2005; Benassai et al., 2005]. A good acid candidate to remove Cl^- as HCl is sulfuric acid from Arctic haze, which can also add SO_4^{2-} to snow resulting in SO_4^{2-} enrichment [Li and Barrie, 1993].

In this paper we study the unique modification mechanisms of Br^-, SO_4^{2-}, Cl^-, NO_3^-, NH_4^+, K^+, Ca^{2+}, and Mg^{2+} in comparison to a sea-salt tracer in snow, Na^+. We also test if Na^+ is efficient as a sea-salt tracer. Our goal is to study the unique modification mechanisms of these species in snow, put constrains onto the extent of source fractionation or atmospheric exchanges based on their modifications, and obtain some valuable insight about their snow-atmosphere chemistry.

2.3 Patterns adopted by modification mechanisms

Figure 2.1 shows two limiting cases of modification patterns to ions in snow shown as log-log correlation plots. Because of the extreme variability of sea salt influences in snow we show each axis on a logarithmic scale. Snow can vary approximately six orders of magnitude in Na^+ concentration from very pure inland snow ($[Na^+] \sim 1\ \mu M$) to cryo-concentrated sea salt brine ($[Na^+] \sim 1$ M). Simple dilution of sea salt with condensed water vapor results in the solid diagonal lines in each panel of the plot. In Figure 2.1a, we consider two source modifications, where sea salt is fractionated at its source either enriching (dashed line) or depleting (dotted line) the ion as compared to the sea-salt tracer. Dilution subsequent to this source fractionation gives diagonal lines parallel to simple sea salt dilution. A common way to express source modification is through enrichment factors,

$$Ef[X] = \frac{\left(\frac{[X]}{[Na^+]}\right)_{Snow}}{\left(\frac{[X]}{[Na^+]}\right)_{Seawater}} \tag{2.1}$$

[X] is the concentration of the ion of interest and [Na^+] is the sodium concentration in snow or seawater. In Figure 2.1a data along the enriched line have Ef = 10, and along the depleted line have Ef = 0.1. Thus, the enrichment factor analysis is highly appropriate to describe source fractionation processes, particularly at high sea-salt tracer concentrations.

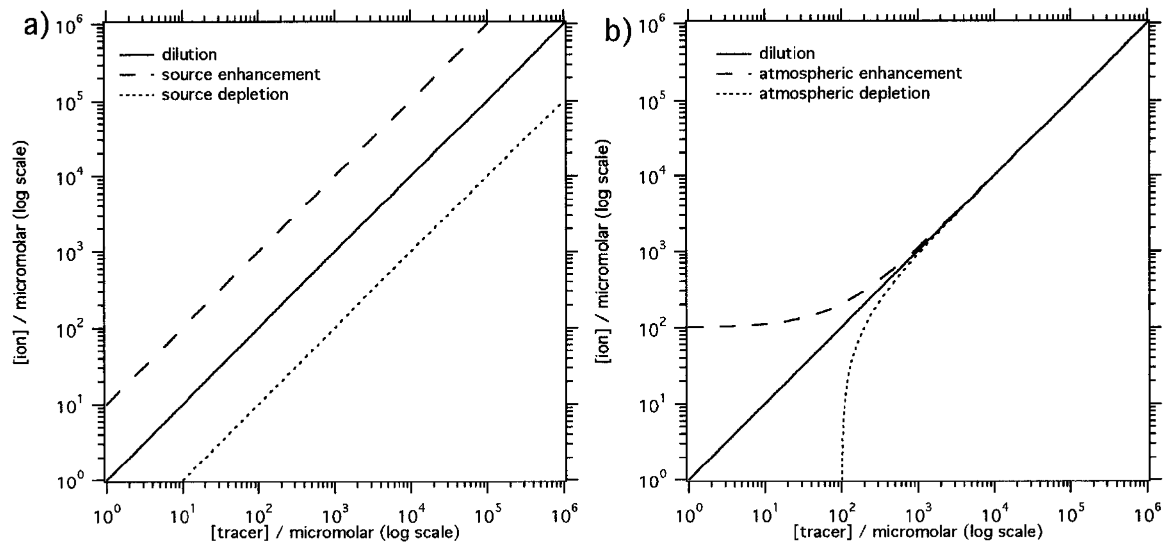

Figure 2.1 A conceptual picture of modification patterns of ions in snow shown on log-log correlation plots. Panel a) shows the expected pattern if the source of ion into the snow was modified to be enriched (dashed line) or depleted (dotted line). Panel b) shows the enrichment (dashed line) and depletion.

Figure 2.1b shows modification by exchange of ions with atmospheric aerosols or acids. Processes of this sort would be addition of atmospheric acidic gases (e.g. sulfuric acid), acid displacement (e.g. removal of Cl^- via addition of SO_4^{2-}), halogen activation (affects Br^-), or addition of dust (affects Ca^{2+}). Because this modification comes from or produces relatively limited fluxes between the snow and the atmosphere, we can model the fluxes as additions or removals of fixed concentrations of the ion of interest, uncorrelated with sea salt abundance. The dashed line is the behavior when a fixed amount (100μM) of the ion is added, and the dotted line corresponds when to fixed amount (100μM) of the ion is removed. These lines curve because of the log-log plotting style. Atmospheric exchanges that result in enrichments and depletions are normally due to addition of non-sea salt ions (nss-ion) to sea-salt or removal of the ion from sea salt.

To quantify the magnitude of ionic exchanges we can calculate the nss-ion (Equation 2.2) from those samples that are affected the most by nss-ion additions. The nss-ion abundance would be the atmospheric enrichment and depletion lines in panel b.

$$nss-[ion]=[ion]_{Sample}-\left\{\left(\frac{[Ion]}{[Na^{+}]}\right)_{Seawater}\times[Na^{+}]_{Sample}\right\}. \tag{2.2}$$

Nss-[ion] is the non-sea salt ion concentration in µM, [Ion]/[Na^+] is ion to Na^+ molar ratio in seawater, [Na^+] is Na^+ concentration in the sample in µM and [Ion] is ion concentration in µM in the sample. Non-sea-salt abundance analysis is appropriate to describe atmospheric exchanges. However, when the sea-salt tracer concentration is high, the removal of sea salt background (the second term in equation 2 becomes problematic due to the magnification of small errors in measurement of [Na^+] and the ion of interest.

From Figure 2.1 we can see these limited snow-air exchanges have little effect in the ion's behavior at high tracer contents but large effects at low tracer concentrations. Conversely, source fractionation affects the behavior at all tracer concentrations. Considering both panels together, we see that at low tracer concentrations, atmospheric exchange is most evident and at high tracer concentrations, source fractionation is most evident. Therefore, we see from these examples how log-log correlation plots allow separation of source fractionation from atmospheric exchange and provide more information than analyses of enrichment factors of non-sea-salt abundances.

2.4 Methodology

2.4.1 Sampling

Samples were collected facing the wind wearing powder free polyethylene disposable gloves and Tyvek suits. All sampling vials were cleaned in the laboratory using 18.2 MΩcm water and were transported to the site packed in 1-gallon Ziploc bags. Snow was collected in the vial using the edge of the vial to scoop the top 2 – 3 cm of the surface snow pack. All samples were transported and stored frozen and away from light until analysis.

The data set used in this paper is a compilation of three years of Arctic snow studies for a total of 936 surface snow samples. Figure 2.2 shows a map of the sampling locations. In 2004, a total of 104 surface snow samples were collected in a 102 km transect inland from Barrow, Alaska. Of these samples, 99 were from inland sites and 5 were from land-fast ice. In March of 2005, 89 surface snow samples were collected on the sea ice portion that is attached to the shoreline (land-fast ice) North of Point Barrow. Surface snow was also collected approximately 3 km on shore, from March to June, 2005 for a total of 122 samples. The samples from 2007 were collected from four different sites, both inland and on the sea ice. The two inland sites were located at 3 km and approximately 15 km from the shoreline in Barrow, Alaska. There were 222 samples collected at the inland sites during the month of March. The two sea ice sites were in the Applied Physics Laboratory Ice Station (APLIS) ice camp and on the land-fast ice in Barrow. A total of 399 surface snow samples were collected on sea ice during the month of March and the first week of April. To unify the three data sets the samples were classified by one of four different environments: land, thin first-year sea ice (thin FYI), thick first-year sea ice (thick FYI) and multi-year sea ice (MYI). Thin FYI was a recently frozen lead (an opening in the sea ice), probably 2-3 weeks old and about 50 cm in sea ice thickness. Thick FYI was 173 cm thick was likely formed in the preceding fall/winter. MYI is ice that has endured at least one summer.

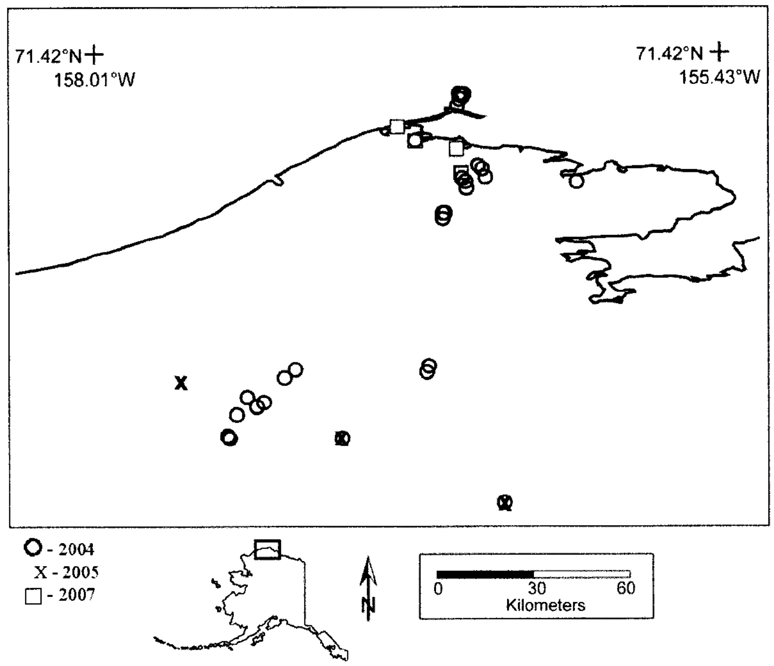

Figure 2.2 A map of sampling locations used in this study.

2.4.2 Analytical Procedures

The samples were melted and an aliquot was removed for specific conductivity analysis using a conductivity meter. According to their conductivity, these samples were then classified in groups for the Ion Chromatography (IC) analysis (Dionex 2000). The surface snow samples were analyzed for Br^-, NO_3^- SO_4^{2-}, Cl^-, NH_4^+, Na^+, K^+, Ca^{2+} and Mg^{2+}. To measure the instrument reproducibility, one sample was run 23 times for anions and 17 times for cations to obtain the error in the measurement. The relative standard deviation for all ions is less than 5%. To measure sampling variability, we sampled some snow in duplicates, and calculated the ratio of the lower value divided by the higher value. The average for all ions was 0.85 indicating a 15% sampling variability. Not all snow was collected in duplicate; 536 samples are single and 402 are duplicates. We report the average of the snow that was collected in duplicates.

Complex matrices like these snow samples contain other chemical species than the ones analyzed for this study. These other chemical species may cause interferences either by affecting the detector's affinity towards certain ions or by affecting the peak resolution. The IC peak resolution for NH_4^+, Mg^{2+} and K^+ was compromised due to other peaks in the area. Thus we expect NH_4^+, Mg^{2+} and K^+ to have more noise associated with the measurement.

2.4.3 Correlation plot construction

For the correlation plots to be efficient in showing modification in comparison to a sea-salt tracer they have to contain both the concentration of the ion of interest versus the concentration of the sea-salt tracer and a sea-salt dilution line. The sea-salt dilution line is defined as the expected concentration of the ion of interest if its only source was sea salt at any sea-salt tracer concentration. The ratio of ion to sea-salt tracer was calculated from Quimby-Hunt and Turekian [1983] standard seawater values. Assuming that the tracer is unmodified, snow samples that fall below the sea-salt dilution line are depleted in the ion of interest and samples above the line are enriched in the ion of interest.

2.4.4 Outlier identification

The ratio of the sum of cations to the sum of anions was used to identify outliers. The charge balance requires that the ratio of the sum of cations to the sum of anions is equal to one. When this ratio is not equal to one, anions or cations present in the snow were either not analyzed or analytical problems occurred. In our analysis, HCO_3^-/CO_3^{2-} and H^+ are unanalyzed species. Panel a in Figure 2.3 shows the distribution of the charge balance ratio as a function of the number of observations of each ratio. When certain ion concentrations were missing we added to the charge balance the expected contribution from sea salt of the missing ion. We calculated the missing ion concentrations using the sea salt ratio of ion to Na^+ and assuming the ion was unmodified from sea salt ratios. We also added 10 μeqL^{-1} to the cation sum to account for the atmospheric addition of H^+, which normally corresponds to a pH of 5 (~10 μeqL^{-1}) [Toom-Sauntry and Barrie, 2002]. The histogram shows a high probability to measure a charge balance ratio of unity, as expected if the majority of ions are accounted for in the analysis. The mean charge balance ratio obtained from the distribution was 0.92, possibly indicating a noise or small (8%) mis-calibration between cation and anion standards (see section 2.4.2). If we consider that the majority of the data appear to be a normal (gaussian) distribution, we expect that a range of the mean $\pm 3\sigma$ would encompass 99% of the normally distributed data. We consider data outside this range, mean $\pm 3\sigma$ (charge balance between 0.70 and 1.21), to be outliers that result from analytical error. We identified the outlier samples beyond the 3σ limits and show in panel b the charge balance plot with outliers in blue and remove them from the data set. A total of 120 of the 936 (13%) surface snow samples are considered outliers and are removed from the data set used in all subsequent analysis. We recognize that samples with low values of anions and cations are more susceptible to atmospheric exchanges. In order not to lose valuable information from samples at low sea-salt tracer concentrations, we keep all samples that contain less than 30 μeqL^{-1} (after the addition of acid, 10 μeqL^{-1}).

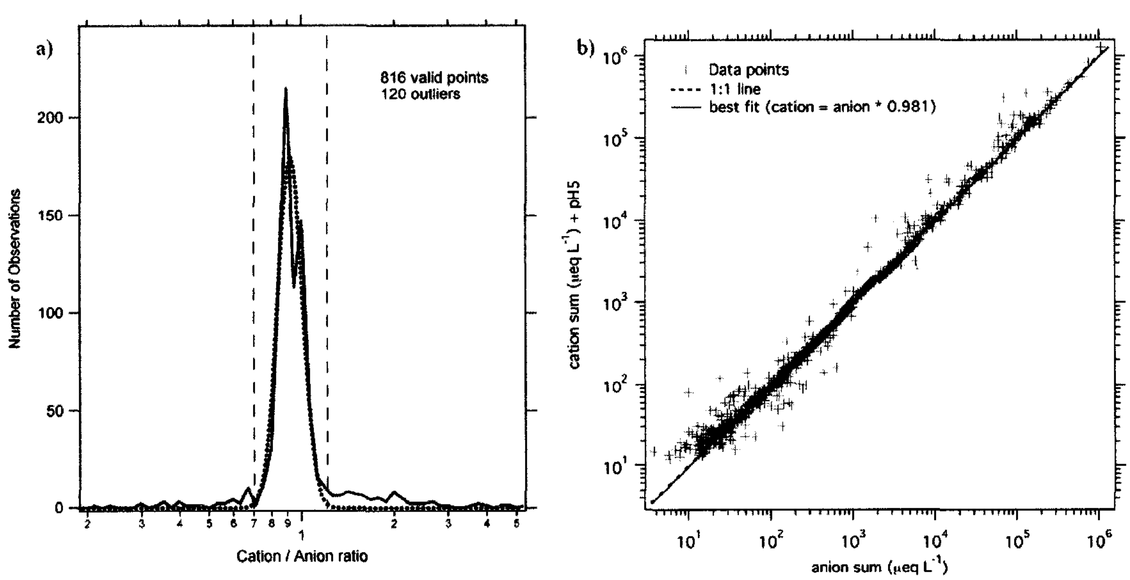

Figure 2.3 Quality control analysis plots used to reject outlying data. Panel a) shows the distribution of the totality of surface snow samples, 936. Panel b) shows the outliers in blue crosses in the sum of anions as a function of the sum of cations.

2.5 Results

2.5.1 Snow ionic content

Table 2.1 summarizes a statistical analysis of each ion's concentrations in all environments. To show a more representative range of concentrations we report here the 10^{th} and 90^{th} percentile; that is after sorting the data in order, the concentrations found at 10% and 90% of the entire set. The 50^{th} percentile is the median, and the average is calculated considering all values of the set.

The overall ionic content on land and on MYI appears to be similar and lower than concentrations on thin and thick FYI. The range of concentrations found on land is larger than on MYI, but the medians indicate that land samples have somewhat lower ionic contents than MYI samples. Thin FYI shows higher values in range of concentrations, average and median than all other environments, therefore it has the highest overall ionic content. Ions that are generally low to absent in seawater (NO_3^- and NH_4^+) show little differences within their variability in the various environments.

Table 2.1 Ranges and averages of each ion concentration in four different environments.

Ion	***Parameter***	***Land (μM)***	***MYI (μM)***	***Thick FYI (μM)***	***Thin FYI (μM)***
Na^+	Average	261	208	19,300	50,500
	Median	64.2	121	1,480	9,110
	10%	4.79	1.36	85.2	489
	90%	734	385	72,700	192,000
Cl^-	Average	366	308	21,100	61,900
	Median	113	175	1,970	11,700
	10%	8.79	7.42	85.9	737.37
	90%	923	585	83,100	250,000
K^+	Average	6.65	5.15	301	838
	Median	3.01	3.32	22.5	86.9
	10%	0.133	0.0932	0.767	5.82
	90%	15.2	11.7	923	2,440
Mg^{2+}	Average	36.1	31.1	1,860	5,200
	Median	14.2	19.6	141	535
	10%	0.501	0.303	5.04	35.2
	90%	94.3	65.1	3,970	13,800
Ca^{2+}	Average	9.28	6.91	394	1,040
	Median	4.58	5.25	27.7	106
	10%	1.19	1.23	2.18	12.1
	90%	22.5	13.2	851	2,930
Br^-	Average	0.259	0.317	30.6	90.7
	Median	0.151	0.247	1.79	17.2
	10%	0.0345	0.0629	0.189	1.16
	90%	0.536	0.413	112	350
SO_4^{2-}	Average	9.09	8.29	2,010	1,910
	Median	5.03	6.80	57.1	82.4
	10%	1.12	2.05	6.15	7.75
	90%	21.1	15.8	5,820	6,350
NO_3^-	Average	6.82	4.11	6.89	6.78
	Median	5.32	3.59	5.24	2.49
	10%	2.36	3.03	2.54	1.81
	90%	10.8	6.75	13.2	9.81
NH_4^+	Average	1.33	0.942	1.11	0.404
	Median	0.723	0.853	0.396	0.451
	10%	0.248	0.513	0.166	0.172
	90%	2.61	1.59	1.76	0.595

2.5.2 Chloride (Cl^-)

Chloride (Cl^-) and sodium (Na^+) are the main constituents of seawater and can be used as sea-salt tracers. Figure 2.4a, shows the correlation plot of Cl^- as a function of Na^+ in all environments. In general, Cl^- is well correlated with Na^+, but shows limited enrichment below 1000 μM Na^+, as observed by Toom-Sauntry and Barrie [2002]. The majority of the data (80%) are within a factor of 2 of the seawater dilution line. The data above 1000 μM Na^+ is found in close proximity to the seawater dilution line. Considering the samples below 1000 μM Na^+, 86% of that subset are enriched, with an average enrichment factor of 1.33 for the enriched samples having less than 1000 μM Na^+. Reasons for the observed deviations and discussion of use of Cl^- as a sea salt tracer are presented in the discussion, section 2.6.1.

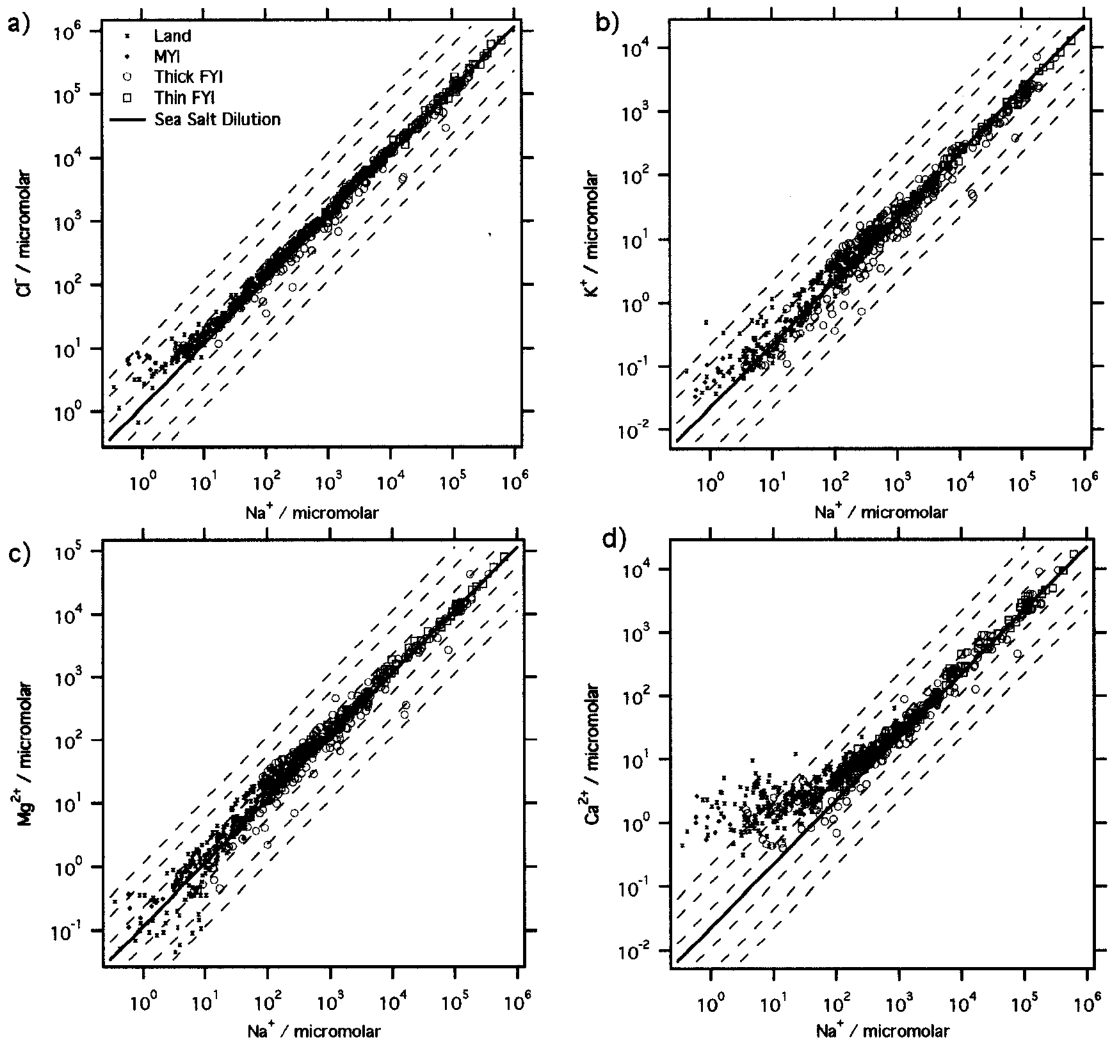

Figure 2.4 Correlation plots of Cl^-, K^+, Mg^{2+}, and Ca^{2+} versus Na^+ in all four environments: land, thin-first-year sea ice (thin FYI), thick-first-year sea ice (thick FYI), and multi-year sea ice (MYI). The dashed lines above the seawater dilution line represent enriched snow with enrichment factors of 2, 5 and 10 times more than sea salt. The dashed lines below the seawater dilution line represents diluted snow with enrichment factors of 2, 5, and 10 times less than sea salt.

2.5.3 Potassium (K^+)

Figure 2.4b shows the correlation plot for K^+. Potassium is correlated with sea salt with some scatter below 100 μM Na^+. The scatter may be due to noise at low K^+ concentration or possibly atmospheric exchanges such as addition from dust. The majority of the samples (85% of the complete data set) are found between the 2 times enriched and 2 times depleted lines. Of these samples that are between the 2x enriched and 2x depleted, half are enriched and half are depleted, indicating little net enrichment or depletion of K^+.

2.5.4 Magnesium (Mg^{2+})

Figure 2.4c shows the Mg^{2+} correlation plot. Magnesium is correlated with sea salt with some scatter. The scatter may result from noise due to analytical errors or atmospheric exchanges such as addition from dust. Similar to Cl^- and K^+, the majority of the samples (86% of the complete data set) are found between the 2 times enriched and 2 times depleted lines. However, unlike K^+, there appears to be a small net enrichment with 77% of all samples showing enrichment and 23% showing depletion. The enriched samples have an average enrichment factor of $Ef(Mg^{2+}) = 1.4$, while the depleted samples show an average enrichment factor of $Ef(Mg^{2+}) = 0.87$. There appears to be some evidence for the enrichment being at least partially correlated with sea salt based upon the fact that low Na^+ samples do not show increasing enrichment.

2.5.5 Calcium (Ca^{2+})

Figure 2.4d is the correlation plot of Ca^{2+} with respect to Na^+. Calcium is correlated with sea salt at high Na^+ (above 100 μM) and shows atmospheric enrichment at low Na^+ (below 100 μM). Almost all of the data below 100 μM Na^+ (91% of this subset) is found above the 2 times enriched line. In addition, a third of the samples below 100 μM are above the 10 times enriched line. At low Na^+ concentrations, the Ca^{2+} concentration becomes uncorrelated with sea salt and varies within a factor of ~5 above and below 1 μM. However, at high Na^+ concentration (above 100 μM), the Ca^{2+} data converges to the sea-salt dilution line. The addition of Ca^{2+} in these data appears to be uncorrelated with sea salt, and is very similar to the atmospheric enrichment model of Figure 2.1b.

2.5.6 Bromide (Br^-)

Figure 2.5a shows the correlation plot of Br^- as a function of Na^+. Thin FYI is generally correlated with sea salt, while the other environments show atmospheric exchanges below 1000 μM Na^+ and correlate with sea salt above 1000 μM Na^+. The data below 1000 μM Na^+ represents 68% of the total data set and half of these samples enriched and half are depleted. Overall, these samples at less than 1000 μM Na^+ appear weakly correlated with sea salt and appear dominated by atmospheric exchanges. The Br^- concentration reaches an asymptote at low Na^+ concentration that is within a factor of 5 of 0.1 μM. Data at high Na^+ concentration converge to the sea salt dilution line.

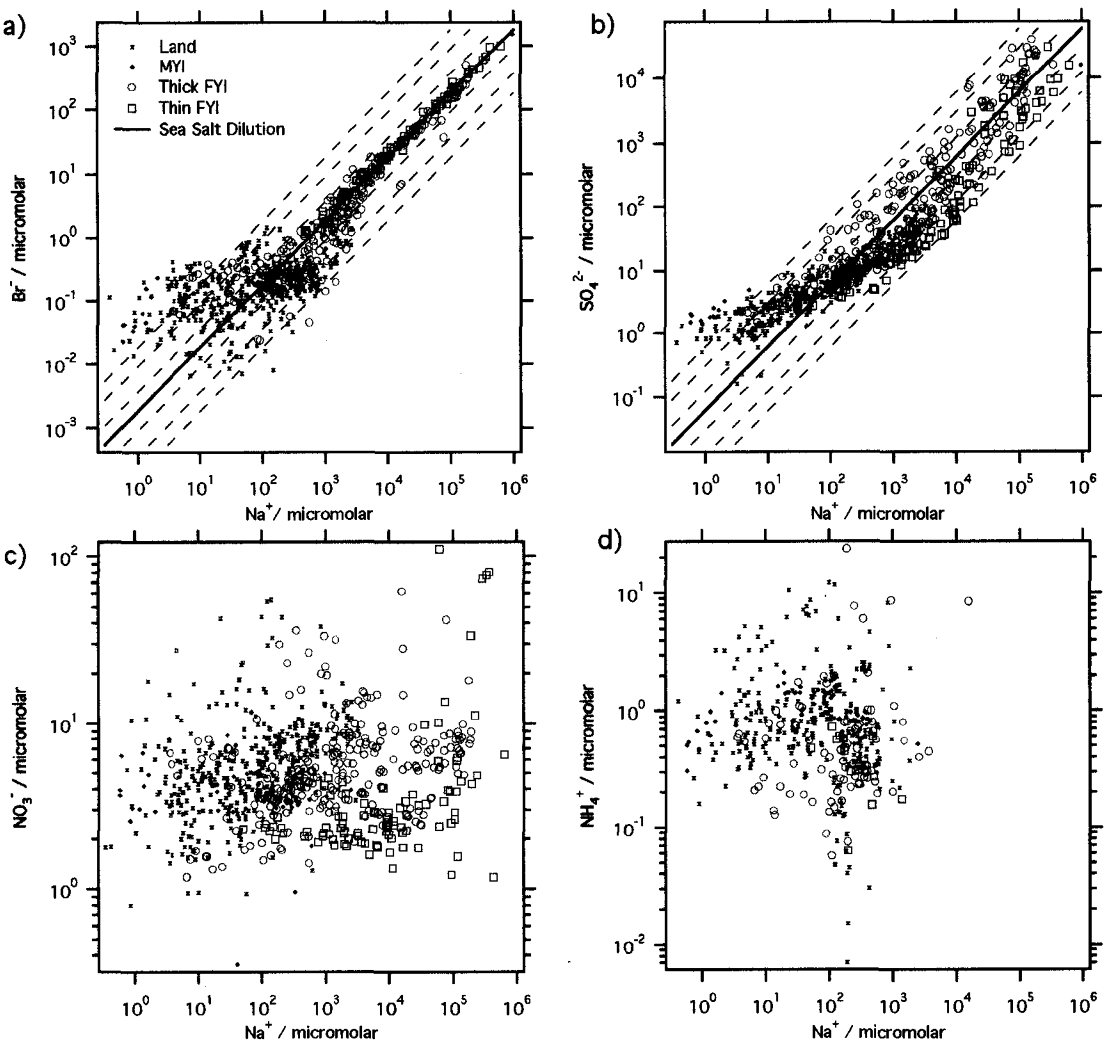

Figure 2.5 Correlation plots of bromine, SO_4^{2-}, NO_3^-, and NH_4^+ versus Na^+ concentrations with enrichment factor lines. Bromide and SO_4^{2-} have a seawater dilution line because they come from sea salt, while NO_3^- and NH_4^+ are not present in sea salt. Ammonium was not quantified at Na^+ concentrations higher 1000μM because the Na^+ peak was too wide and was not separated from NH_4^+.

2.5.7 Sulfate (SO_4^{2-})

Figure 2.5b shows SO_4^{2-} versus Na^+ in all environments. In contrast to all other ions, SO_4^{2-} shows enrichments and depletions at high Na^+ concentrations, above 1000 μM, probably from source fractionation. Most samples above 1000 μM belong to thin and thick FYI. There appears to be a difference between thick and thin FYI, with thin

FYI showing more depletion, while thicker FYI is more scattered across the sea salt dilution line. The majority of the thin FYI samples (84% of thin FYI samples having >1000 μM Na^+) are depleted as compared to 16% of the same subset that are enriched. In comparison, a thick FYI shows 60% of the samples having >1000 μM Na^+ are depleted as compared to 40% of the same subset that are enriched. Below 100 μM Na^+, SO_4^{2-} appears to reach an asymptote of approximately 1 μM.

2.5.8 Nitrate (NO_3^-) and Ammonium (NH_4^+)

Table 2.1 and Figures 2.5c and 2.4d show that NO_3^- and NH_4^+ are not correlated with sea salt. Because they are biologically utilized, the abundance of these two ions is variable and low in seawater; thus, the correlation plots do not show a seawater dilution line. The median concentration and ranges of each ion are in the same order of magnitude for all environments showing that both ions vary less than the sea-salt ions. Ammonium measurements are not available in highly saline samples (above 10,000 μM of Na^+), because the ratio of NH_4^+ to Na^+ concentration was too small to meet reliable analysis criterion.

2.6 Discussion

2.6.1 Sodium and chloride as sea-salt tracers

Sodium and Cl^- are good sea-salt tracers and can be used to track modifications to sea salt. Still, Na^+ and Cl^- are subject to modifications, and consideration of how these modifications affect the sea-salt tracer helps to weight the importance of these modifications. Chloride can be modified via acid displacement reactions, R2.1 [Finlayson-Pitts, 2003]. The observed enrichment in Figure 2.3a is due to the addition of hydrochloridic acid to sea salt Cl^- in snow. The effect of HCl addition to snow diminishes as the sea-salt tracer concentration increases. Below 1000 μM Na^+ most samples are within a factor of 2 from sea salt concentration and they get closer to seawater concentration at higher Na^+ concentrations (above 1000 μM Na^+), indicating that Cl^- is generally a good sea-salt tracer except for snow of very low marine influence.

Sodium can be modified via mirabilite ($NaSO_2 \bullet 6H_2O$) precipitation. Mirabilite precipitation removes SO_4^{2-} and Na^+, but because there is much more Na^+ than SO_4^{2-} (16.6:1, molar ratio), if all SO_4^{2-} is removed via mirabilite precipitation, only a 13% of the sea salt Na^+ is lost [Rankin and Wolff, 2002]. If we were to represent a 13% depletion in Na^+ as one of the dashed lines in Figure 2.4a, it would be a 1.1 times enriched line which is difficult to differ from the sea water dilution line in a log-log plot. Therefore, mirabilite precipitation is not a large modifier of Na^+, and Na^+ can be a good sea-salt tracer for log-log plots. The same way depletion occurs via mirabilite precipitation, Na^+ enrichment could originate from addition of the precipitated mirabilite crystals to snow. However, these effects appear small and we can use either Na^+ or Cl^- as a good proxy for sea salt influence. We generally use Na^+ as the tracer, but have found that for anions, Cl^- is a lower noise tracer and will use Cl^- in some interpretation plots.

2.6.2 Ions correlated with seawater: Potassium and Magnesium

Magnesium and K^+ are correlated with seawater and show some values that we attribute to noise and possible addition from dust. The lack of net enrichment in the case of K^+ appears to indicate that noise or weak source fractionation is responsible for its variations. The small net enrichment of Mg^{2+} appears to argue for a small non-sea-salt source like dust. However, this addition might be at least partially correlated with sea salt as evidenced by the lack of a plateau at the lowest Na^+ concentrations that is seen in Ca^{2+}, Br^-, and SO_4^{2-}. Source fractionation of Mg^{2+} and K^+ can occur through precipitation that becomes thermodynamically favorable at temperatures below -34°C. According to our field notes the air temperature ranged from -10°C to -30°C for all three campaigns, thus precipitation of Mg^{2+} and K^+ was not favored. However, it could be that the conditions for precipitation of Mg^{2+} and K^+ were met at earlier times before sample collection. Therefore, we cannot rule out that source fractionation for Mg^{2+} and K^+

occurs in the snow. In any case, any modifications from sea salt composition are fairly small for these ions.

2.6.3 Ion affected by atmospheric addition: Calcium

Sea-salt Ca^{2+} is the predominant Ca^{2+} source in snow samples with Na^+ concentrations above 100 μM and dust sources dominate the total amount of Ca^{2+} in snow samples below 100 μM of Na^+. Calcium addition from dust sources is significant at low Na^+ concentrations when a small addition carries more influence as compared to the same small addition to a highly concentrated sample. Dust sources normally contain both Ca^{2+} and Mg^{2+}, but the Mg^{2+} correlation plot is better correlated with sea salt at low Na^+ than the Ca^{2+} plot. One reason for this effect is that there is about 5 times more Mg^{2+} in sea water than Ca^{2+}, allowing enrichments in Ca^{2+} to be observed more easily over a lower sea salt "background". The enriched snow appears to reach an asymptotic Ca^{2+} concentration of around 1.7 μM. We obtained this value from the average of the nss-Ca^{2+} concentration (Equation 2.2) in enriched snow at Na^+ concentrations below 100 μM. Figure 2.6 contains a solid line that describes the overall pattern of Ca^{2+}. If the dust source had this magnitude of Mg^{2+}, the correlation plot should have shown it at low Na^+ concentration (see Figure 2.4c), therefore, it appears that the dust source has less Mg^{2+} than Ca^{2+} on a molar basis.

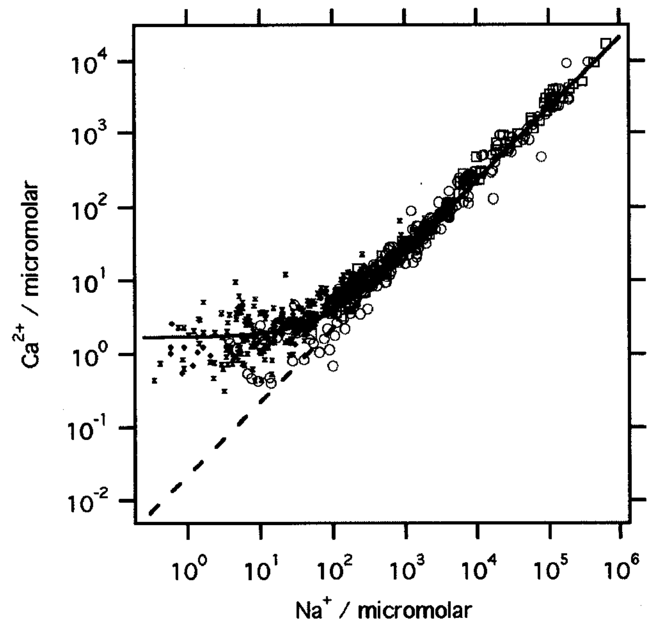

Figure 2.6 Calcium modification models shown on a correlation plot of Ca^{2+} versus Na^+. The solid line represents the expected behavior for Ca^{2+}. The curvature at low Na^+ concentrations is the product of dust sources adding nss-Ca^{2+} to snow. As the sea-salt tracer concentration increases, nss-Ca^{2+} influences are not significant and sea-salt Ca^{2+} dominates the total amount of Ca^{2+}.

2.6.4 Ion affected by atmospheric addition and removal: Bromide

Snow can be a source and sink of Br^- via heterogeneous reactions that take part in halogen activation chemistry. As Br^- is removed from the snow (a source of atmospheric Br), the atmosphere transports the reactive bromine species (bromine atoms and BrO) farther from their removal site. This reactive bromine can react with aldehydes, HO_2, and VOCs to form HBr, which is ultimately returned to the snow pack. The addition of HBr to snow with low sea-salt Br^- concentration results in enrichments and the removal due to activation results in depletions. However, it is likely that the same snow has been subject to removal and addition of Br^- throughout time, which tends to cloud the overall picture of snow Br^- exchanges with the atmosphere enriched and depleted samples below 1000 μM of sea-salt tracer. However, at the lowest sea salt tracer concentrations, we expect that atmospheric addition dominates over removal. We calculated the average of the minimum concentration range to be 0.2 μM using the nss-Br^- calculation (Equation 2.2).

Figure 2.7 solid line shows the expected behavior when nss-Br^- is added to snow with low Br^- concentrations. The depleted samples below 1000 μM of Cl^- are found in the range of the minimum Br^- concentration and when considering nss-Br^- calculation result in negative values. Depletions below 1000 μM indicate that this snow served as a source of Br^- to the atmosphere and that the added HBr is not enough to result in positive nss-Br^-.

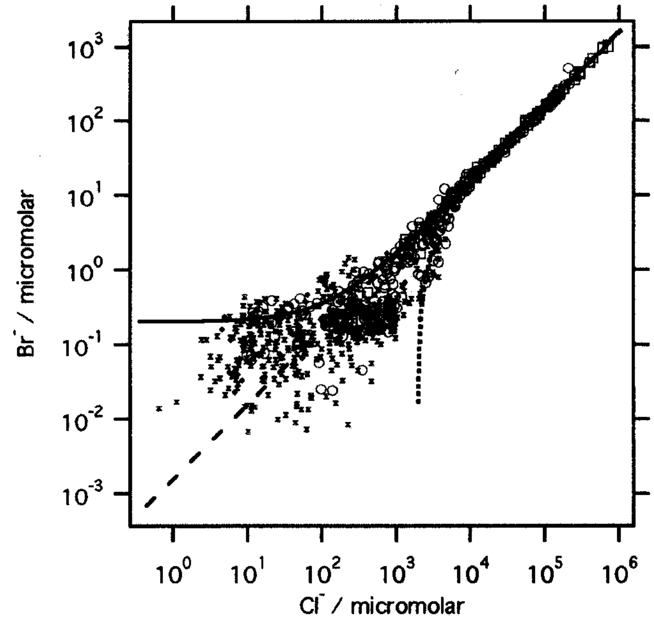

Figure 2.7 Bromine modification models shown on a correlation plot of Br^- versus Cl^-. The Br^- atmospheric addition solid line shows that snow is a sink of nss-Br^- from halogen chemistry. The dotted line represents snow that has lost Br^- and is a source of active bromine species. We plotted versus Cl^- to show that both Na^+ and Cl^- are good sea-salt tracers and can reproduce the same results about modifications to sea salt.

Samples in the range from about 100 to 1000 μM of Cl^- appear to be depleted with little enrichment because at this Br^- concentrations small additions of nss-Br^- are not significant. Because a mix of exchanges between the snow and atmosphere clouds the overall picture of Br^- modifications, we estimate that the maximum removal of Br^- from snow that is observable on a log-log plot is 3 μM. The dotted line in Figure 2.7 represents the removal of Br^-, and most of the samples lie between the enrichment and depletion models shown in this figure.

2.6.5 Ion affected by all modification mechanisms: Sulfate

At low Cl^- concentrations, all environments show the same modification pattern for SO_4^{2-}, atmospheric addition (see Figure 2.8). Arctic haze and other phenomena may be responsible for SO_4^{2-} addition into the snow pack as sulfuric acid (H_2SO_4) or ammonium sulfate ($(NH_4)_2SO_4$) [Shaw, 1995]. The addition found at Cl^- concentrations less than 100 μM was calculated by averaging nss-SO_4^{2-} concentration in all enriched samples less than 100 μM, resulting in an asymptotic concentration of around 1.7 μM.

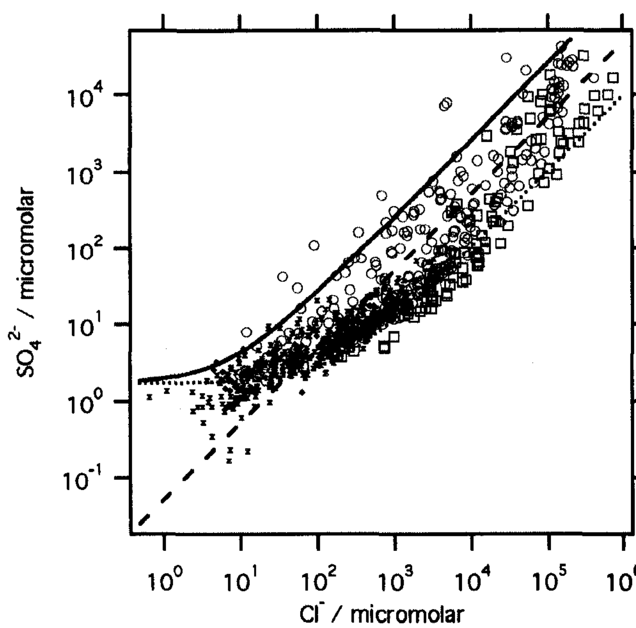

Figure 2.8 Sulfate fractionation models shown on a correlation plot of SO_4^{2-} versus Cl^-. Both dashed and solid lines are enriched at low sea-salt tracer concentrations indicating addition from non-sea-salt sources. The dashed line represents source fractionation, which is present in all environments indicating that the main source of SO_4^{2-} into snow is depleted. The solid line represents source fractionation that results in enrichment, which was unique to first-year sea ice. We plotted versus Cl^- to show that both Na^+ and Cl^- are good sea-salt tracers and can reproduce the same results about modifications to sea salt.

At high Cl^- concentrations, SO_4^{2-} demonstrates source fractionation as shown in figure 2.8 by two approximately limiting models that are shown by dotted and solid lines.

Limiting cases of enrichment and depletion appear to be roughly factors of 5 above and below the sea salt dilution line (see figure 2.8). Sea-salt SO_4^{2-} depletion occurs when Na^+ and SO_4^{2-} precipitate as $Na_2SO_4{\bullet}10H_2O$ (mirabilite), which is thermodynamically favored below -8°C. The mirabilite precipitate separates from the brine that contained sea-salt SO_4^{2-} resulting in SO_4^{2-}-depleted brine. This SO_4^{2-}-depleted brine can migrate upward to the snow pack surface and result in the observed SO_4^{2-} depletions in surface snow.

Thin-FYI samples are more depleted in SO_4^{2-} than thick-FYI samples. A possible explanation for this finding is that in young FYI, mirabilite precipitates and the brine that wicks up to surface snow is generally depleted in SO_4^{2-}. As the snow on FYI ages, wind may mix up snow layers and scour regions of the sea ice that have little snow cover. This mixing process could bring up mirabilite crystals to the surface of the snow pack, where they could enrich SO_4^{2-} in our surface snow samples. The fact that both MYI and land samples, which lack brine wicking as a possible ion transport mechanism, generally show depletions in their most Na^+ concentrated samples appears to indicate that aerosol arising from sea salts is generally depleted in SO_4^{2-}, as has been observed by Rankin and Wolff [2003].

2.6.6 Ions uncorrelated with sea salt: Nitrate (NO_3^-) and Ammonium (NH_4^+)

Nitrate and ammonium (NO_3^- and NH_4^+) are essentially absent in seawater and thus are not correlated with sea salt. The range of concentrations in NO_3^- and NH_4^+ show little variability (see Table 2.1). It appears that sources of NO_3^- and NH_4^+ into the snow pack are more constant than sea salt over the region that covers all sampled environments and that NO_3^- and NH_4^+ transport similarly to all these environments. We speculate that episodes of Arctic haze can spread over a wide area and add similar amounts of NO_3^- to surface snow, which agrees with the presence of nss-SO_4^{2-} in all environments.

Figure 2.9 shows NO_3^- as a function of nss-SO_4^{2-}. Because both NO_3^- and non-sea-salt SO_4^{2-} are anthropogenic pollutants, one might expect that they would be correlated, and past aerosol and snow studies have found reasonable correlations between these two quantities [Joranger and Semb, 1989; Toom-Sauntry and Barrie, 2002; Yalcin et al., 2006]. However, the correlation we find in these data is very weak. The solid lines represent the range of ratios between NO_3^- and nss-SO_4^{2-} that encompass most of our data and the dashed line the models from Toom-Sauntry and Barrie [2002]. Our range for NO_3^- to nss-SO_4^{2-} (0.9 – 9) is roughly an order of magnitude higher than that reported by Toom-Sauntry and Barrie [2002] for snow (0.2 – 0.6) when compared to aerosol ratios (0.05 – 0.18), the snow ratios indicated to the authors that snow more efficiently scavenged gaseous NO_3^- compounds than gaseous SO_4^{2-} compounds from the atmosphere. Our snow NO_3^- to nss-SO_4^{2-} ratios are much higher than Toom-Sauntry and Barrie [2002], which could indicate stronger NO_3^- sources for our pollution. Alternatively, we have demonstrated that SO_4^{2-} is fractionated at the source, leading often to SO_4^{2-} depletion in the aerosols and negative initial nss-SO_4 values. If our environment has a larger influence of SO_4^{2-}-depleted brine, the nss-SO_4^{2-} values would be decreased, increasing the slope of the NO_3^- to nss-SO_4^{2-} correlation.

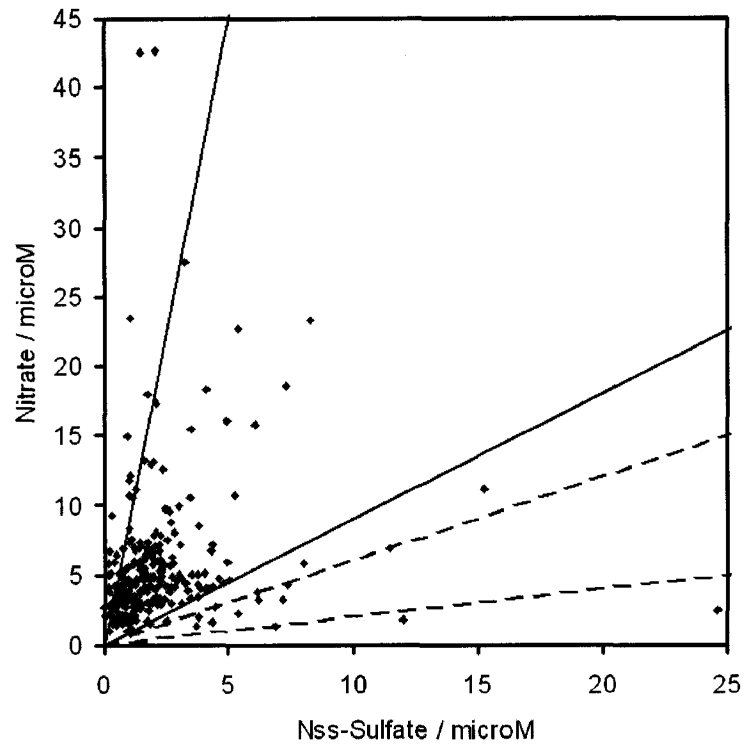

Figure 2.9 Nitrate as a function of nss-SO_4^{2-}. The solid lines are the range of our data NO_3^- to nss-SO_4^{2-} ratio, (0.9 – 9) and the dashed lines are Toom-Sauntry and Barrie [2002] ratios (0.2 – 0.6) in snow.

2.6.7 Ionic abundances in snow in relation to atmospheric species

The abundance of certain ions in snow can be compared to the atmospheric abundance of related compounds to provide information on the role of snow as a source or sink of species in the atmosphere. We consider the values obtained from the interpreted correlation plots in previous sections that referred to atmospheric exchanges and utilize them to calculate a time-integrated flux. A flux is the molecules per area per time that are emitted or deposited into the snow pack. If we consider the integral of a flux over time, we get the unit of molecules per area, which is the column density if the exchange simply went to a fixed atmospheric column directly above the snow, and if we assume a height of the atmospheric column, we can calculate the atmospheric concentration produced. Because the air moves and transports these species horizontally, we cannot directly relate these time-integrated fluxes to atmospheric column densities or concentrations. However, we sampled Arctic environments that represent a good portion of the Arctic terrain. Therefore, we expect that the average exchanges are order-of-magnitude estimates. For conversion between snow concentrations modification and time-integrated fluxes we consider the atmosphere to be a well-mixed column of 1 km height, and the portion of the snow pack undergoing exchange to be 3 cm deep and have a density of 0.33 g/cm^3. The water-equivalent height of the exchanging snow pack is 1 cm under the conditions above and we assume the air molecular density to be 3×10^{19} $molecules/cm^3$. Considering that the atmosphere and snow pack height can change by an order of magnitude, each of these estimates is expected to be accurate to an order of magnitude.

Calcium exhibits atmospheric addition that we interpret to be from crustal sources. From the correlation plot of Ca^{2+} (Figure 2.6) we approximated the influence of these crustal sources to add an average of 1.7 μM of Ca^{2+} to snow. Using the assumptions discussed above, we calculate the equivalent atmospheric concentration of aerosol-particle-bound Ca^{2+} to be 0.7 $\mu g/m^3$. The calculated Ca^{2+} is an order of magnitude larger than observations of aerosol particle Ca^{2+} concentration which at Alert is ~0.046 $\mu g/m^3$ [Kawamura et al., 2007] and at Ny Ålesund is ~0.032 $\mu g/m^3$ [Teinilä et al., 2003]. The difference between observations of aerosol and snow Ca^{2+} concentrations could be because different sources of dust bring Ca^{2+} to different parts of the Arctic. Many of our Ca^{2+}-enriched samples are from inland are as in Alaska near the Brooks mountain range, while Alert lies at higher latitudes in the Arctic and Ny Ålesund experiences more marine conditions due to persistent nearby open water.

Interpretation of the Br^- correlation plot, Figure 2.7, provided an approximation of the maximum atmospheric removal of Br^- from the snow to be 3 μM (section 2.6.4) and of maximum addition of Br^- to be 0.2 μM. Again, using the above assumptions, we obtain a maximum addition of 40 pptv atmospheric bromine added the snow pack surface and a maximum removal of 600 pptv of atmospheric bromine leaving the snow. The addition of bromine to the snow pack is in reasonable agreement with observations of BrO that indicate levels around 50 pptv [Wagner et al., 2001; Höenninger and Platt, 2002]. The maximal removal from snow is an order of magnitude larger than typical atmospheric abundances, which might indicate that some limited regions of relatively saline snow produce large amounts of reactive bromine that then spread over wider geographic regions, resulting in lower observed mixing ratios. Many of these samples that show decreases in bromide concentration are from samples taken from the sea ice, particularly the more saline FYI, which is in agreement with the idea that snow on FYI is a source of reactive bromine [Simpson et al., 2007b]. It is also possible that, if frost flowers produce large amounts of sea-salt aerosol, this aerosol could release reactive bromine before depositing to the snow pack. This deposition of concentrated and bromide depleted sea salt to snow would then appear in our samples as Br^- depleted snow.

Sulfate at low Na^+ concentrations shows atmospheric addition from sources other than sea salt. This SO_4^{2-} addition was approximated to be 1.4 μM from Figure 2.7 in section 2.6.5. Using the same considerations as discussed above, the equivalent aerosol SO_4^{2-} concentration is 1.3 μg/m^3. This concentration is in agreement with observations of nss-SO_4^{2-} at Alert (1 - 2 μg/m^3) [AMAP, 1998], which is in agreement with the idea that Arctic Haze can add SO_4^{2-} from non-sea-salt sources to the snow pack. At high Na^+ concentrations there are SO_4^{2-} enrichments and depletions that are not explained by atmospheric fluxes, and thus we interpret them as source fractionation of SO_4^{2-} through mirabilite precipitation and sea ice formation processes as explained in section 2.6.5.

2.7 Conclusions

Correlation plots of major ions in snow with respect to sea-salt tracers show unique modification patterns for each ion. The modification pattern's shape depends on how the ion is affected by source fractionation and atmospheric exchanges. Potassium and Mg^{2+} are comparable to the values observed in sea salt, and Ca^{2+} is observably enhanced by dust sources. Atmospheric aerosol Ca^{2+} concentrations appear to be in reasonable agreement with snow enhancements. Bromide is affected by atmospheric exchanges that both remove and add Br^- through reactive bromine chemistry. The magnitude of bromine's time-integrated atmospheric exchange fluxes is reasonably accounted for by atmospheric abundances. Maximal depletion of bromine from snow is roughly an order of magnitude larger than maximal enhancement, indicating that bromine may be sourced from limited geographic regions, and the resulting atmospheric bromine is deposited over wider geographic regions. Sulfate modifications suggested that SO_4^{2-}-depleted brine is the main source of SO_4^{2-} for surface snow and that SO_4^{2-}-enriched brine is unique to first-year sea ice. Addition of non-sea-salt SO_4^{2-} at atmospheric aerosol abundances accounts for enrichment of SO_4^{2-} in surface snow that is observed at low sea salt tracer abundance. These observations provide valuable insight about the chemical composition of surface snow and snow-air interactions.

2.7 References

AMAP (1998). AMAP Assessment Report: Arctic Pollution Issues, Arctic Monitoring and Assessment Programme (AMAP), Oslo, Norway, IX, 627-630.

Aristarain, A. J. and R. J. Delmas (2002), Snow chemistry measurements of James Ross Island (Antarctic Peninsula) showing sea-salt aerosol modifications, ***Atmos. Env., 36***, 765-772.

Barrie, L. A., Bottenheim, J. W., Schnell, R. C., Crutzen, P. J., and Rasmussen, R. A. (1988), Ozone destruction and photochemical reactions at polar sunrise in the lower Arctic atmophere, ***Nature, 334***, 138-141.

Benassai, S., S. Becagli, R. Graganani, O. Magand, M. Proposito, I. Fattori, R. Traversi, R. Udisti (2005), Sea-spray deposition in Antarctic coastal and plateau areas from ITASE traverses, ***Annals of Glaciology, vol. 41***, 32.

Bottenheim, J. W., L. Barrie, E. Atlas, L. E. Heidt, H. Niki, R. A. Rasmussen and P. B. Shepson (1990), Depletion of lower tropospheric ozone during Arctic spring: The Polar Sunrise Experiment 1988, ***J. Geophys. Res., vol. 95***, no. D11, 18,555-18,568.

Davidson, C. I., J. R. Harrington, M. J. Stephenson, M. J. Small, F. P. Boscoe, and R. E. Gandley (1989), Seasonal variations in sulfate, nitrate and chloride in the Greenland ice sheet: relation to atmospheric concentrations, ***Atmos. Env., vol. 23***, no. 11, 2483-2493.

de Caritat, P., G. Hall, S. Gislason, W. Belsey, M. Braun, N. I. Goloubeva, H. K. Olsen, J. O. Scheie, J. E. Vaive (2005), Chemical composition of arctic snow: concentration levels and regional distribution of major elements, ***Science of the Total Environment, 336***, 183-199.

Dominé, F. and P. B. Shepson (2002), Air-Snow interactions and atmospheric chemistry, ***Science vol. 297***, 1506.

Dominé, F., R. Sparapani, A. Ianniello, and H. J. Beine (2004), The origin of sea salt in snow on Arctic sea ice and in coastal regions, ***Atmos. Chem. Phys., 4***, 2259-2271.

Fan, SM. and Jacob, D. J. (1992), Surface ozone depletion in Arctic spring sustained by bromine reactions on aerosols, ***Nature, vol. 359***, 522-524.

Finlayson-Pitts, B. J. (2003), The tropospheric chemistry of sea salt: a molecular-level view of the chemistry of NaCl and NaBr, ***Chem. Rev., 103***, 4801.

Gragnani, R., C. Smiraglia, B. Stenni, and S. Torgini (2002), Chemical and isotopic profiles from snow pits and shallow firn cores on Campbell Glacier, northern Victoria Land, Antarctica, ***Annals of Glaciology, vol. X***, 679.

Höenninger, G., and U. Platt (2002), Observations of BrO and its vertical distribution during surface ozone depletion at Alert, ***Atmos. Env.***, ***36***, 2481-2490.

Joranger, E. and A. Semb (1989), Major ions and scavenging of sulphate in the Norwegian Arctic, ***Atmos. Env., vol. 23***, no. 11, 2463-2469.

Kawamura, K., M. Narukawa, S.-M. Ling and L. A. Barrie (2007), Size distribution of dicarboxylic acids and inorganic ions in atmospheric aerosols collected during polar sunrise in the Canadian high Arctic, ***J. Geophys. Res., 112***, D10307, doi:10.1029/2006JD008244.

Khalizov, A. F., B. Viswanathat, P. Larregaray and P. A. Ariya (2003), A theoretical study on the reactions of Hg with halogens: atmospheric implications, ***J. Phys. Chem., 107***, 6360-6365, doi:10.1021/jp0350722.

Li., S. M, and L. A. Barrie (1993), Biogenic sulphur aerosol in the Arctic troposphere: I. Contributions to sulphate, ***J. Geophys. Res., 98D***, 20613-20622.

Lindberg, S., S. Brooks, C.-J. Lin, K. J. Scott, M. S. Landis, R. K. Stevens, M. Goodsite, A. Richter (2002), Dynamic oxidation of gaseous mercury in the Arctic troposphere at Polar Sunrise, ***Environ. Sci. Technol., 36***, 1245-1256.

McConnell, J. C., Henderson, G. S., Barrie, L., Bottenheim, J., Nili, H., Langford, C. H., and Templeton, E. M. J. (1992), Photochemical bromine production implicated in Arctic boundary-layer ozone depletion, ***Nature***, ***355***, 150-152.

Nikus, U. (2003), Ion content of the snowpack on Franz Josef Land, Russia, ***Arctic, Antarctic and Alpine Research, vol. 35***, no. 3, 399-408.

Platt, U. and G. Hönninger (2003), The role of halogen species in the troposphere, ***Chemosphere, 52***, 325-338.

Quimby-Hunt, M. S. and Turekian, K. K. (1983), Distribution of Elements in Sea Water, *Eos, vol. 64*, No. 14, 130-132.

Rankin, A. M., Auld, V., and Wolff, E. W. (2000), Frost flower as a source of fractionated sea salt aerosol in the polar regions, *Geophys. Res. Lett.*, *27* (21), 3469-3472.

Rankin, A. M. and Wolff, E. W. (2002), Frost flowers: Implications for tropospheric chemistry and ice core interpretation, *J. Geophys. Res.*, *107* (D23), 4683, doi:10.1029/2002JD002492.

Rankin, A. M. and Wolff, E. W. (2003), A year-long record of size-segregated aerosol composition at Halley, Antartica, *J. Geophys. Res.*, *108* (D24), 4775, doi:10.1029/2003JD003993.

Sander, R., J. Burrows and L. Kaleschke (2006), Carbonate precipitation in brine – a potential trigger for tropospheric ozone depletion events, *Atmos. Chem. Phys., 6*, 4653-4658.

Schröeder, W. H. and J. Munthe (1998), Atmospheric mercury-An overview, *Atmos. Env.*, *32*, 809-822.

Shaw, G. E., The Arctic haze phenomenon (1995), *Bulletin American Meteorological Society, 76*, 2403-2413.

Simpson, W. R., Alvarez-Aviles, L., Douglas, T. A., Sturm, M., and Dominé, F. (2005), Halogen in the coastal snow pack near Barrow Alaska: Evidence for active bromine air-snow chemistry during springtime, *Geophys. Res. Lett.*, *32*, L04811, doi:10.1029/2004GL021748.

Simpson, W. R., R. von Glasow, K. Riedel, P. Anderson, P. Ariya, J. Bottenheim, J. Burrows, L. Carpenter, U. Frieß, M. E. Goodsite, D. Heard, M. Hutterli, H.-W. Jacobi, L. Kaleschke, B. Neff, J. Plane, U. Platt, A. Richter, H. Roscoe, R. Sander, P. Shepson, J. Sodeau, A. Steffen, T. Wagner, E. Wolff (2007a), Halogens and their role in polar boundary-layer ozone depletion, *Atmos. Chem. Phys., 7*, 4375-4418.

Simpson, W. R., D. Carlson, G. Hoenninger, T. A. Douglas, M. Sturm, D. K. Perovich, and U. Platt (2007b), The Dependence of Arctic Tropospheric Halogen Chemistry on Sea Ice Conditions, ***Atmos. Chem. Phys., 7***, 621 – 627, doi: 10.1029/2004GL022132.

Tang, T. and McConnell, J. C. (1996), Autocatalytic release of bromine from Arctic snow pack during polar sunrise, ***Geophys. Res. Lett.***, ***23***, 2633-2636.

Teinilä, K., R. Hillamo, V.-M. Kerminen, and H. J. Beine (2003), Aerosol chemistry during the NICE dark and light campaigns, ***Atmos. Env., 37***, 563-575.

Toom-Sauntry, D. and L. A. Barrie (2002), Chemical composition of snowfall in the high Arctic: 1990-1994, ***Atmos. Env., 36,*** 2683-2693.

Udisti, R., S. Begagli, E. Castellano, R. Traversi, S. Vermigli, and G. Piccardi (1999), Sea-spray and marine biogenic seasonal contribution to snow composition at Terra Nova Bay, Antarctica, ***Annals of Glaciology, vol. 29***, 77.

Vogt, R., P. J. Crutzen, and R. Sander (1996), A mechanism for halogen release from sea salt aerosol in the romote marine boundary layer, ***Nature, 338,*** 327-330.

Wagner, T., Leue, C., Wenig, M., Pfeilstcker, K., and Platt, U. (2001), Spatial and temporal distribution of enriched boundary layer BrO concentrations measured by the GOME instrument aboard ERS-2, ***J. Geophys. Res.***, ***106*** (D20), 24,225 – 24,235.

Wang, Z. and S. O. Pehkonen (2004), Oxidation of elemental mercury by aqueous bromine: atmospheric implications, ***Atmos. Env., 38,*** 3675-3688.

Yalcin, K., C. P. Wake, J. E. Dibb and S. I. Whitlow (2006), Relations between aerosol and snow chemistry at King Col, Mt. Logan Massif, Yukon Canada, ***Atmos. Env., 40,*** 7152-7163.

Chapter 3. Frost flower chemical composition during growth and its implications for aerosol production and bromine activation[2]

3.1 Abstract

Frost flowers have been proposed to be the major source of sea-salt aerosol to the atmosphere during polar winter and a source of reactive bromine during polar springtime. However, little is known about their bulk chemical composition or microstructure, two important factors that may affect their ability to produce aerosols and provide chemically reactive surfaces for exchange with the atmosphere. Therefore, we chemically analyzed 28 samples of frost flowers and parts of frost flowers collected from sea ice off of northern Alaska. Our results support the proposed mechanism for frost flower growth that suggests water vapor deposition forms an ice skeleton that wicks brine present on newly grown sea ice. We measured a high variability in sulfate enrichment factors (with respect to chloride) in frost flowers and seawater from the vicinity of freezing sea ice. The variability in sulfate indicates that mirabilite precipitation ($Na_2SO_4 \cdot 10\ H_2O$) occurs during frost flower growth. Brine wicked up by frost flowers is typically sulfate depleted, in agreement with the theory that frost flowers are related to sulfate-depleted aerosol observed in Antarctica. The bromide enrichment factors we measured in frost flowers are within error of seawater composition, constraining the direct reactive losses of bromide from frost flowers. We combined the chemical composition measurements with temperature observations to create a conceptual model of possible scenarios for frost flower microstructure development.

3.2 Introduction

Frost flowers are vapor-deposited ice crystals that wick brine from the sea-ice surface and thus they contain high bulk salinities. Early studies of frost flowers focused

[2] Alvarez-Aviles, L., W. R. Simpson, T. A. Douglas, M. Sturm, D. Perovich, F. Dominé (2008), Frost flower chemical composition during growth and its implications for aerosol production and bromine activation, J. Geophys. Res., in press.

on their physical properties and the sea ice environment where they form [Perovich and Richter-Menge, 1994]. Laboratory experiments investigated the temperature dependence of frost flower growth and the infrared emission of frost flowers [Martin et al., 1995; 1996]. Frost flowers may be responsible for a significant fraction of the salt aerosol available during winter and spring in polar regions [Rankin et al., 2000; Rankin and Wolff, 2002; 2003], and have also been proposed to be a source of reactive bromine to the Polar lower atmosphere [Rankin and Wolff, 2002, Kaleschke et al., 2004; Jones et al., 2006]. However, due to difficulties in locating and collecting frost flowers, only a few studies have observed their chemical composition, and often with small sample numbers [Rankin et al., 2000; Rankin and Wolff, 2002 and 2003; Simpson et al., 2005; Douglas et al., 2005; Kalnajs and Avallone, 2006].

3.2.1 Impacts of frost flowers on atmospheric chemistry

Due to their formation in the polar regions and their potential for mediating exchange between the atmosphere and sea ice surface, frost flowers may play a major role in the tropospheric chemistry of polar regions during the winter. It is widely established that aerosol particles provide sites for heterogeneous chemistry and at the same time, they transport with the wind, dispersing chemical constituents far from their original source [Wagenbach et al., 1998; Ianniello et al., 2002; Rankin and Wolff, 2003]. Possible sea-salt aerosol sources include ocean spray, blowing of snow containing sea salts, and frost flowers [Dominé et al., 2004]. Aerosol particle generation from frost flowers, or the brine that surrounds them, could explain events of high salt loading in winter months, when young sea ice (nilas) replaces open water near coastal sampling sites [Rankin et al., 2000]. In a year-long study of size segregated aerosol compositions at Halley, Antarctica, Rankin and Wolff [2003] estimated that at least 60% of the total sea salt arriving at Halley is from brine and frost flowers on the sea ice surface rather than from sea spray sourced from open water. The primary evidence that brine and/or frost flowers are a source of sea-salt aerosol is that aerosol SO_4^{2-} is depleted with respect to Cl^- in comparison to seawater [Rankin et al., 2000; Rankin and Wolff, 2002]. In this paper, we concentrate on the chemical composition of frost flowers, brine, and seawater, and we use these measurements to make constraints on the role of frost flowers in aerosol particle formation.

Chemical models indicate that gas-phase bromine forms when Br^- present in ice reacts with HOBr to release Br_2 that is in turn photolyzed to produce bromine atoms [Fan and Jacob, 1992; McConnell et al., 1992; Tang and McConnell, 1996; von Glasow and Crutzen, 2007; Simpson et al., 2007a]. Frost flowers could promote Br^- activation if HOBr reacted with Br^- in frost flowers. Or, frost flowers could release aerosols containing Br^- that react with HOBr. Bromine monoxide, BrO, forms from the reaction of gas-phase bromine atoms and ozone. The catalytic reactions of bromine atoms and BrO result in episodes of almost total destruction of tropospheric ozone [Barrie et al., 1988]. The origin and formation of BrO-enriched air masses during tropospheric ozone destruction events are not yet fully understood. Satellite observations of BrO spatially match air masses rich in BrO with potential frost flower (PFF) formation sites [Kaleschke et al., 2004]. However, ground-based observations of BrO at Barrow, Alaska find no correlation between BrO and potential frost flowers, but show good correlation between BrO and first-year sea-ice contact [Simpson et al., 2007b]. In this paper, we present observations of bromide in frost flowers to consider their possible role in halogen activation.

3.2.2 Frost flower growth process

Figure 3.1 shows a model of the frost flower growth process. This figure was made by combining our field observations from three years of field campaigns on the sea ice north of Barrow, Alaska with proposed mechanisms of frost flower growth [Perovich and Richter-Menge, 1994; Rankin and Wolff, 2002]. The age stages of formation, keyed to the panels in Figure 3.1, are (i) growth of small (0.5 cm) nodules (ice bumps, as described in Perovich and Richter-Menge [1994]) on the nilas (newly formed sea ice) surface, (ii) growth of young frost flowers on the nodules, and (iii) further growth and cooling into mature frost flowers. Panel (iv) represents other ice crystals that are common where frost flowers grow or are found in close proximity, as described later. Brine, cryo-concentrated salt solutions, is present on the surface of the nilas because the salts are rejected from the freezing ice lattice. Most brine sinks, but some is forced to the surface [Richardson, 1976]. Wicking of brine is indicated in Figure 3.1 by arrows in the upward position from brine on the sea-ice surface towards the frost flower ice-skeleton, in panel (ii) and (iii).

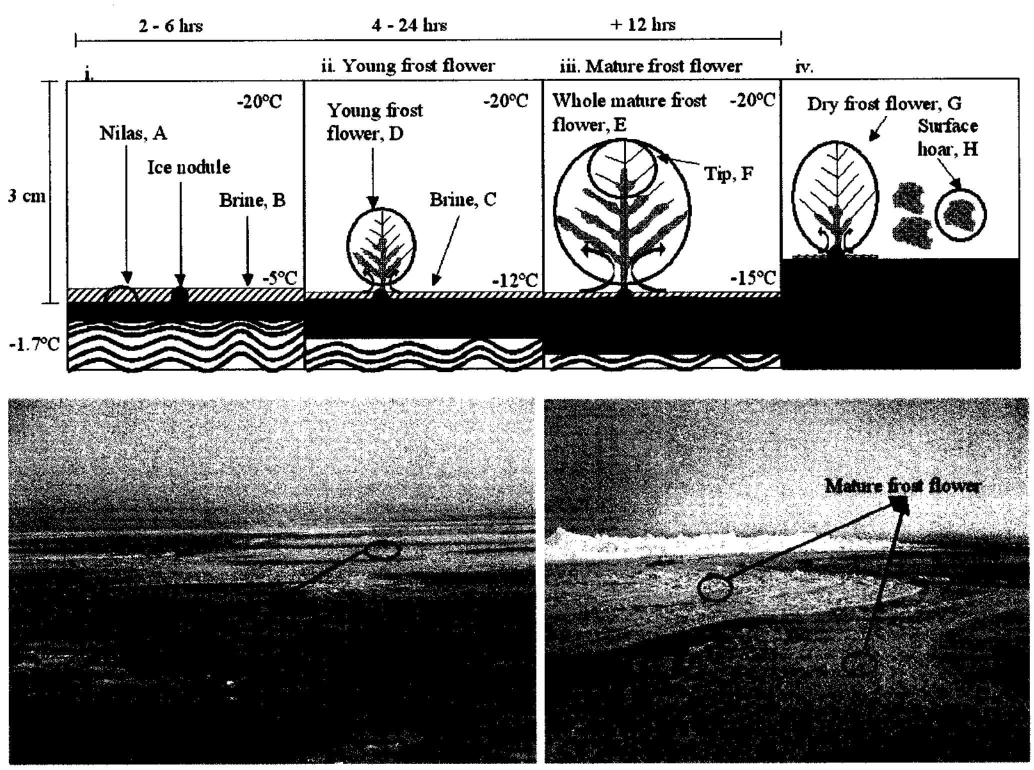

Figure 3.1 A conceptual model of frost flower growth. The first three panels represent life stages of frost flower growth: (i) Nilas and ice nodules, (ii) Young frost flowers, and (iii) Mature frost flowers. Panel (iv) represents different environments that are physically close to or related to the frost flower growth process, like "dry" frost flowers (*i.e.* frost flowers that do not have as much brine available to wick) and surface hoar. These types are predominantly comprised of water vapor condensed as ice. The circles represent the types of samples collected from the field. All black lines and black shaded areas indicate ice and blue lines or blue shaded areas are brine or snow. The photographs at the bottom illustrate different frost flower growth environments.

The large temperature gradient between seawater (~ -1.7°C) and ambient air above the water surface (~ -20°C in these cases) leads to water vapor supersaturation with respect to ice [Andreas et al., 2002]. The supersaturated vapor in the air condenses as ice onto the nodules. The source of water vapor at the warm brine/ice surface and rapid growth on a limited number of nucleation points on the surface leads to Mullins-Sekerka growth instabilities [Mullins and Sekerka, 1963], explaining the dendritic crystal shapes. Over the course of a few hours, the sea ice grows thicker and the ice surface temperature drops, causing two things to occur: first, brine on the sea ice surface is drawn up onto the frost flower by capillary forces raising their bulk salinity. Second, the brine cools and salts begin to precipitate based on the temperature at which they exceed saturation; however, slow nucleation dynamics may allow for some degree of supersaturation on short timescales.

When the supersaturated salts nucleate, these precipitation processes modify the chemical composition of the frost flowers and residual brine. At -8°C Na^+ and SO_4^{2-} are thermodynamically predicted to precipitate as mirabilite ($Na_2SO_4 \bullet 10\ H_2O$). Hydrohalite ($NaCl \bullet 2\ H_2O$) does not crystallize from the brine until temperatures are below -22°C. Magnesium (Mg^{2+}) and potassium (K^+) do not precipitate until below -34°C, as $MgCl_2 \bullet 6\ H_2O$ and $KCl \bullet 6\ H_2O$. However, it is important to remember that there is a large temperature gradient in the vicinity of frost flowers, so the flowers themselves are typically warmer than the overlying air. Martin et al. [1996] observed that frost flower tips are 4-6°C warmer than the air temperature, and their IR emission temperature is 12-16°C warmer than the air temperatures, depending upon actual conditions. Therefore, although the air temperature often may go below the -22°C threshold for hydrohalite precipitation, it is less common that frost flowers growing on thin ice cool to temperatures where hydrohalite and Mg^{2+} and K^+ precipitate.

The main purpose of this paper is to propose a conceptual model of the chemical fractionation processes that occur during frost flower growth. We present results from chemical analyses of frost flowers and their components at various life stages of their growth to support our conceptual model. We also consider the chemical composition of frost flowers and their possible role in bromine activation and aerosol production in the lower troposphere.

3.3 Methods

3.3.1 Sample collection

We collected frost flowers near Barrow Alaska, from an active open lead (71.43° N, 156.47° W) located approximately 3 km from Point Barrow during springtime, on 25 March and 1 April 2005. Some of the samples were collected from newly formed ice by the edge of the lead, some were collected from a floating slab that came close to the ice edge. Other samples were collected in the same lead from a boat, and include nilas and very young frost flowers. Air temperatures were stable at around -22°C during both of these sampling events. Ages or growth stages of frost flowers were estimated in reference to the growth scheme described in the introduction. Seawater was sampled at this time and in later years by submerging a polypropylene sampling vial in water either near the sea ice edge or through a hole chopped through the ice. All samples were transported and stored frozen and away from light until analysis about 5 months later. Samples were collected facing into the wind following clean protocols with powder-free gloves and Tyvek suits. To collect frost flower tips, we used tweezers and for brine on sea ice we used a cleaned glass eyedropper. When sampling whole frost flowers, we collected them with the edge of the polypropylene sampling vial. All sampling vials and tools were cleaned in the laboratory using 18.2 MΩ cm water and were transported to the site packed in 1-gallon Ziploc bags.

3.3.2 Analytical Procedures

We weighed the sampling vials, 50 mL polypropylene centrifuge tubes, prior to sampling, and after melting the sample to obtain the mass of the sample. The samples were then diluted by adding ultrapure water until the conductivity of the sample indicated it was in the proper analytical range. The volume of ultrapure water added divided by the mass of the frost flower sample constituted a dilution factor that was later used to back-calculate the samples' total salinity. Major anions (F^-, Cl^-, Br^-, SO_4^{2-}, and NO_3^-) were measured using an Ion Chromatograph (Dionex ICS-2000), using a Dionex AS17 separation column. Standards were made using analytical grade reagents with ion ratios designed to mimic the sample matrix and were verified by commercial standards (Dionex).

We use enrichment factors (*Ef*) to compare the ionic concentration ratios we measured in our samples to the values in standard seawater from Quimby-Hunt and Turekian [1983]. For example, the enrichment factor with respect to chloride for a given ion, X, is defined by:

$$Ef(X) = \frac{\left(\frac{[X]}{[Cl^-]}\right)_{Sample}}{\left(\frac{[X]}{[Cl^-]}\right)_{Seawater}}. \tag{3.1}$$

Here, Ef(X) is the ion enrichment factor, [X] is the ion concentration in moles per liter, and [Cl^-] is the chloride concentration in moles per liter. Chloride is chosen as the reference instead of the more traditional Na^+ for a number of reasons. First, Cl^- is analyzed in the same chromatograph as the other anions; so fewer possible error sources enter into the measurement. Second, Na^+ is partially removed when mirabilite precipitates thus making it a poorer reference than Cl^-, which is not removed until hydrohalite precipitates at temperatures below -22C. Third, for aerosol or snow samples, addition or removal of Cl^- by atmospheric processes make it a poorer tracer than Na^+ (which does not undergo volatilization reactions). However, mass-balance considerations, discussed further below, indicate that frost flowers contain orders of magnitude more Cl^- than can be affected by relatively weaker atmospheric chlorine fluxes. Therefore, Cl^- is an appropriate tracer of sea-salt content in these samples. We also performed analysis using either Na^+ or Mg^{2+} as the sea salt tracer and find completely consistent results but slightly poorer measurement precision and small systematic deviations consistent with mirabilite depletion in the case of using Na^+ as the sea-salt tracer.

A statistical analysis was performed to quantify uncertainties in the measured enrichment factors. We find that the relative standard deviation (RSD = standard deviation / mean) of the analyzed enrichment factors for bromide is 0.02, and for sulfate is 0.07, which was mostly due to variability between differing IC analysis days with less variability on individual days. These RSD values correspond to precisions of the analysis of enrichment factors for each ion.

We use the chloride concentration to calculate the total salt mass fraction, or bulk salinity, and to compare the salt content in the samples. The bulk salinity is calculated from the Cl^- measurement via:

$$\boldsymbol{S} = \frac{[Cl^-] \times \boldsymbol{DF} \times \boldsymbol{MW}_{Cl}}{\boldsymbol{MF}(Cl)_{Seawater}}. \tag{3.2}$$

In this equation, $\boldsymbol{S}$ is the salinity (g salt per g of frost flower), $[Cl^-]$ is the Cl^- concentration (moles per liter), $\boldsymbol{DF}$ is the dilution factor (liters of diluted solution per gram of frost flowers), $\boldsymbol{MW}_{Cl}$ is the molecular mass of Cl^- (35.453 g/mol), and $\boldsymbol{MF}(Cl^-)_{Seawater}$ is the mass fraction of Cl^- in standard sea water (0.553 g(Cl^-)/g(sea salt) [Quimby-Hunt and Turekain, 1983]). This calculation yields the bulk salinity as a mass fraction in grams of salt per gram of frost flower, and is multiplied by 1000 to present the results in parts per thousand by weight (‰). We note that precipitation reactions modify the composition of the brine, for instance, complete removal and separation of mirabilite would remove ~10% of the salt mass. However, none of our samples are completely sulfate depleted, indicating that this effect causes <10% error in calculation of bulk salinity from Cl^- abundance.

3.4 Results

The enrichment factors (Ef) for Br^- and SO_4^{2-} and the calculated salinity values of sea ice processed seawater samples are shown in Table 3.1. The term "sea-ice processed seawater" refers to ocean water that has been in contact with forming and melting sea ice. There are seven samples of sea-ice processed seawater: one from 2004, from a hole cut in the sea ice; one from 2005, from the lead edge and five from 2007, from holes on the sea ice. Table 2 shows enrichment factors for Br^- and SO_4^{2-} and the calculated salinity values of frost flowers and their components. The sample letters in Table 3.2 correspond to the letters and circles in Figure 3.1. There are 28 samples of different types of frost flower components: six samples correspond to forming sea ice or brine, six are young frost flowers, 10 are mature frost flowers, two are tips of mature frost flowers, two are dry frost flowers, and two are surface hoar.

3.4.1 Sea-ice processed seawater

In this study, enrichment factors and salinity values are calculated with respect to standard seawater, equation (3.1). We collected seawater samples on the sea ice from different sites with the original purpose of quality assurance of our ion chromatographic analyses. However, through replicate analyses of these samples we find that some are significantly different from standard seawater (see Table 3.1). We found that salinity in the sea-ice processed seawater samples is variable and below that of standard sea water, with a range of more than a factor of two. This effect is expected because of sea ice freezing dynamics, which separates ice from brine. Brine that is more concentrated than the underlying sea water sinks, leaving a fresher surface layer. The Ef(Br^-) is close to unity (standard seawater ratio) while Ef(SO_4^{2-}) shows enrichment at low salinity values and approaches unity as the salinity increases towards that of standard seawater (35‰). Samples that originate from holes in the sea ice seem to have higher salinity values while the ones from the lead edge have the lowest salinity values and the greatest SO_4^{2-} enrichment. After observing that our sea-ice processed seawater samples show enrichment factors different from that of standard seawater we called these samples sea-ice processed seawater to make a clear distinction from standard sea water.

Table 3.1 Sea-ice processed seawater Br^- and SO_4^{2-} enrichment factors (Ef), and salinity values. In the case of replicate analysis, the value in the parenthesis is the standard deviation. For samples that have more than 1 analyses of the same sample (N), we report the average of the enrichment factors.

Site	Ef (Br^-)	Ef(SO_4^{2-})	Salinity (‰)	N
Lead edge (2005)	1.00 (± 0.04)	2.11 (± 0.08)	15.3 (± 0.7)	9
Hole on sea ice (2007)	1.00 (± 0.03)	1.40 (± 0.05)	17.7 (± 0.6)	23
Hole on sea ice (2007)	1.06 (± 0.01)	1.02 (± 0.01)	25.7 (± 0.2)	3
Hole on sea ice (2007)	0.95	1.00	35.6	1
Hole on sea ice (2007)	1.01	1.02	27.4	1
Hole on sea ice (2007)	1.01	1.01	27.5	1
Hole on sea ice (2004)	1.09	0.93	32.6	1

3.4.2 Bulk salinity of frost flowers

Bulk salinity of the samples in the frost-flower environment range from 16‰ for nilas to 107‰ for mature whole frost flowers. The high variability in bulk salinity where frost flowers form has been previously reported [Perovich and Richter-Menge, 1994; Rankin et al., 2000] and is attributable to the thermodynamics of sea ice and frost flower formation processes. As sea ice freezes, the new ice, nilas, contains nearly pure ice and brine channels that contain concentrated brine, some of which drains out of the ice, decreasing the bulk salinity, as observed in our nilas samples (type A in Table 3.2 and referring to the type from Figure 3.1). The brine fractionated to the surface is concentrated with respect to ocean water, and as the ice thickens and brine channels constrict (removing water), one would expect the sea-ice surface brine salinity to increase. This effect is exhibited by our salinity measurements, where the brine salinity on 1 cm thick nilas (type B), is ~36 ‰, and increases as the ice ages and thickens to ~4 cm thick nilas, where the brine (type C) salinity averages ~75 ‰. Frost flower samples are generally, but not always, enriched in bulk salinity as compared to ocean water. For young frost flowers, all samples are more saline than seawater with an average bulk salinity of ~75 ‰. Bulk salinity of mature frost flowers (type E) range from 16 to 105 ‰, and the average is 62 ‰, which is comparable to our young frost flower samples. The mature frost flower tips (type F) show lower bulk salinity, ~16‰, than standard seawater. These bulk salinity measurements show that the tips possess more vapor deposited ice and/or less brine than whole mature frost flowers (type E). Dry frost flower samples, which appear dry because they have wicked less brine, (type G) show low bulk salinity values, 16 and 25 ‰, compared to standard ocean water. The surface hoar samples (type H) have the lowest salinity values, 2 ‰. As opposed to frost flowers, surface hoar crystals have no brine source from underlying sea ice, and their salinity may be a result of incorporation of sea-salt aerosols, sea spray, or atmospheric gases (e.g. H_2SO_4 or HCl) during their growth.

Table 3.2 Salinity values, SO_4^{2-} and Br^- enrichment factors in frost flowers, brine and surface hoar in different life stages of frost flower growth.

Sample	Description	Salinity (‰)	Ef(Br^-)	Ef(SO_4^{2-})
A	Nilas (ice and surface brine)	16	0.98	1.03
		23	0.98	1.03
B	Brine on 1 cm thick nilas	38	0.96	1.01
		35	0.96	1.02
C	Brine on moving slab	80	0.96	1.04
		69	0.97	1.05
D	Young whole frost flower	96	0.98	0.88
		91	0.98	0.96
		87	0.97	1.05
		49	0.97	1.08
		46	0.97	1.08
		81	0.98	1.12
E	Mature whole frost flower	107	0.98	0.35
		85	0.98	0.35
		106	0.98	0.82
		16	0.96	0.92
		22	0.96	0.92
		94	0.97	0.94
		94	0.98	0.97
		20	0.96	0.98
		24	0.96	0.99
		58	0.98	1.43
F	Mature frost flower tip	17	0.97	0.78
		14	0.97	0.89
G	Mature dry whole frost flower	26	0.97	0.8
		16	0.98	0.91
H	Surface hoar	2	0.30	0.66
		2	0.56	0.66

3.4.3 Sulfate enrichment factor of frost flowers

Temperature changes and nucleation dynamics at different frost flower growth stages dictate if precipitation processes are to occur. Fairly young (1 to 2 hours old) samples that have not yet cooled below -8C (temperature at the sampling point – e.g. the nilas) likely do not contain mirabilite crystals and would be expected to have enrichment factors near unity. Sample types A-C all show this behavior, with the SO_4^{2-} enrichment factor range in nilas and brine comparable to unity. Because the brine and mirabilite crystals probably wick differently up frost flowers, we expect that the sulfate enrichment factor will show variability, and in fact there is a high variability of Ef(SO_4^{2-}) between different types of frost flowers and even for the same types. Of the six young frost flower samples (type D),. four have a small enrichment and the other two have a small depletion. Nine of ten mature frost flower samples (type E) are depleted in sulfate, with two depleted down to Ef(SO_4^{2-}) = 0.35. The two mature flower tip samples show moderate depletion, Ef(SO_4^{2-}) = 0.89 and 0.78. The two dry frost flower samples (type G) show moderate depletion with Ef(SO_4^{2-}) = 0.91 and 0.80. The surface hoar samples are depleted, with both samples showing Ef(SO_4^{2-}) = 0.66.

3.4.4 Bromide enrichment factor of frost flowers

The Br^- enrichment factors for all the frost flower components we collected range from 0.96 to 0.98 while the two surface hoar samples yield values of 0.30 and 0.56. According to our statistical analysis for Br^-, the RSD of the Ef(Br^-) has a 1-σ precision of 0.02 (this includes day-to-day variability). Thus, it is evident that the Ef(Br^-) does not vary among any of the components that make up frost flowers or among young or old frost flowers. This findings stands in contrast to the high variability of Ef(SO_4^{2-}) we measured. Although there appears to be a slight depletion of ~3 % in all samples, this apparent depletion is not variable and is not dependent on the sample age. Therefore, we expect that analytical uncertainties in the instrument calibration account for this small deviation from unity. Taken in total, our analysis shows that none of the brine-sourced frost flowers or related samples are significantly depleted in Br^-. The surface hoar samples are the only samples that show a considerable depletion in Br^-. Variability of Br^- in snow and a lack of depletion or enrichment in frost flowers has been previously reported [Simpson et al., 2005], although they reported the results from only a few frost flower samples.

3.5 Discussion

Physical and chemical processes involved in frost flower growth govern where salts are stored on the frost flower ice crystals. In the following sections, we discuss sulfate and bromide enrichment factors and their implication in aerosol formation and bromine activation in the atmosphere and synthesize the results from our detailed chemical analysis into a conceptual model of frost flower growth and microstructure.

3.5.1 Sea-ice processed seawater

Frost flowers and brine on the sea-ice surface form from seawater that is available; therefore at early stages of frost flower growth they mostly reflect the chemical composition of the seawater from which they originated. Some of our sea-ice processed seawater samples, particularly ones characterized by low salinity, show Ef(SO_4^{2-}) different than standard seawater. Figure 3.2 shows Ef(Br^-) and Ef(SO_4^{2-}) versus salinity for the sea-ice processed seawater samples. Figure 3.2 reinforces what Table 3.1 summarizes: Ef(Br^-) is close to unity with no apparent trend in salinity, and Ef(SO_4^{2-}) shows greater enrichment at low salinity and is comparable to standard seawater as salinity increases. Based on what is presented in Figure 3.3 the SO_4^{2-} enrichment in low salinity samples could be attributable to mixing mirabilite precipitate on the surface of young sea ice with seawater. As mirabilite crystallizes on the sea-ice surface and the sea ice cracks, the mirabilite crystals can mix with seawater that is being diluted by the incorporation of broken sea ice or forming crystals (frazil ice). Salts present in seawater can be diluted when sea ice melts and other processes that add fresh water to seawater altering the salinity, [Comiso et al., 2003]. Adding mirabilite to seawater adds SO_4^{2-}, thereby increasing Ef(SO_4^{2-}). If the water is fresher than standard seawater, it would float on top of the denser sea water, and would have been measured by our surface water sample. If this sulfate-enriched sea-ice processed seawater were to be involved in new nilas formation that formed frost flowers, there could be some degree of SO_4^{2-} enrichment in the initially formed nilas and frost flowers.

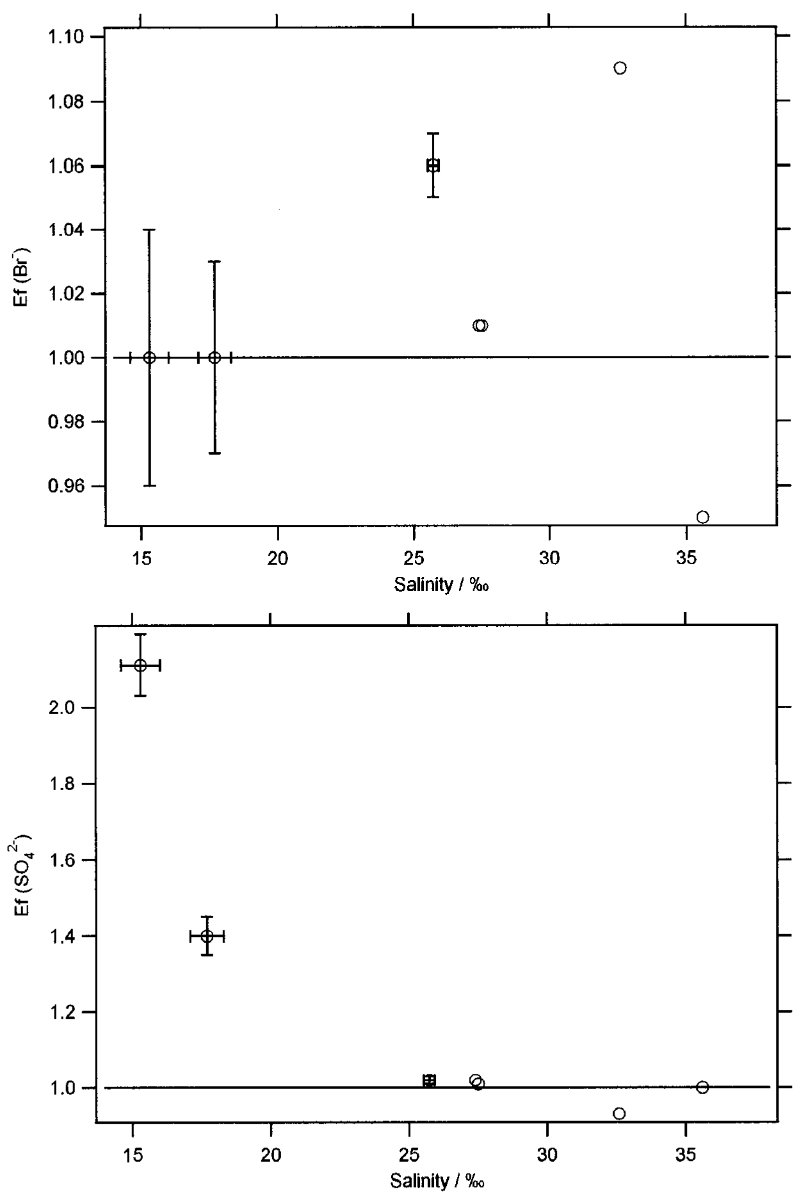

Figure 3.2 Bromide and SO_4^{2-} enrichment factors as a function of Arctic seawater salinity (in parts per thousand, ‰).

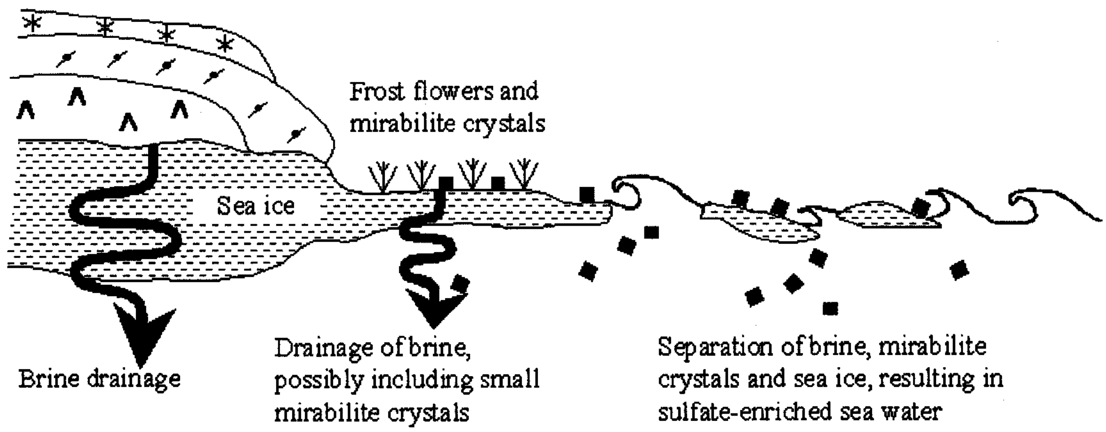

Figure 3.3 A schematic diagram of sea-ice processed seawater formation. The left portion of the figure shows frost flowers on nilas in the presence of mirabilite precipitate (red squares), and sea salt migration upward and downward through channels in the sea ice (arrows). As mirabilite forms the fractionated brine is separated from the mirabilite precipitate. The separation of fractionated brine and mirabilite precipitate occurs when the fractionated brine migrates or drains away from the nilas area. The right portion of the figure shows an opening on the sea ice where surface brine drains into the ocean. If this sample contains mirabilite, and ice, they will melt when in contact with warmer seawater, resulting in less saline, sulfate enriched sea-ice processed seawater that will float on the denser normal seawater.

3.5.2 Salinity of frost flowers

The bulk salinity of frost flowers provides important constraints on their growth mechanism and resulting microstructure. Our salinity findings are similar to what was previously reported by Perovich and Richter-Menge [1994] who found that as the temperature of the environment in which the frost flowers form decreases, the bulk salinity of the frost flowers increases. Our observation that the tips of frost flowers are of lower bulk salinity than the frost flowers as a whole is in agreement with the idea that the dendritic tips of frost flowers grow by rapid vapor condensation or that brine has not yet wicked to this point. Dominé et al. [2005] observed that the morphology of frost flower tips was consistent with rapid vapor deposition. These observations indicate that frost flowers grow largely by vapor deposition of ice to form a "skeleton" that defines the overall macroscopic morphology followed by brine wicking that provides salts.

Temperature affects frost flower skeletal morphology, as noted in Martin et al. [1996]. Other evidence that the skeleton formation is not related to the presence of brine is that frost flowers grow on freshwater ice [Dominé et al., 2005; Gosnell, 2005].

The frost flowers become saline by wicking brine from the young sea-ice surface. The bulk salinity of frost flowers (~50–100 ‰) and the ambient temperatures of the environment in which they form (approximately -10°C, at the frost flowers base) locate frost flowers in a two-phase region of the phase diagram for sea ice [Weeks and Ackley, 1982]. The composition and temperature indicate roughly equal parts of ice and brine. For this reason, we present the conceptual picture of the frost flower macrostructure shown in Figure 3.4, left panel.

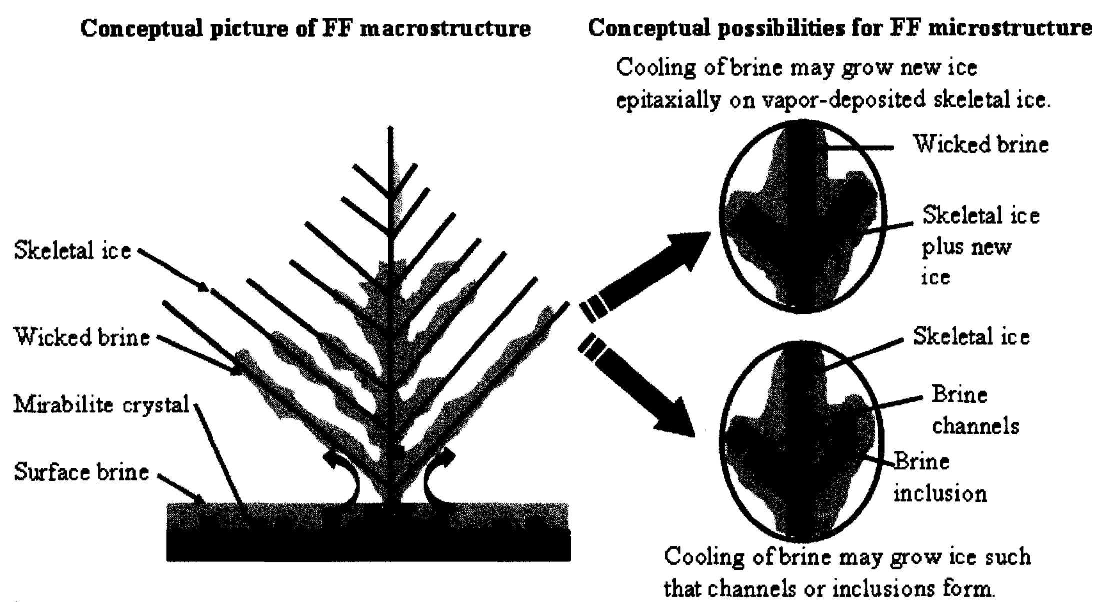

Figure 3.4 A conceptual model of possible macro- and micro- structures involved in frost flower growth and the related chemical separation. The tips of the frost flowers are shown as not yet wetted by brine and they are primarily vapor-deposited "skeletal ice". The ice surface is covered with brine that cools and precipitates mirabilite crystals, leading to wicked brine that is depleted in sulfate. The ice-sea salt phase diagram indicates that frost flowers are two or more phase systems (ice, brine, and precipitate), but the microstructure of the ice is unknown. Skeletal ice may grow as the brine cools (right top), or ice may overgrow brine forming pockets and channels (right bottom).

The microstructure of frost flowers is not well defined by the bulk measurements presented here, but we can identify two limiting cases, as shown in the right panel of Figure 3.4. In the first case, brine is assumed to be present only on the outside of an ice skeleton, and in the second case, brine inclusions or channels also form in the ice lattice. The photomicrographs presented in Dominé et al. [2005] appear to show that at least some brine is present on the surface and rounds the angular forms of the vapor-deposited ice skeleton. As frost flowers cool, the sea ice phase diagram [Weeks and Ackley, 1982] shows that the brine becomes more concentrated as water molecules add to existing ice or form new ice. Depending on the morphology of the frost flower ice skeleton and the availability of brine, all or some of the frost flower surface area is likely to be wetted by brine. The composition of brine is a function of temperature, as predicted by the phase diagram, and not a function of the bulk salinity. Higher bulk salinity simply indicates a higher fraction of brine than ice. Therefore, if we consider a hypothetical frost flower fully wetted by brine, its surface composition is that of the brine, while measuring its bulk composition will yield the proportion of skeletal ice to wicked brine. On the other hand, if freezing brine within frost flowers leads to the growth of inclusions or channels, included brine may not be available on the frost flower surface. Formation of channels could cause pressurization and pumping of brine could occur, as it does when bulk sea ice freezes. The microstructural details of this process are unclear at this point and should be further studied.

3.5.3 Sulfate in frost flowers

The sea ice phase diagram is useful when considering the chemical composition of frost flowers. Unfortunately, the thermodynamics expressed in the phase diagram are most useful for closed systems, and frost flowers, sea ice, and all of the samples considered here are not closed systems because we only collected parts of the complete system. Specifically, liquid brine is more mobile than ice or precipitates, thus brine wicking is likely to be associated with salts that have a different composition than seawater once precipitation occurs. Sea ice samples show salinity deviations from seawater (ice–salt separation), but as long as they are warmer than -8°C, no mirabilite precipitation should occur. Therefore, nilas and sea-ice surface brine at early stages should have SO_4^{2-} enrichment factors near their seawater source, in agreement with the observations of types A to C (Table 3.2 and Figure 3.1). As time advances and the temperature decreases below -8°C, mirabilite precipitation should become thermodynamically favorable. Some spatial regions within the frost flowers / ice-surface brine / sea-ice environment where mirabilite precipitation occurs could contain more (or less) mirabilite crystals than others and thus be enriched (or depleted) in SO_4^{2-}. Therefore, we interpret the variability in $Ef(SO_4^{2-})$ as evidence that our samples are from the spatial location of mirabilite precipitation and separation of mirabilite from SO_4^{2-} depleted brine.

Mirabilite is denser than brine (1.46 vs. about 1.08 g cm^{-3}, [Porter and Spiller, 1956; Dougherty, 2001]) so its crystals would sink and are expected to be less likely to be wicked up along with brines colder than -8°C. However, the fall velocity of a spherical $1 \mu m$ diameter mirabilite crystal [Light et al., 2003] through brine would be about 0.2 mm per hour (derived by application of the Stokes Law assuming a brine viscosity of 0.003 Pa s, which corresponds to 100‰ salinity) so that sedimentation may be too slow to lead to fractionation in all cases. Likewise, mirabilite may fail to nucleate even when it is supersaturated, so that SO_4^{2-} depletion would not always be observed, especially for young frost flowers. This slow rate of sedimentation is consistent with the observation that aged frost flowers are more depleted in SO_4^{2-} than younger frost flowers.

Our observations of SO_4^{2-} fractionation in frost flowers helps develop a conceptual model of frost flower growth and chemical fractionation, shown in Figure 3.4. Mirabilite crystals (red squares) are precipitated mostly in the sea-ice surface brine, and the brine that is wicked by the frost flower is SO_4^{2-} depleted. We can generally characterize our observations of SO_4^{2-} fractionation in the samples into classes of warmer samples, which are unfractionated or slightly enriched SO_4^{2-} and older, colder samples (e.g. older frost flowers or tips), which generally exhibit SO_4^{2-} depletion.

Sea-ice processed seawater can be a source of SO_4^{2-} enriched nilas and brine that is wicked by frost flowers. Enrichment in mature frost flowers is less likely to occur according to our observations, so our one highly enriched mature frost flower could be explained in multiple ways. First, while collecting the mature frost flowers it is possible that we accidentally sampled mirabilite from the brine at the base of the frost flowers. This brine contains mirabilite precipitate crystals that when added to the SO_4^{2-} depleted frost flower could result in SO_4^{2-} enrichment. We mentioned previously that as time advances, brine on the sea ice surface diminishes but mirabilite precipitate crystals left behind may be more available, and therefore, easier to collect. Second, as mirabilite precipitation occurs on the frost flower, external processes can remove the liquid brine leaving behind attached to the frost flower the mirabilite precipitate resulting in enhancement. External processes that remove liquid brine from the frost flower could include brine droplets being blown away from the frost flower, or the mechanical breakage of frost flower parts that have depleted brine around it. And third, if the brine from which the frost flowers originate is SO_4^{2-}-enriched due to sea-ice processed seawater, these frost flowers should show enrichment in SO_4^{2-}. Fourth, enrichment of sulfate could result from attachment of non-sea-salt sulfate (e.g. Arctic haze-derived sulfate); however, Toom-Sauntry and Barrie [2002] indicate that atmospheric addition to fresh snow typically adds on the order of 10 μM sulfate, which is undetectably small as compared to sea-salt sulfate in these samples (1,000 – 80,000 μM).

Frost flowers are believed to be a major source of sea salt aerosol [Rankin et al., 2000; Rankin and Wolff, 2002; 2003], but the mechanism by which frost flowers produce aerosol particles is not well established. Rankin and Wolff [2003] propose mechanical breakage of frost flowers as the aerosol source. However, our sampling of frost flowers shows that they are fairly mechanically rigid and appear difficult to fracture or break, at least on the macroscopic scale. This macrosocopic rigidity was also observed by Dominé et al. [2005]. Drying of frost flowers could increase their fragility and allow production of salt fragments. Another possible aerosol particle formation mechanism would be for brine to blow from the frost flower structure, producing aerosol directly from the brine.

An even more extreme mechanism might be if brine channels form, as discussed in section 4.3, pressurization of the channel could produce brine that might produce aerosol particles. If inclusions form, their partial freezing during the cooling of the frost flower would probably lead to ice/brine particle production, in a manner similar to the rime-splintering mechanism of Hallett and Mossop [1974] that was proposed to explain the formation of large numbers of ice particles in clouds.

It is useful to use the aerosol observations to consider the size of brine or frost flower fragments that would be needed to produce the observed aerosol particles. Rankin and Wolff [2003] reported that winter sea-salt aerosol particle diameters measured in Antarctica commonly range from 0.2 to 2 μm. To produce a dry salt aerosol particle of this size, the diameter of a 75‰-brine droplet is approximately 4 times larger than a dry aerosol particle. Thus, 0.2-2 μm salt aerosol particles would be the result of drying brine droplets on the order of 0.8 – 8 μm. Direct aerosol production by mechanical breakage of frost flowers would require similar sized fragments based upon the bulk composition of the frost flowers; however, it is quite likely that there is a great deal of heterogeneity in the chemical composition of frost flowers at the microscopic scale.

3.5.4 Bromide in frost flowers

Depletion of Br^- can occur when Br^- ions have been activated to gas-phase reactive bromine species. Field observations of snow samples have shown a significant number of snow samples are depleted in Br^-, which was taken as evidence of production of reactive bromine [Simpson et al., 2005]. Enrichment would result from the addition of Br^- through the termination step of reactive bromine chemistry, reaction of bromine atoms with VOCs, which produces HBr. Addition of Br^- through HBr could explain the enrichment in Br^- reported in aerosols [Barrie et al., 1988; Ianiello et al., 2002], in some snow pack samples [Simpson et al., 2005], and in model simulations [Sander et al., 2006].

We found that only the surface hoar collected close to frost flowers was significantly depleted in Br^-, but none of the frost flower samples or brine samples were significantly depleted or enriched in Br^-. These observations agree with the idea that salts in the surface hoar are likely to come from the atmosphere, while salts in all of the other samples come from the ocean via sea-ice processes. Douglas et al., [2008] proposed that surface hoar is an efficient mercury scavenger, thus it is likely that surface hoar is also an efficient sea-salt aerosol scavenger. Atmospheric salts are affected by bromine chemistry and aerosol formation mechanisms while the directly ocean-derived salts are primarily affected by precipitation reactions (e.g. mirabilite precipitation). The lack of Br^- depletion in frost flowers might imply they do not play a role in Br^- activation chemistry. However, a consideration of the bromine mass balance shows that significant atmospheric abundance of reactive bromine could be produced with small depletions of Br^- from the extremely saline frost flowers. Observed BrO levels near the ground could be as large as 50 pptv during ozone depletion events [Wagner et al., 2001, Höenninger and Platt, 2002]. If we assume 50 pptv of BrO for a 1 km high atmosphere column at -40°C, there are 2 x 10^{14} molecules/cm^2 of bromine. Frost flower salinities can be more than 100‰, which implies a Br^- concentration of approximately 3 x 10^{-3} moles per liter. For 1 cm high frost flowers with a density of 0.02 g/cm^3 [Dominé et al., 2005] there are 4 x 10^{16} molecules/cm^2 of Br^-. Thus, the frost flower column density is 200 times larger than the atmospheric column density value. As a consequence, for a frost flower to satisfy the total atmospheric budget of Br^- there has to be a 0.5% Br^- depletion in frost flowers. This 0.5% depletion is smaller than our measurement precision and thus is not detectable, yet it could significantly affect lower tropospheric halogen chemistry. This simple calculation ignores the fact that many airmasses do not have such a high BrO column density and that frost flowers do not cover the whole region below BrO events and thus should be taken to be only an order-of-magnitude estimate. However, it is still clear that frost flowers could release bromine in amounts that significantly affect the atmosphere while only changing Ef(Br) by small enough amounts to escape detection (a few percent). Our results constrain the bromine release budget from frost flowers better than any previous measurements and show that it is maximally on the order of atmospheric column abundances.

3.6 Conclusions

The bulk chemical analysis of numerous frost flowers and related samples presented here reinforces the previously proposed formation mechanism for frost flowers [Perovich and Richter-Menge, 1994; Rankin and Wolff, 2002]. In this mechanism, the bulk morphology is determined by vapor deposition of water in a supersaturated environment followed by wicking of brine up the ice skeleton. Consideration of the phase diagram for sea ice indicates that the structure of frost flowers is a multi-phase system with nearly pure ice, cryoconcentrated brine, and precipitate crystals. The brine has a composition controlled by the temperature and the mobility of brine, which allows separation of brine from ice and precipitates. However, the microstructure of the frost flowers remains unknown by our studies of bulk composition. This microstructure could be relatively simple, with a brine liquid layer coating an ice skeleton, or much more complex with brine channels or inclusions. The microstructure is critical to understanding chemical reactions on the surface of frost flowers because it controls the surface composition of reactants on the flowers. The observation of high variability in SO_4^{2-} enrichment factors is consistent with the frost flower / ice-surface brine / sea ice environment being the location where mirabilite crystals separate from SO_4^{2-}-depleted brine. Typically, younger, warmer samples have sulfate enrichment factors near unity, while older, colder samples appear depleted in sulfate. From this consideration, we support the argument that mirabilite crystals separate from brine that is SO_4^{2-}-depleted in this environment and that frost flowers may produce sulfate depleted aerosol through this mechanism. Clearly, field and laboratory measurements should be directed towards observations of aerosols produced from frost flowers. Bromide enrichment factors are essentially all unity, indicating no fractionation of Br^- in frost flowers, in agreement with previous observations [Rankin and Wolff 2002, Simpson et al., 2005]. While this observation appears to argue against frost flowers as a source of reactive bromine to the atmosphere, a mass balance shows that frost flowers contain a greater bromine pool than the typical lower atmospheric burden so they could still be a significant bromine source to the atmosphere.

3.7 Acknowledgements

This work was funded by the National Science Foundation Office of Polar Programs Arctic Sciences Section: Sturm, Douglas and Perovich (OPP-0435989) and Simpson (OPP-0435922). Alvarez-Aviles was supported by a DOE-GREF fellowship. The Barrow Arctic Science Consortium provided logistical support and their assistance is greatly appreciated. We thank Professor Hajo Eicken and his research group for insightful discussions on sea ice.

3.8 References

Andreas, E.L., Guest, P.S., Persson, P.O.G., Fairall, C.W., Horst, T.W., Moritz, R.E., and Semmer, S.R. (2002), Near-surface water vapor over polar sea ice is always near ice saturation, ***J. Geophys. Res., 107***(C10), doi: 10.1029/2000JC000411.

Barrie, L. A., Bottenheim, J. W., Schnell, R. C., Crutzen, P. J., and Rasmussen, R. A. (1988), Ozone destruction and photochemical reactions at polar sunrise in the lower Arctic atmophere, ***Nature, 334***, 138-141.

Comiso, J. C., J. Yang, S. Honjo, and R. A. Krishfield (2003), Detection of change in the Arctic using satellite and in situ data, ***J. Geophys. Res., 108*** (C12), 3384, doi:10.1029/2002JC001347.

Dominé, F., Sparapani, R., Ianniello, A., and Beine, H. J. (2004), The origin of sea salt in snow on Arctic sea ice and coastal regions, ***Atmospheric Chemistry and Physics, 4***, 2259-2271.

Dominé, F., Taillandier, A.-S., Simpson, W. R., and Severin, K. (2005), Specific surface area, density and microstructure of frost flowers, ***Geophys. Res. Lett., 32***, L13502, doi:10.1029/2005GL023245.

Dougherty, R.C. (2001), Density of salt solutions: effect of ions on the apparent density of water. ***J. Phys. Chem. B, 105***, 4515-4519.

Douglas, T., M. Sturm, W. Simpson, S. Brooks, S. Lindberg and D. Perovich (2005), Elevated mercury measured in snow and frost flowers near arctic sea ice leads, ***Geophys. Res. Lett., 32***(4), L04502, doi:10.1029/2004GL022132.

Douglas, T., M. Sturm, W. Simpson, S. Brooks, S. Lindberg and D. Perovich (2008), Influence of snow and ice crystal formation and accumulation on mercury deposition to the Arctic, ***Environ. Sci. Technol. 42***, 1542-1551.

Fan, SM. and Jacob, D. J. (1992), Surface ozone depletion in Arctic spring sustained by bromine reactions on aerosols, ***Nature, 359***, 522-524.

Gosnell, M. (2005), ***Ice: The nature, the history, and the uses of an astonishing substance***, Alfred A. Knopf, New York, USA.

Hallett, J. and Mossop, S. C. (1974), Production of secondary ice particles during the riming process, *Nature*, *249*, 26–28.

Hoenninger, G., and U. Platt (2002), Observations of BrO and its vertical distribution during surface ozone depletion at Alert, *Atmos. Env.*, *36*, 2481-2490.

Ianniello, A., Beine, H. J., Sparapani, R., Di Bari, F., Allegrini, I., and Fuentes, J. D. (2002), Denuder measurements of gas and aerosol species above Arctic snow surfaces at Alert 2000, *Atmospheric Environment*, *36*, 5299-5309.

Jones, A. E., P. S. Anderson, E. W. Wolff, J. Turner, A. M. Rankin, and S. R. Colwell (2006), A role for newly forming sea ice in springtime polar tropospheric ozone loss? Observational evidence from Halley station, Antarctica, *J. Geophys. Res., vol. 111*, D08306, doi:10.1029/2005JD006566.

Kaleschke, L., Richter, A., Burrows, J., Afe, O., Heygter, G., Notholt, J., Rankin, A. M., Roscoe, H. K., Hollowedel, J., Wagner, T., and Jacobi, H.-W. (2004), Frost flowers on sea ice as a source of sea salt and their influence on tropospheric halogen chemistry, *Geophys. Res. Lett.*, *31*, L16114, doi:10.1029/2004GL020655.

Kalnajs, L. E. and Avallone, L. M. (2006), Frost flower influence on springtime boundary-layer ozone depletion events and atmospheric bromine levels, *Geophys. Res. Lett.*, *33*, L10810, doi:10.1029/2006GL025809.

Light, B., G. A. Maykut, and T. C. Grenfell (2003), Effects of temperature on the microstructure of first-year Arctic sea ice, *J. Geophys. Res.*, 108(C2), 3051, doi:10.1029/2001JC000887.

Martin, S., Drucker, R, and Fort, M. (1995), A laboratory study of frost flower growth on the surface of young sea ice, *J. Geophys. Res.*, *100*, 7,027-7,036.

Martin, S., Yu, Y, and Drucker, R (1996), The temperature dependence of frost flower growth on laboratory sea ice and the effect of the flowers on infrared observations of the surface, *J. Geophys. Res., 101*, 12,111—12,125.

McConnell, J. C., Henderson, G. S., Barrie, L., Bottenheim, J., Nili, H., Langford, C. H., and Templeton, E. M. J. (1992), Photochemical bromine production implicated in Arctic boundary-layer ozone depletion, *Nature*, *355*, 150-152.

Mullins, W. W., and R. F. Sekerka (1963), Morphological stability of a particle growing by diffusion or heat flow, *J. Appl. Phys, 34*, 323-329.

Perovich, D. K. and Richter-Menge, J. A. (1994), Surface characteristics of lead ice, *J. Geophys. Res.*, *99*, 16,341-16,350.

Porter, M.W. and Spiller, R.C. (1956), *The barker index of crystals: a method for the identification of crystalline substances*, W. Heffer, Cambridge, UK.

Quimby-Hunt, M. S. and Turekian, K. K. (1983), Distribution of Elements in Sea Water, *Eos*, *64*, (14), 130-132.

Rankin, A. M., Auld, V., and Wolff, E. W. (2000), Frost flower as a source of fractionated sea salt aerosol in the polar regions, *Geophys. Res. Lett.*, *27* (21), 3469-3472.

Rankin, A. M. and Wolff, E. W. (2002), Frost flowers: Implications for tropospheric chemistry and ice core interpretation, *J. Geophys. Res.*, *107* (D23), 4683, doi:10.1029/2002JD002492.

Rankin, A. M. and Wolff, E. W. (2003), A year-long record of size-segregated aerosol composition at Halley, Antartica, *J. Geophys. Res.*, *108* (D24), 4775, doi:10.1029/2003JD003993.

Richardson, C. (1976), Phase relationship in sea ice as a function of temperature, *Journal of Glaciology*, *17* (77), 507-519.

Sander, R., Burrows, J., and Kaleschke, L. (2006), Carbonate precipitation in brine – a potential trigger for tropospheric ozone depletion events, Atmos. Chem. Phys., 6, 4653–4658, www.atmos-chem-phys.net/6/4653/2006/

Simpson, W. R., Alvarez-Aviles, L., Douglas, T. A., Sturm, M., and Dominé, F. (2005), Halogen in the coastal snow pack near Barrow Alaska: Evidence for active bromine air-snow chemistry during springtime, *Geophys. Res. Lett.*, *32*, L04811, doi:10.1029/2004GL021748.

Simpson, W. R., R. von Glasow, K. Riedel, P. Anderson, P. Ariya, J. Bottenheim, J. Burrows, L. Carpenter, U. Frieß, M. E. Goodsite, D. Heard, M. Hutterli, H.-W. Jacobi, L. Kaleschke, B. Neff, J. Plane, U. Platt, A. Richter, H. Roscoe, R. Sander, P. Shepson, J. Sodeau, A. Steffen, T. Wagner, E. Wolff (2007a), Halogens and their role in polar boundary-layer ozone depletion, ***Atmos. Chem. Phys., 7***, 4375-4418.

Simpson, W. R., D. Carlson, G. Hoenninger, T. A. Douglas, M. Sturm, D. K. Perovich, and U. Platt (2007b), The Dependence of Arctic Tropospheric Halogen Chemistry on Sea Ice Conditions, ***Atmos. Chem. Phys., 7***, 621 – 627, doi: 10.1029/2004GL022132.

Tang, T. and McConnell, J. C. (1996), Autocatalytic release of bromine from Arctic snow pack during polar sunrise, ***Geophys. Res. Lett.***, ***23***, 2633-2636.

Toom-Sauntry, D. and L. A. Barrie (2002), Chemical composition of snowfall in the high Arctic: 1990-1994, ***Atmos. Env.***, ***36***, 2683-2693.

von Glasow, R. and Crutzen, P. J. (2007), ***Tropospheric halogen chemistry, in: The Atmosphere***, ***4*** Treatise on Geochemistry, Elsevier-Pergamon, Oxford, UK.

Wagenbach, D., Ducroz, F., Mulvaney, R., Keck, L., Minikin, A., Legrand, M., Hall, J. S., and Wolff, E. W. (1998), Sea-salt aerosol in coastal Antarctic regions, ***J. Geophys. Res.***, ***103*** (D9), 10,961-10,974.

Wagner, T., Leue, C., Wenig, M., Pfeilstcker, K., and Platt, U. (2001), Spatial and temporal distribution of enriched boundary layer BrO concentrations measured by the GOME instrument aboard ERS-2, ***J. Geophys. Res.***, ***106*** (D20), 24,225 – 24,235.

Weeks, W.F. and Ackley, S.F. (1982), The growth, structure, and properties of sea ice, Open file rep. Monograph, 82-1. 130 pages, CRREL, USA.

Chapter 4. Time series of the chemical composition of aerosol particles and snow collected near Barrow, Alaska[3]

4.1 Abstract

Reactive bromine chemistry is responsible for springtime ozone depletion and mercury deposition in the polar regions. The ultimate source of this bromine is primarily sea salts, but how these salts are chemically activated and how this chemistry depends upon the state of the sea ice is not well understood. We report a time series of Br^- and Cl^- in snow surfaces and aerosol particles in addition to gas-phase bromine monoxide (BrO) to explore exchanges of bromine among the reservoirs. Using a mass-balance approach, we find that the largest bromine reservoir in this system is the snowpack and that surface snow contains amounts of bromine comparable to atmospheric abundances. Observations of aerosol particles show that they contain too little Br^- to source the atmospheric abundance, indicating that they most likely are not a primary source. Larger aerosol particles show near sea-salt Br^-/Cl^- composition ratios, while submicron diameter particles show evidence of gaining Br^-. We extend the mass-balance approach to include consideration of the prevalence of ice surfaces (e.g. snow on sea ice, land, and frost flowers) in the Arctic system to show that frost flowers are an unlikely direct source of reactive bromine and that snowpack shows the strongest signatures of reactive bromine release.

4.2 Introduction

Bromine is involved in a series of reactions that destroy tropospheric O_3 [Barrie et al., 1988] and oxidize elemental mercury to more reactive and possibly toxic mercury species [Schroeder et al., 1998]. Models and field measurements indicate that during the springtime in the Arctic, bromide (Br^-) stored in the snow pack and other ice surfaces is transformed into highly reactive species, Br and BrO (bromine atoms and bromine

---

[3] Alvarez-Aviles, L., W. R. Simpson, D. Carlson, M. Sturm, T. A. Douglas, A. Laskin (2008), Time series of the chemical composition of aerosol particles and snow collected near Barrow, Alaska. Prepared for submission in Atmospheric Chemistry and Physics.

monoxide). Bromide is liberated from ice surfaces by reacting with HOBr to produce Br_2, which is quickly outgased and photolyzed to form bromine atoms, which, in the presence of ozone, are quickly oxidized to BrO [Fan and Jacob, 1992; McConnell et al., 1992; Vogt et al., 1996]. These bromine activation reactions deplete Br^- from the ice surfaces. The termination of the reactive bromine chemistry occurs when volatile organic compounds (VOC) react with bromine to produce HBr. The HBr product can be scavenged by ice surfaces resulting in addition of Br^-. Addition and/or removal of Br^- to/from snow and aerosol surfaces has been observed in many polar studies [Ianniello et al., 2002; Hara et al., 2002; Toom-Sauntry and Barrie, 2002; Simpson et al., 2005; Alvarez-Avilés et al., in preparation 2008, Chapter 2].

Chemical concentrations in snow and aerosol particles are controlled by seasonal source variability [Udisti, et al., 1999; Sirois and Barrie, 1999], spatial location [Proposito, et al., 2002] and exchange with atmospheric gases and acids [Aristarain and Delmas, 2002]. The snow and aerosol particle samples in this study belong to a coastal site under marine aerosol influences during the springtime. Therefore, we expect most of the Br^- and Cl^- content in snow and particles to originate from sea salt and any modifications of sea-salt Br^- and Cl^- to be due to atmospheric exchanges and heterogeneous reactions.

Newberg et al. [2005] conducted a study of modifications to sea-salt particles and found depletions in Cl^- and Br^- suggesting that acid-dependent oxidation reactions formed photoactive bromine species that volatilized from the particles. Although the Newberg et al., [2005] study is not in the Arctic, their findings can help to study aerosol particles without the presence of snow. Ianniello et al. [2002] measured Br^- in Arctic aerosol particles and gas-phase HBr and reported enrichments in Br^- on aerosol particles and suggested that the enrichment was due to HBr addition to the aerosols. Measurements of Br^- in aerosol particles and gas phase by Hara et al. [2002 and 2004] also indicate that aerosol particles could be a good storage or recycling reservoir for bromine species.

Our goal was to measure a time series of Br^- and Cl^- in different ice surfaces, snow, aerosols, and related gas phase species, to determine each surfaces' role in the bromine activation chemistry.

4.3 Methods

4.3.1 Experimental design

Aerosol particles were collected at the National Oceanic and Atmospheric Administration Earth System Reserach Laboratory, Global Monitoring Division (NOAA/ESRL/GMD, formerly NOAA/CMDL) facility approximately 2 km from the snow-sampling site. Both sites are in close proximity (a few km) to the frozen ocean and the village of Barrow, Alaska. The dominant meteorology provides clean air, uncontaminated by Barrow's emissions, to our sites. Snow samples were collected twice a day, once in the morning in between at 10:00 and 11:00 hours local time, and once in the afternoon around 16:00 and 17:00 hours every day starting March 8, 2007 (DOY 67) and ending on March 30, 2007 (DOY 89). During DOY 79 – 84 we undertook an "intensive operations period" (IOP), sampling snow every 6 hours to match the same sampling time resolution of the aerosol collector. The snow-sampling site was located approximately 5 km from the nearest open water (depending on sea ice changes and refreezing of open water), and 3 km from the coastline. Gas-phase BrO was measured using Differential Optical Absorption Spectroscopy, approximately 3 km from the snow-sampling site.

4.3.2 Snow sampling

We sampled snow wearing powder-free gloves and approaching the sampling site from the down-wind side. We sampled surface snow from the top three cm of the snow pack. We also sampled the vertically integrated snow column from the wall of a snow pit. The whole snow column was equally sampled and the typical total depth of snow pack was 10 to 30 cm. Lastly, we sampled freshly deposited snow from Pyrex trays set on a table 1 m above the ground. All snow samples were collected in pre-cleaned 50 mL polypropylene vials and the edge of the vial was used to scoop the sample. For every surface snow samples there is a corresponding vertically integrated snow column sample, but freshly deposited snow was only collected after a snowfall.

4.3.3 Aerosol particle sampling

A three-stage Davis Rotating Universal-size-cut Monitoring (DRUM) impactor collected aerosol particles in the following diameter size ranges 2.5 to 0.84 μm, 0.84 to 0.30 μm and 0.30 to 0.12 μm. The modified DRUM used in this study was programmed to stay stationary at the same impaction site for six hours then rotate 1 cm, resulting in discrete 6-hour averaged data. After sampling, the Teflon strip was cut into 1 cm squares containing each discrete-time-sampled aerosol sample.

4.3.4 Analytical procedures

We analyzed Cl^-, Br^-, and Na^+ in snow and aerosol samples using Ion Chromatography (IC) and Proton Induced X-Ray Emission (PIXE). All snow samples were analyzed with IC. Snow samples were melted and analyzed for their specific conductance. Samples were then sorted by conductance to select the appropriate injection volume on the IC. The first 18 days of aerosol particle samples were analyzed by IC. Aerosol samples were collected on Teflon strips, that were cut in 1 cm squares, then transferred to IC autosampler vials. Immediately after transferring each square to the vial, 2 mL of ultrapure water (18.2 MΩ) was added, and the samples were eluted by ultrasonification for 40 minutes, and analyzed with the IC. Because of limited sample size, only anion (Cl^- and Br^-) analysis of the aerosol samples was carried out. The IC detection limits for Br^- and Cl^- in snow were 0.001 and 0.02 micromolar, respectively. In the aerosol particles, IC detection limits were 0.13 ng/m^3 and 1.2 ng/m^3, for Br^- and Cl^-, respectively. During the last three days, aerosol particles were analyzed by PIXE.

4.4. Results

4.4.1 Aerosol particle and snow sea salt correlations

Figure 4.1 shows Br^- concentration as a function of Cl^- concentration for the three size ranges of aerosol particles. Most (91%) of the larger sized particles, 0.84 to 2.5 µm, are not shown in Figure 4.1 (crosses) because were under detection limit for Br^-. The solid line is the seawater dilution line that helps to identify modifications in Br^- with respect to Cl^- (sea-salt tracer). Smaller particles, 0.12 – 0.30 µm, are mostly enriched in Br^- and larger particles, 0.30 to 0.84 µm, and 0.84 to 2.5 µm are closer to the dilution line.

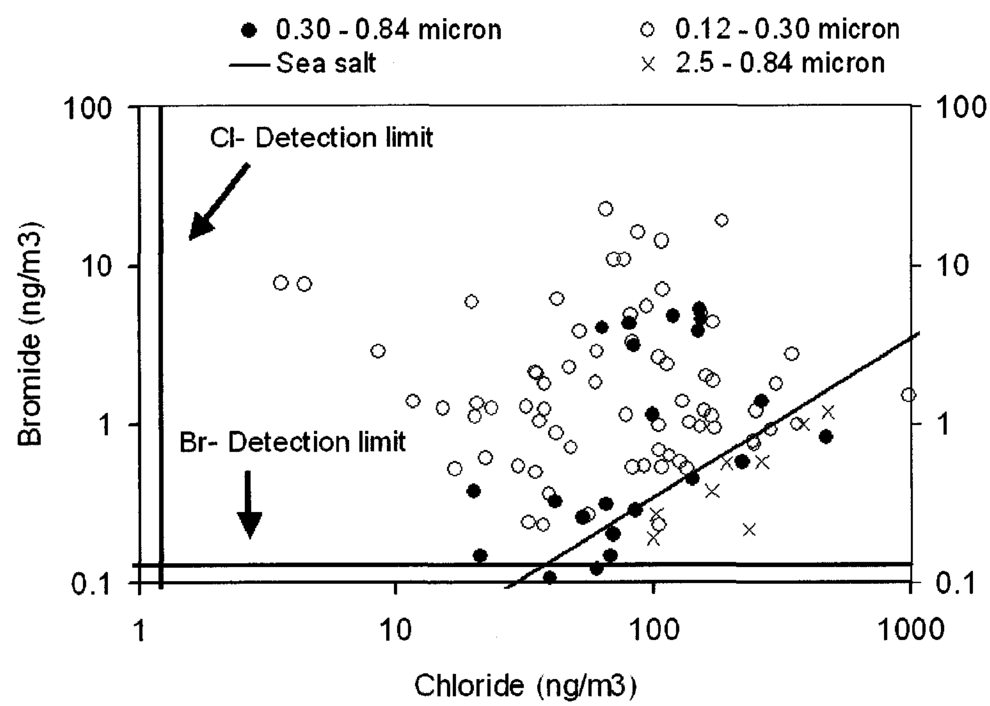

Figure 4.1 Bromide versus Cl^- observed in aerosol particles. Bromide concentration (ng/m^3) as function of Cl^- concentration (ng/m^3) in a three-stage DRUM aerosol collector. Sizes ranges are 0.12 to 0.30 microns, 0.30 – 0.84 microns, and 0.84 – 2.5 microns. The straight solid lines indicate the detection limit for Cl^- and Br^-.

Figure 4.2 shows Na^+ versus Cl^- concentration in different snow ice surfaces. Most samples are within a factor of two of the sea salt ratio of Cl^- to Na^+ as seen by the closeness of the data points to the seawater dilution line. Surface snow (full circles) and freshly deposited snow (hollow circles) Cl^- concentration shows a wide range from 10 to 2000 μM, while the vertically integrated snow pack (crosses) range starts at higher Cl^- concentrations, 100 μM and continues to a similar upper limit, 2000 μM. Snow samples show moderate enrichment of Cl^- with respect to Na^+ at low Na^+ concentration and converge to the sea-salt dilution line at higher Na^+ as observed by Toom-Sauntry and Barrie, [2002] and Alvarez-Avilés et al., [in preparation, 2008, Chapter 2].

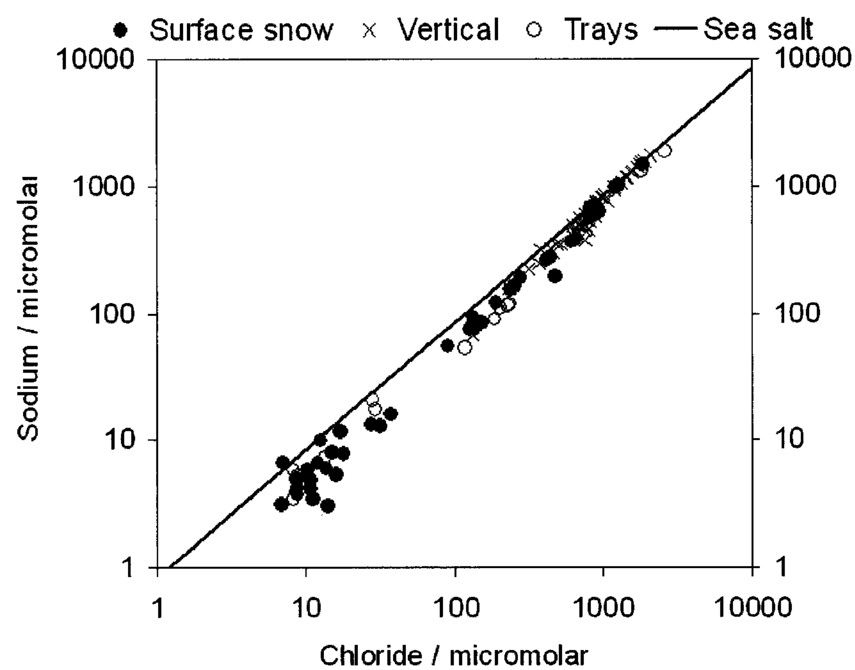

Figure 4.2 Snow Na^+ correlation plot. Chloride (μM) concentration versus sodium (μM) concentration in different snow types.

4.4.2 Temporal variation in aerosol particle and snow chemical composition

A relatively long precipitation event occurred from day of the year (DOY) 75 to 85. Figure 4.3a and b shows a plot of Cl^- concentration in snow surface, freshly deposited snow (trays) and aerosols as a function of time. The Cl^- concentration range in surface snow is 10 – 1,000 μM. Surface snow collected during DOY 67 to 70, first few days of the experiment, was older and the snow layer was dense and wind packed. These samples show high Cl^- concentrations (more than 200 μM). The fresh snow from the precipitation event covered the older surface snow. We collected fresh snow sample on the snow pack surface and in trays during the precipitation event, DOY 75 to 85. The Cl^- concentration in freshly deposited snow is comparable to that of the snow pack surface snow, and is considered low Cl^- concentrations (less than 100 μM). After the precipitation event some of the old hard snow pack was re-exposed DOY 86 to 88 due to wind blowing some of the freshly deposited snow. We sampled the re-exposed older snow from DOY 86 to 88 and fresh snow in the last day 89. We observed that the fresher snow (Figure 4.3a square) is lower in Cl^- concentrations than older snow pack (outside the square with the exception of DOY 89).

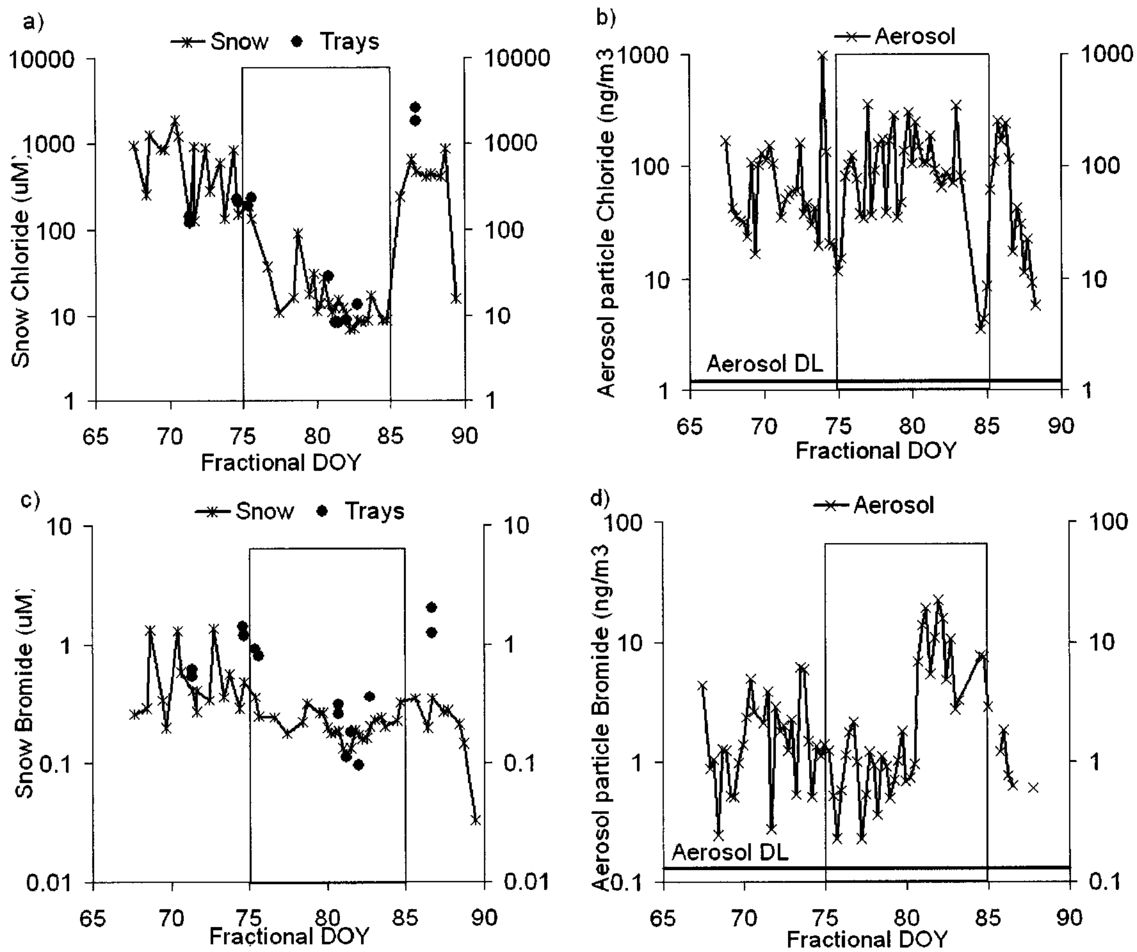

Figure 4.3 Concentration of Cl^- (panel a and b) in snow and aerosol particles and Br^- (panel c and d) in snow and aerosol as a function of time.

Figure 4.3c and 4.3d shows Br^- concentrations as a function of time in surface snow, freshly deposited snow, and aerosol particles. The Br^- concentration in snow is less variable than the concentration of Cl^-. The Br^- concentration in surface snow can be found in a stable range, 0.1 – 1.3 μM for snow, and 0.2 – 22 ng/m^3 for aerosols. Also as observed for Cl^-, the Br^- concentration in freshly deposited snow is similar to that of surface snow.

The aerosol particle Cl^- concentration ranges from 4 to 400 ng/m^3 showing great variability in the Cl^- concentration. The aerosol particle Br^- concentration ranges from

0.2 to 22 ng/m^3, showing similar variability than the Cl^- concentration in aerosol particles.

4.4.3 Temporal variation in aerosol particles and snow enrichments

Figure 4.4 contains 4 panels showing Cl^- and Br^- as a function of time in a) aerosol particles, b) surface snow, c) freshly deposited snow, and d) vertically integrated snow. Predicted Br^- indicates the expected Br^- concentration from sea salt based upon using Cl^- as the sea-salt tracer. We calculated the expected sea-salt Br^- concentrations using the Cl^- concentration in the sample and multiplying by the molar ratio of Br^- to Cl^- in sea salt, 0.0015 [Quimby-Hunt and Turekian, 1983]. If the observed Br^- is above the predicted Br^- line, the sample is enriched, while if the observed Br^- is below the predicted Br^-, the sample is depleted. [[I deleted this section because you don't discuss it later]] The older surface snow (DOY 67-70 and 86-88) is either close to sea-salt ratios or sometimes depleted. The surface snow sampled during the precipitation event (inside the square) is significantly enriched in Br^- Figure 4.4b. Vertically integrated snow, Figure 4.4d, has a higher and more stable Cl^- content and Br^- is near sea salt ratios. Because Cl^- is in higher concentrations and the snow is near sea-salt Br^- composition, this snow typically has higher Br^- concentrations than surface snow.

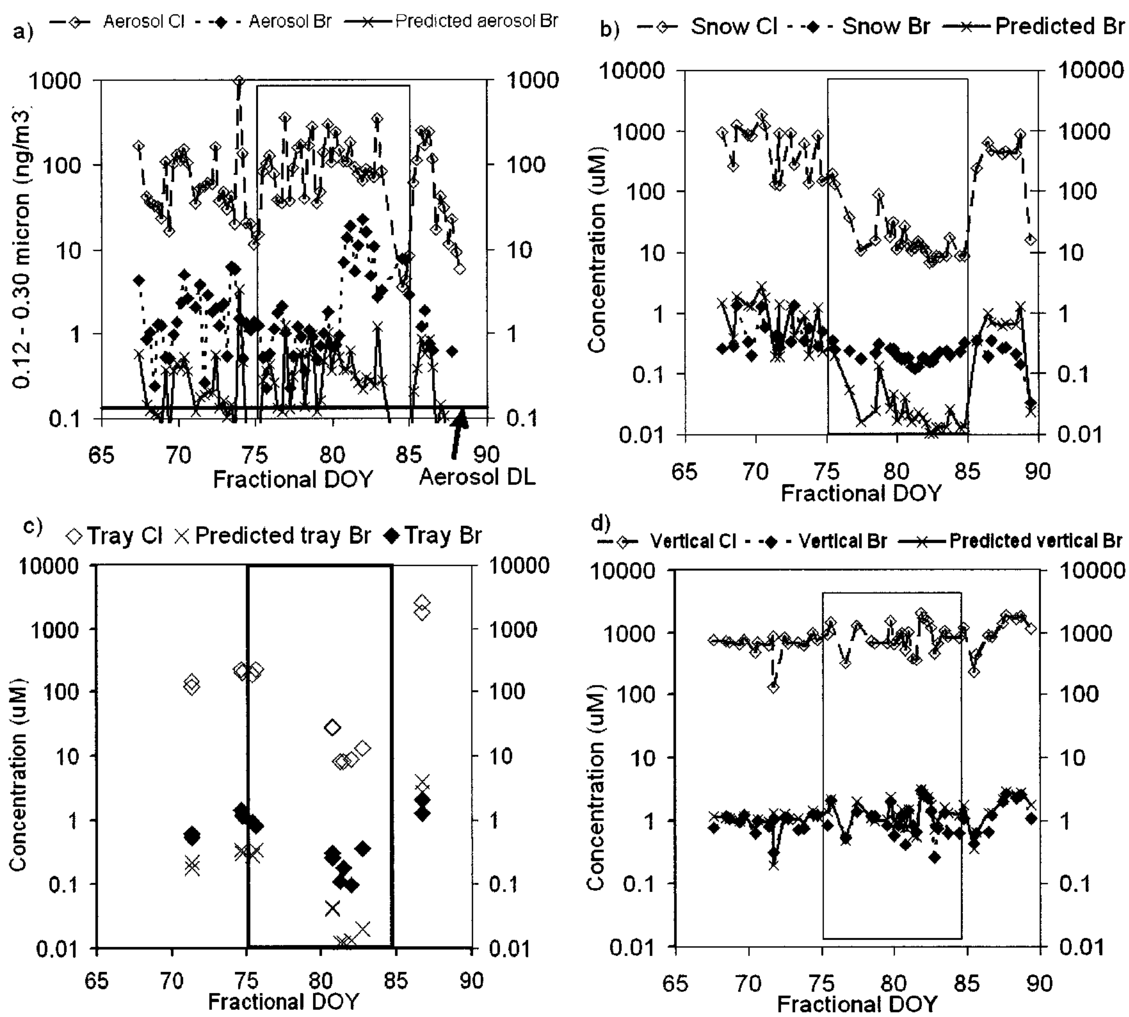

Figure 4.4 Chloride and Br^- concentrations in all studied reservoirs as a function of time during the extent of the study. All panels contain the Cl^- and Br^- concentration and the predicted sea-salt Br^- concentration. Panel a) shows the time series of Cl^-, Br^- and predicted sea-salt Br^- in the smaller aerosol particles, panel b) shows the same for surface snow, panel c) for the freshly deposited snow and panel d) for the vertically integrated snow.

4.5 Discussion

4.5.1 Sea-salt influences and bromide exchanges

The wide range in the Cl^- concentrations in surface snow indicates differing sea-salt influences on snow at various times. The older surface snow from DOY 67 to 70 and 86 to 88 have a high Cl^- concentration. Surface snow and freshly deposited snow from the precipitation event have similar, lower Cl^- concentrations probably due to dilution of ionic content by condensed water vapor on surface (e.g. particulate or ice) during snow formation.

The large aerosol particles are closer to the seawater dilution line (Figure 4.1), indicating that these particles consist of relatively unaltered sea-salt. The smaller particles are mostly enriched (Figure 4.1) indicating that they have undergone some modification from sea salt composition. The enrichment in smaller particles is consistent with HBr scavenging, which is expected to enrich smaller particles to a greater degree because of their larger surface-area to volume ratio, as compared to larger particles.

Although the Cl^- concentration in surface snow changes according to different sea-salt influences, the Br^- concentration shows a relatively more stable range of concentrations, varying by approximately an order of magnitude (0.1 – 1.3 μM). The reduced concentration range, as compared to the range of Cl^-, suggests that sea-salt Br^- is modified and that the concentration of Br^- in snow is evened by nearby sources and sinks.

4.5.2 Ice surfaces bromide abundances

To investigate the role of various ice surfaces as a source or sink of bromine into the atmosphere we use a mass-balance approach. We initially assume that the Arctic region that experiences halogen chemistry is a closed system and that our measurements of bromine concentrations are representative of the Arctic as a whole. For the atmospheric components (BrO and aerosol), we assume a well-mixed 500 m deep boundary layer. For the snow pack components, we assumed that surface snow is 3 cm deep, and the average snow depth for the vertically integrated snow was 9 cm. We used a snow density of 0.35 g/cm^3 from Dominé et al., [2005]. Table 4.1 shows the calculated column density for each component. The range of mixing ratios used in the vertical column abundance (VCA) calculation for BrO was 0 to 40 pptv, at -30°C resulting in a column density of 0 – 60 x 10^{12} Br atoms/cm^2. Aerosol particles average Br^- concentration was 1 ng/m^3 and the maximum Br^- concentration reported in this study was 10 ng/m^3, so we calculate 0.4 – 4 x 10^{12} Br atoms/cm^2. Surface snow average Br^- concentration was 0.1 μM, and the maximum Br^- concentration reported in this study was approximately 1 μM. The column density surface snow calculation resulted in 60 – 600 x 10^{12} Br atoms/cm^2. Vertical average Br^- concentration is a stable 1 μM all throughout the experiment extent, and the column density calculation resulted in a 1000 x 10^{12} Br atoms/cm^2.

Table 4.1 Vertical column abundances (VCA) of Br for some important ice surfaces, gas phase and aerosols.

Component	***Species***	***Concentration***	***VCA (Br atoms / cm^2)***
Gas phase	BrO	0 – 40 pptv	0 – 60 x 10^{12}
Aerosol particle	Br^-	0.1 – 10 ng/m^3	0.4 – 4 x 10^{12}
Surface snow	Br^-	0.1 – 1 μM	60 – 600 x 10^{12}
Vertically integrated snow	Br^-	1 μM	1000 x 10^{12}

The largest reservoir is the snow pack, followed by the surface snow, which has comparable abundance to the atmospheric BrO column. The aerosol contains less Br^- than any other reservoir and according to the column density results, is not likely that the aerosol content can satisfy either the gas phase or surface snow abundance levels. The column density results indicate that surface snow could be a significant source of bromine to the atmosphere, and that underlying snow contains sufficient Br^- to source Br^- to surface snow.

The atmospheric columns move significant distances on the timescale of the effective BrO lifetime. Models indicate that BrO may live for a couple days, allowing transport hundreds of kilometers horizontally. Therefore, the BrO detected in this study could have originated in geographic environments that are different from this study's sampling site. Figure 4.5 shows Br^- in the small particles and surface snow along with gas-phase BrO. There is no obvious correlation between gas-phase BrO enhancement and losses of Br^- from the local condensed phases, in agreement with the idea that BrO may transport long distances. In past studies, our group has used a trajectory model to calculate the ice contact history of airmasses arriving at Barrow and found that BrO abundance was correlated to first-year sea ice contact over the preceding three days [Simpson et al., 2007]. Therefore, there is a need to consider horizontal transport of airmasses over various ice environments in the case of the atmospheric components.

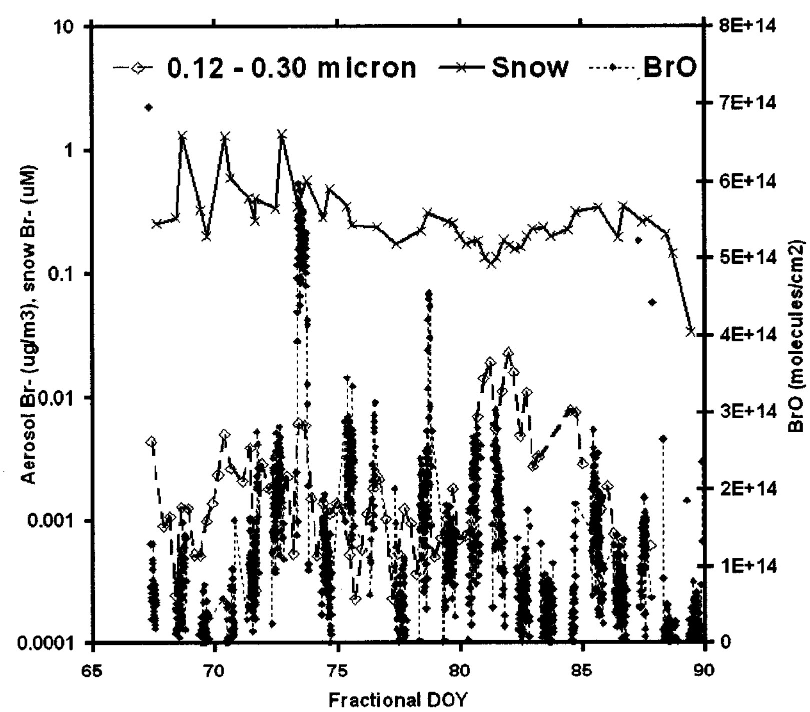

Figure 4.5 Snow, aerosol particles and gas-phase bromine concentration time series. Br^- concentration in snow and small aerosol particles and gas-phase BrO concentration versus fractional day of the year. The BrO shown in this plot is the 2 degree elevation angle slant column density, a proxy for boundary layer BrO.

Some ice surfaces can have Br abundances much larger than the BrO abundance, such as frost flowers, [Rankin and Wolff, 2002; Simpson et al., 2005; Alvarez-Avilés et al., 2008, in press, chapter 3]. From the data presented in Alvarez-Avilés et al. [2008, in press, chapter 3], we can calculate a frost flower column density of ~4000 x 10^{12} Br atoms/cm^2. When the column density of frost flowers is compared to the atmospheric BrO column (0 – 60 x 10^{12} Br atoms/cm^2), it confirms that frost flowers contain sufficient Br^- to satisfy atmospheric BrO abundances with little depletion of the frost flower Br^-. However, there are two complications that have to be considered. First, frost flowers are not always present across the whole Arctic, as we implicitly assume in the simple calculation above. Second, frost flowers are a two-phase system [Alvarez-Aviles et al., 2008, in press, chapter 3], with separate brine and ice, and it is likely that snow is also a two-phase system. Due to brine-ice separation, the bulk composition is not directly related to the surface available bromide, and therefore, the mass-balance calculations presented here may not represent rates of bromine evolution from the surfaces. However, the mass-balance approach does place constraints on the maximum amount of bromine present in a type of ice and thus is still useful. We consider the mass balance approach first.

Frost flower are normally found on refreezing sea ice and open leads (opening on sea ice that exposes seawater). Refreezing sea ice and open leads can occupy up to 12% of the Arctic ice area [Piot and von Glasow, 2008, and references therein]. If we consider that frost flowers grow under low wind conditions and cold temperatures and that these conditions are not always available, then we assumed the presence of frost flowers in the Arctic to be smaller than the occurrence of open leads and refreezing ice, 1%. If we consider frost flowers as a dominant source of Br atoms to the atmosphere, we need to deplete the frost flower's Br by roughly 100 times the atmospheric BrO abundance, which would imply up to 6000 x 10^{12} Br atoms/cm^2 would be removed from frost flowers. This removal is of the order of the total available Br^- in frost flowers (~4000 x 10^{12} Br atoms/cm^2), yet all observations of the Br^- in frost flowers shows undetectable depletions [Rankin and Wolff, 2002; Simpson et al., 2005; Alvarez-Aviles et al., 2008, in press; chapter 3]. Therefore, the vertical column abundance approach, when combined with realization of the limited spatial extent of frost flowers, indicates that frost flowers do not appear to be the direct source of reactive halogens to the atmosphere.

The concentration of Br^- in brine associated with frost flowers and snow crystals can be predicted by bulk thermodynamics [Koop et al., 2000] and is a strong function of temperature. However, the microstructure of the brine/ice system is not predicted by thermodynamics. The brine may wet the surface of the ice, as is probably the case for frost flowers [Domine et al., 2005; Alvarez-Avlies et al., 2008, in press, chapter 3], or may form inclusions or surface islands that present less of the ice surface containing bromide. If we were to assume that a frost flower and snow were both at the same temperature, and that their brine wetted the surface of each structure completely, then both would present the same concentration of bromide to the atmosphere, and even though the snow is of much lower bulk bromide concentration, it may be equally reactive. Therefore, the total mass-balance calculations presented here, while useful to constrain the problem, are likely to not accurately constrain the kinetics of bromine evolution. More work needs to be done on the microstructure of frost flowers and snow surfaces to address these possible kinetic limitations. However, to the extent that brine wets the surfaces, snow and frost flowers may be similarly kinetically facile in bromine evolution, in which case the increased prevalence of snow makes it a more important reactive bromine source.

4.6 Conclusion

Submicron aerosol particles and fresh snow in trays appeared enriched in Br^- as compared to seawater sources, which is consistent with gaining Br^- by HBr deposition to the particles. Older surface snow is less enriched in Br^- than aerosol or tray snow, indicating that it has lost Br^-, most likely to the gas phase in the form of Br atoms and BrO. The high Br^- abundance in vertically integrated snow suggests that underlying snow pack contains sufficient Br^- to source surface snow Br^-. The similarity of the bromine abundances between surface snow and atmospheric BrO indicates that surface snow contains sufficient amounts of Br^- to source the observed BrO levels and that snow pack may be a major source of Br^- to the atmosphere. Further consideration of other ice forms like frost flowers and their presence in the Arctic and surface concentration in comparison to snow, suggested that the frost flowers are not the dominant direct source of reactive bromine to the atmosphere. When combined with the observation that fine aerosol particles (<2.5 micron diameter) do not contain sufficient bromine to source reactive bromine, these observations indicate that surface snow is the dominant source of reactive bromine to the Arctic atmosphere. It is also possible that larger aerosols / sea spray (larger than the 2.5 micron diameter cutoff of our inlet) are an important reactive bromine source, and we observe the depletion of Br^- in surface snow after these coarse-mode aerosols deposit to the snow pack.

4.7 References

Alvarez-Avilés, L., W. R. Simpson, T. A. Douglas, M. Sturm, D. K. Perovich, and F. Dominé (2008), Frost flower chemical composition during growth and its implications for aerosol production and bromine activation, ***J. Geophys. Res.***, in press.

Alvarez-Avilés, L., W. R. Simpson, D. Carlson, T. A. Douglas, M. Sturm (2008), Chemical composition of Arctic surface snow, in preparation for ACPD.

Aristarain, A. J., and R. J. Delmas (2002), Snow chemistry measurements on James Ross Island (Antarctic Peninsula) showing sea-salt aerosol modifications, ***Atmos. Environ., 36***, 765-772.

Dominé, F., Taillandier, A.-S., Simpson, W. R., and Severin, K. (2005), Specific surface area, density and microstructure of frost flowers, ***Geophys. Res. Lett.***, ***32***, L13502, doi:10.1029/2005GL023245.

Fan, S.-M. and D. J. Jacob (1992), Surface ozone depletion in Arctic spring sustained by bromine reactions on aerosols, N***ature***, ***359***, 522-524.

Foster, K. L., R. A. Plastridge, J. W. Bottenheim, P. B. Shepson, B. J. Finlayson-Pitts, and C. W. Spicer (2001), The role of Br_2 and BrCl in surface ozone destruction at polar sunrise, ***Science, 291***, 471-474.

Hara, K., K. Osada, K. Matsunaga, Y. Iwasaka, T. Shibata (2002), Atmospheric inorganic chloride and bromine species in Arctic boundary layer of the winter/spring, ***J. Geophys. Res., vol. 107***, no. D18, 4361, doi:10.1029/2001JD001008.

Hara, K., K. Osada, M. Kido, M. Hayashi, K. Matsunaga, Y. Iwasaka, T. Yamanouchi, G. Hashida, T. Fukatsu (2004), Chemistry of sea-salt particles and inorganic halogen species in Antarctic regions: Compositional differences between coastal and inlad stations, ***J. Geophys. Res., vol. 109***, D20208, doi:10.1029/2004JD004713.

Ianniello, A., Beine, H. J., Sparapani, R., Di Bari, F., Allegrini, I., and Fuentes, J. D. (2002), Denuder measurements of gas and aerosol species above Arctic snow surfaces at Alert 2000, ***Atmos. Env.***, ***36***, 5299-5309.

Kawamura, K., M. Narukawa, S.-M. Li, L. Barrie (2007), Size distribution of dicarboxylic acids and inorganic ions in atmospheric aerosols collected during polar sunrise in the canadian high Arctic, *J. Geophys. Res., vol. 112*, D10307, doi:10.1029/2006JD008244.

Koop, T., A. Kapilashrami, L. T. Molina, and M. J. Molina (2000), Phase transitions of sea-salt/water mixtures at low temperatures: Implications for ozone chemistry in the polar marine boundary layer, *J. Geophys. Res., 105*, *vol.* 26 393–26 402.

Langendörfer, U., E. Lehrer, D. Wagenbach, and U. Platt (1999), Observation of filterable bromine variabilities during Arctic tropospheric ozone depletion events in high (1 hour) time resolution, *J. Atmos. Chem.*, *34*, 39-541.

Lehrer, E., G. Hönninger, and U. Platt (2004), Aerosol chemical composition during tropospheric ozone depletion at Ny Alesund/Svalbard, *Tellus., 49B*, 486-495.

McConnell, J. C., Henderson, G. S., Barrie, L., Bottenheim, J., Nili, H., Langford, C. H., and Templeton, E. M. J. (1992), Photochemical bromine production implicated in Arctic boundary-layer ozone depletion, *Nature*, vol. 355, 150-152.

Newberg, J. T., B. m. Matthew, C. Anastasio (2005), Chloride and bromide depletions in sea-salt particles over the northeastern Pacific Ocean, *J. Geophys. Res., vol. 110*, D06209, doi:10.1029/2004JD005446.

Piot, M. and R. von Glasow (2008), The potential importance of frost flowers, recycling on snow, and open leads for ozone depletion events, *Atmos. Chem. Phys., 8*, 2437-2467.

Proposito, M., S. Becagli, E. Castellano, O. Flora, L. Genoni, R. Gragnani, B. Stenni, R. Traversi, R. Udisti, M. Frezzotti (2002), Chemical and isotopic snow variability along the 1998 ITASE traverse from Terra Nova Bay to Dome C, East Antarctica, *Annals of Glaciology, 35*, 187.

Quimby-Hunt, M. S. and Turekian, K. K. (1983), Distribution of Elements in Sea Water, *Eos*, *64*, (14), 130-132.

Schröeder, W. H., K.G. Anlauf, L.A. Barrie, J.Y. Lu, A. Steffen, D.R. Schneeberger, T. Berg (1998), Arctic spring time depletion of mercury, *Nature*, *394*, 331-332.

Simpson, W. R., Alvarez-Aviles, L., Douglas, T. A., Sturm, M., and Dominé, F. (2005), Halogen in the coastal snow pack near Barrow Alaska: Evidence for active bromine air-snow chemistry during springtime, ***Geophys. Res. Lett.***, ***32***, L04811, doi:10.1029/2004GL021748.

Simpson, W. R., D. Carlson, G. Hoenninger, T. A. Douglas, M. Sturm, D. K. Perovich, and U. Platt (2007), The Dependence of Arctic Tropospheric Halogen Chemistry on Sea Ice Conditions, ***Atmos. Chem. Phys., 7***, 621 – 627, doi: 10.1029/2004GL022132.

Sirois, A. and L. A. Barrie (1999), Arctic lower tropospheric aerosol trends and composition at Alert, Canada: 1980-1995, ***J. Geophys. Res., vol. 104***, No. D9, p. 11,599-11,618.

Toom-Sauntry, D. and L. A. Barrie (2002), Chemical composition of snowfall in the high Arctic: 1990-1994, ***Atmos. Env.***, ***36***, 2683-2693.

Udisti, R., S. Begagli, E. Castellano, R. Traversi, S. Vermigli, G. Piccardi (1999), Sea-spray and marine biogenic seasonal contribution to snow composition at Terra Nova Bay, Antarctica, ***Annals of Glaciology***.

Vogt, R., P. J. Crutzen, and R. Sander (1996), A mechanism for halogen release from sea salt aerosol in the romote marine boundary layer, ***Nature, 338***, 327-330.

Chapter 5. Conclusion and outlook for the future

The main goal of this thesis is to observe the chemical composition of ice surfaces so as to gain knowledge on these surfaces' role in reactive bromine chemistry in the Arctic. Improving knowledge on ice surface's involvement in halogen chemistry is critical because the Arctic cryosphere is rapidly changing [NSIDC 2007] and is predicted to continue to change [Holland et al., 2006]. It is only with mechanistic knowledge on how various ice surfaces participate in halogen activation that we can make meaningful predictions as to how a changing Arctic climate may affect pollutants in the Arctic such as ozone and mercury.

Our measurements of the chemical composition of ice surfaces, presented in Chapter 2, improved our understanding of exchanges between snow and the atmosphere. We studied modifications to sea-salt ions in surface snow using log-log correlation plots. This analysis is complementary to two traditional methods of snow analysis, enrichment factors and non-sea-salt abundances, and we have described how our analysis is related to these traditional methods. The unique modification pattern of each sea-salt ion in surface snow permits the identification of a specific modification mechanism. Two important modification mechanisms are source fractionation and atmospheric exchange. The ability to observe certain modifications depends upon the sea-salt tracer concentration; lower sea-salt tracer levels allow observations of atmospheric exchange that are masked at high tracer levels. Bromide showed significant depletions and enrichments at low sea-salt tracer concentrations indicating that Br^- in surface snow is highly affected by atmospheric influences. The depletions are consistent with liberation of reactive bromine, and the enrichments indicate the capacity of snow to scavenge HBr. Nevertheless, at high sea-salt tracer concentrations, Br^- was well correlated with sea salt Br^-, indicating that at high sea salt concentrations exchanges with the atmosphere cannot result in detectable alterations and that Br^- is not fractionated at its source (for example by a precipitation process). Calcium is added to snow by dust sources, which is evident at low sea-salt tracer concentrations, but at higher concentrations, Ca^{2+} is correlated with sea salt.

Sulfate modifications with respect to sea salt in frost flowers and surface snow contributed valuable information on frost flower formation, aerosol production from frost flowers or the brine source of these crystals, and sea ice formation processes. We found SO_4^{2-} to be affected by both source fractionation processes and atmospheric addition, most likely from Arctic haze. Source fractionation occurs when Na^+ and SO_4^{2-} precipitate as $Na_2SO_4{\cdot}6H_2O$ (mirabilite) at temperatures colder than -8°C. Based upon measurements, presented in Chapter 2, of surface snow in many Arctic environments (e.g. land, multi-year sea ice, and first-year sea ice), we observe significant source fractionation of SO_4^{2-}, consistent with mirabilite precipitation.

In Chapter 3, we observed the chemical composition of frost flowers directly. These observations showed the frost flowers enrichment factors with respect to seawater are variable for sulfate but are unfractionated for bromide. The variability in SO_4^{2-} is consistent with mirabilite precipitation, and we observe evidence for differential transport of SO_4^{2-}-depleted brine away from mirabilite crystals. The lack of variability in Br^- indicates that frost flowers do not directly lose appreciable amounts of Br^- to the atmosphere, limiting their direct involvement in halogen activation. Further analysis along these lines was carried out in Chapter 4, as summarized below. Based upon the chemical observations, we corroborated proposed frost flower growth models and suggested possible microstructures. We propose that frost flowers are made up of an ice skeleton coated by brine, although some brine may also be in inclusions or channels in the frost flower. This model of frost flower growth has important implications for surface chemistry on frost flowers, as discussed in Chapter 4 and at the end of this chapter.

Our surface snow study, Chapter 2, shows enrichments and depletions in Br^-, but further investigation was needed to investigate if surface snow is a direct source of reactive bromine to the atmosphere. A direct involvement in the bromine chemistry occurs when the snow contains the Br^- that is transformed to reactive bromine. An indirect involvement occurs when bromine activation occurs from some other surface formed that is correlated to an ice form. For example, if halogen release happened from aerosol produced from frost flowers, then frost flowers would be indirectly involved in halogen activation. We studied Br^- modifications with respect to Cl^- in the snow pack, aerosol particles and reactive bromine in the gas-phase in Chapter 4. Our observations of enrichments and calculations of vertical column abundances of surface snow, aerosol particles and frost flowers suggested that the surface snow contains enough Br^- to satisfy the BrO gas-phase abundance, but fine aerosols (<2.5 micron diameter) alone cannot satisfy the BrO budget. We also found that the underlying snow pack could be a source of Br^- to the surface snow. Frost flowers contain sufficient amounts bromine to produce the atmospheric BrO abundance in a column above the frost flowers with very small depletions in Br^- that could escape detection. However, considering that frost flowers are rare (~1% of the Arctic is covered by frost flowers), direct release of the full atmospheric abundance should have resulted in detectable depletion of Br^- from frost flowers. Therefore, our observations indicate that frost flowers are not the primary direct source of reactive halogens. This process of elimination then leaves coarse-mode aerosol particles (>2.5 micron diameter) and surface snow as dominant reactive bromine sources to the atmosphere.

The most important result of our studies is an improved understanding of the fundamental processes that govern snow and ice chemical composition and their interactions with the atmosphere. Some of these fundamental processes have been overlooked by the community and these omissions have compromised their conclusions. We found that consideration of the sea-salt tracer concentration can put into perspective exchanges between snow and the atmosphere, allowing us to identify the tools needed to detect modifications, such as log-log correlation plots, enrichment factors and the concept of non-sea-salt ions. Another overlooked aspect is the idea of using bulk composition to pinpoint which ice surfaces contain enough bromine to supply the atmosphere's abundance.

An important area for future work lies in the elucidation of the microstructure of ice and snow. We used the phase diagram to explore availability and concentration of ionic species on ice structures. The temperature controls the concentration of the ionic species found on the brine liquid layer that is in equilibrium with the ice structure, while the bulk composition provides information on the ratio of ice to brine layer. How this brine is distributed in snow and ice was not determined in our studies, but is clearly critical to understand for the surface reactivity of these systems. If brine is present on the surface, it is available for gas-surface reactions, while if it is buried in inclusions, it will not affect gas-surface reactions. Photomicrographs of frost flowers [Domine et al., 2005] show rounding, which probably indicates wetting by liquid brine. Phase diagram arguments then indicate very thick (~> 10s of microns) surface layers. Snow possesses orders of magnitude less salts, but if these salts still partition to the surface, they would produce micron to sub-micron surface brine layers, which are still hundreds of water molecules thick. Therefore, snow may be coated with brine of the same surface composition as those that coat frost flowers, which would allow snow to be as highly reactive as the less common frost flowers, and thus dominate the reactive bromine source to the arctic atmosphere.

Without the actual microscopic structure measurements and a determination of the location of the chemical species within the ice surface, we can only speculate on how various ice forms release bromine to the atmosphere. Therefore, we consider the study of the ice forms' microscopic structure vital to investigating surface reactivity of these ice forms in the future.

Introduction and conclusions references:

Adams, J. W., N. S. Holmes, and J. N. Crowley (2002), Uptake and reaction of HOBr on frozen and dry salt surfaces, ***Atmos. Chem, Phys., 2***, 79-91.

AMAP (2005), AMAP Assessment 2002: Heavy Metals in the Arctic, Oslo, Arctic Monitoring and Assessment Programme (AMAP), XVI, 265.

Ariya, P., A. P. Dastoor, M. Amyot, W. H. Schroeder, L. Barrie, K. Anlauf, F. Raofie, A. Ryzhkov, D. Davignon, J. Lalonde, A. Steffen (2004), The Arctic: a sink for mercury, ***Tellus, 56B***, 397-403.

Ariya, P. A., A. Khalizov, and A. Gidas (2002), Reactions of gaseous mercury with atomic and molecular halogens: kinetics, products studied, and atmospheric implications, ***J. Phys. Chem. A, 106***, 7310-7320.

Barrie, L. A., Bottenheim, J. W., Schnell, R. C., Crutzen, P. J., and Rasmussen, R. A. (1988), Ozone destruction and photochemical reactions at polar sunrise in the lower Arctic atmophere, ***Nature, 334***, 138-141.

Bottenheim, J. W., L. A. Barrie, E. Atlas, L. E. Heidt, H. Niki, R. A. Rasmussen, and P. B. Shepson (1990), Depletion of lower tropospheric ozone during arctic spring: the Polar Sunrise Experiment 1988, ***J. Geophys. Res., vol. 95***, no. D11, 18,555-18,568.

Bottenheim, J. W., J. D. Fuentes, D. W. Tarasick, K. G. Anlauf (2002), Ozone in the Arctic lower troposphere during winter and spring 2000 (ALERT2000), ***Atmos. Env, 36***, 2535-2544.

Carpenter, L. J. and P. S. Liss (2000), On temperature sources of bromoform and other reactive organic bromine gases, ***J. Geophys. Res., vol. 105***, no. D16, 20,539-20,547.

Davidson, C. I., J. R. Harrington, M. J. Stephenson, M. J. Small, F. P. Boscoe, and R. E. Gandley (1989), Seasonal variations in sulfate, nitrate and chloride in the Greenland ice sheet: relation to atmospheric concentrations, ***Atmos. Env., vol. 23***, no. 11, 2483-2493.

de Caritat, P., G. Hall, S. Gislason, W. Belsey, M. Braun, N. I. Goloubeva, H. K. Olsen, J. O. Scheie, J. E. Vaive (2005), Chemical composition of arctic snow: concentration levels and regional distribution of major elements, ***Science of the Total Environment, 336,*** 183-199.

Dehn, L.-A., E.H. Follomann, D. L. Thomas, G. G. Sheffield, C. Rosa, L. K. Duffy, T. M. O'Hara (2006), Trophic relationships in an Arctic food web and implications for trace metal transfer, ***Science of the total Environment,*** 362 (1-3), 103-123.

Dominé, F. and P. B. Shepson (2002), Air-Snow interactions and atmospheric chemistry, ***Science vol. 297,*** 1506.

Dominé, F., Sparapani, R., Ianniello, A., and Beine, H. J. (2004), The origin of sea salt in snow on Arctic sea ice and coastal regions, ***Atmospheric Chemistry and Physics, 4,*** 2259-2271.

Dominé, F., Taillandier, A.-S., Simpson, W. R., and Severin, K. (2005), Specific surface area, density and microstructure of frost flowers, ***Geophys. Res. Lett., 32,*** L13502, doi:10.1029/2005GL023245.

Douglas, T., M. Sturm, W. Simpson, S. Brooks, S. Lindberg and D. Perovich (2005), Elevated mercury measured in snow and frost flowers near arctic sea ice leads, ***Geophys. Res. Lett., 32*** (4), L04502, doi:10.1029/2004GL022132.

Douglas, T., M. Sturm, W. Simpson, S. Brooks, S. Lindberg and D. Perovich (2008), Influence of snow and ice crystal formation and accumulation on mercury deposition to the Arctic, ***Environ. Sci. Technol. 42,*** 1542-1551.

Enami, S., C. D. Vecitis, J. Cheng, M. R. Hoffmann, and A. J. Colussi (2007), Global inorganic source of atmospheric bromine, ***J. Phys. Chem. Lett., 111,*** 8749-8752.

Fan, S.-M. and D. J. Jacob (1992), Surface ozone depletion in Arctic spring sustained by bromine reactions on aerosols, N***ature, 359,*** 522-524.

Fickert, S., J. W. Adams, and J. N. Crowley (1999), Activation of Br_2 and BrCl via uptake of HOBr onto aqueous salt solutions, ***J. Geophys. Res., 104,*** 23719-23727.

Finlayson-Pitts, B. J. (2003), The tropospheric chemistry of sea salt: a molecular-level view of the chemistry of NaCl and NaBr, ***Chem. Rev., 103,*** 4801.

Frieβ, U., J. Hollwedel, G. König-Langlo, T. Wagner, and U. Platt (2004), Dynamics and chemistry of tropospheric bromine explosion events in the Antarctic coastal region, ***J. Geophys. Res., vol. 109***, D06305, doi:10.1029/2003JD004133.

Hara, K., K. Osada, K. Matsunaga, Y. Iwasaka, T. Shibata (2002), Atmospheric inorganic chloride and bromine species in Arctic boundary layer of the winter/spring, ***J. Geophys. Res., vol. 107***, no. D18, 4361, doi:10.1029/2001JD001008.

Hara, K., K. Osada, M. Kido, M. Hayashi, K. Matsunaga, Y. Iwasaka, T. Yamanouchi, G. Hashida, T. Fukatsu (2004), Chemistry of sea-salt particles and inorganic halogen species in Antarctic regions: Compositional differences between coastal and inlad stations, ***J.Geophys. Res., vol. 109***, D20208, doi:10.1029/2004JD004713.

Hara, K., K. Osada, M. Kido, K. Matsunaga, Y. Iwasaka, G. Hashida, and T. Yamanouchi (2005), Variations of constituents of individual sea-salt particles at Syowa station, Antarctica, ***Tellus, 57B***, 230-246.

Hess, M., U. K. Krieger, C. Marcolli, T. Huthwelker, M. Ammann, W. A. Lanford, and Th. Peter (2007), Bromine enrichment in the near-surface region of Br-doped NaCl single crystals diagnosed by Rutherford backscattering spectrometry, ***J. Phys. Chem. A, 111***, 4312-4321.

Holland, M. M., C. M. Bitz, and B. Tremblay (2006), Future abrupt reductions in the summer Arctic sea ice, ***Geophys. Res. Lett., 33***, L23, 503, doi:10.1029/2006GL028 024.

Hopper, J. F., L. A. Barrie, A. Silis, W. Hart, A. J. Gallant, and H. Dryfhout (1998), Ozone and meteorology during the 1994 Polar Sunrise Experiment, ***J. Geophys. Res., vol. 103***, no. D1, 1481-1492.

Hönninger, G., and U. Platt (2002), Observations of BrO and its vertical distribution during surface ozone depletion at Alert, ***Atmos. Environ., 36***, 2481-2489.

Huff, A. K. and J. P. D. Abbatt (2000), Gas-phase Br_2 production in heterogeneous reactions of Cl_2, HOCl, and BrCl with halide-ice surface, ***J. Phys. Chem., A***, 104, 7284-7293.

Huff, A. K. and J. P. D. Abbatt (2002), Kinetics and product yields in the heterogeneous reactions of HOBr with ice surfaces containing NaBr and NaCl, ***J. Phys. Chem., A***, 106, 5279-5287.

Ianniello, A., Beine, H. J., Sparapani, R., Di Bari, F., Allegrini, I., and Fuentes, J. D. (2002), Denuder measurements of gas and aerosol species above Arctic snow surfaces at Alert 2000, ***Atmos. Env.***, ***36***, 5299-5309.

Iraci, L. T., R. R. Michelsen, S. F. M. Ashbourn, T. A. Rammer, and D. M. Golden (2005), Uptake of hypobromous acid (HOBr) by aqueous sulfuric acid solutions: low-temperature solubility and reaction, ***Atmos. Chem. Phys.***, ***5***, 1577-1587.

Jewett, S. C., X. Zhang, A. S. Naidu, J. J. Kelley, D. Dasher, L. K. Duffy (2003), Comparison of mercury and methylmercury in northern pike and Arctic grayling from western Alaska rivers, ***Chemosphere, 50 (3)***, 383-392.

Jewett, S. C., and L. K. Duffy (2007), Mercury in fishes of Alaska, with emphasis on subsistence species, ***Sci. Total Environ., (1-3):3-27***, 15,387.

Jones, H. G., T. D. Davies, J. W. Pomeroy, P. March, and M. Tranter (1993), Snow-Atmosphere interactions in Arctic snowpacks net fluxes of NO_3, SO_4 and influence of solar radiation, ***Proceedings of the annual eastern snow conference***, 255-264.

Jones, A. E., P. S. Anderson, E. W. Wolff, J. Turner, A. M. Rankin, and S. R. Colwell (2006), A role for newly forming sea ice in springtime polar tropospheric ozone loss? Observational evidence from Halley station, Antarctica, ***J. Geophys. Res., vol. 111***, D08306, doi:10.1029/2005JD006566.

Joranger, E. and A. Semb (1989), Major ions and scavenging of sulphate in the Norwegian Arctic, ***Atmos. Env., vol. 23***, no. 11, 2463-2469.

Jourdain, B., and M. Legrand (2002), Year-round records of bulk and size-segregated aerosol composition and HCl and HNO_3 levels in the Dumont d'Urville (coastal Antarctica) atmosphere: Implications for sea-salt aerosol fractionation in the winter and summer, ***J. Geophys. Res., vol. 107***, no. D22, 4645, doi:10.1029/2002JD002471.

Kaleschke, L., Richter, A., Burrows, J., Afe, O., Heygter, G., Notholt, J., Rankin, A. M., Roscoe, H. K., Hollowedel, J., Wagner, T., and Jacobi, H.-W. (2004), Frost flowers on sea ice as a source of sea salt and their influence on tropospheric halogen chemistry, ***Geophys. Res. Lett.***, ***31***, L16114, doi:10.1029/2004GL020655.

Kalnajs, L. E. and Avallone, L. M. (2006), Frost flower influence on springtime boundary-layer ozone depletion events and atmospheric bromine levels, ***Geophys. Res. Lett.***, ***33***, L10810, doi:10.1029/2006GL025809.

Langendörfer, U., E. Lehrer, D. Wagenbach, and U. Platt (1999), Observation of filterable bromine variabilities during Arctic tropospheric ozone depletion events in high (1 hour) time resolution, ***J. Atmos. Chem.***, ***34***, 39-541.

Lehrer, E., G. Honninger, and U. Platt (2004), A one dimensional model study of the mechanism of halogen liberation and vertical transport in the polar troposphere, ***Atmos. Chem. Phys.***, ***4***, 2427-2440.

Lin, C. J. and S. O. Pehkonen (1999), The chemistry of the atmospheric mercury: a review, ***Atmos. Env., vol. 33***, no. 13, 2067-2079.

Lindberg, S., S. Brooks, C.-J. Lin, K. J. Scott, M. S. Landis, R. K. Stevens, M. Goodsite, A. Richter (2002), Dynamic oxidation of gaseous mercury in the Arctic troposphere at Polar Sunrise, ***Environ. Sci. Technol.***, ***36***, 1245-1256.

Lu, J. Y., W.H. Schroeder, L.A. Barrie, A. Steffen, H.E. Welch, K. Martin, L. Lockhart, R.V. Hunt, G. Boila, A. Richter (2001), Magnification of atmospheric mercury deposition to polar regions in springtime: the link to tropospheric ozone depletion chemistry, ***Geophys. Res. Lett.***, ***28***, 3219-3222.

Martin, S., Drucker, R, and Fort, M. (1995), A laboratory study of frost flower growth on the surface of young sea ice, ***J. Geophys. Res.***, ***100***, 7,027-7,036.

Martin, S., Yu, Y, and Drucker, R (1996), The temperature dependence of frost flower growth on laboratory sea ice and the effect of the flowers on infrared observations of the surface, ***J. Geophys. Res.***, ***101***, 12,111—12,125.

McConnell, J. C., Henderson, G. S., Barrie, L., Bottenheim, J., Nili, H., Langford, C. H., and Templeton, E. M. J. (1992), Photochemical bromine production implicated in Arctic boundary-layer ozone depletion, ***Nature*, *355***, 150-152.

McElroy, C. T., C. A. McLinden, and J. C. McConnell (1999), Evidence of bromine monoxide in the free troposphere during the Arctic polar sunrise, ***Nature*, *397***, 338-341.

National Snow and Ice Data Center (NSIDC 2007), Arctic sea ice news fall 2007, http://nsidc.org/news/press/2007_seaiceminimum/20070810_index.html.

Newberg, J. T., B. m. Matthew, C. Anastasio (2005), Chloride and bromide depletions in sea-salt particles over the northeastern Pacific Ocean, ***J. Geophys. Res.***, ***110***, D06209, doi:10.1029/2004JD005446.

Perner, D., T. Arnold, J. Crowley, T. Klüpfel, M. Martinez, and R. Seuwen (1999), The measurements of active chlorine in the atmosphere by chemical amplification, ***J. Atmos. Chem.*, *34***, 9-20.

Platt, U., and G. Hönninger (2003), The role of halogen species in the troposphere, ***Chemosphere*, *52***, 325-338.

Rankin, A. M., Auld, V., and Wolff, E. W. (2000), Frost flower as a source of fractionated sea salt aerosol in the polar regions, ***Geophys. Res. Lett.***, ***27***(21), 3469-3472.

Rankin, A. M. and Wolff, E. W. (2002), Frost flowers: Implications for tropospheric chemistry and ice core interpretation, ***J. Geophys. Res.***, ***107*** (D23), 4683, doi:10.1029/2002JD002492.

Rankin, A. M. and Wolff, E. W. (2003), A year-long record of size-segregated aerosol composition at Halley, Antartica, ***J. Geophys. Res.***, ***108*** (D24), 4775, doi:10.1029/2003JD003993.

Ridley, B. A., E. L. Atlas, D. D. Montzka, E. V. Browell, C. A. Cantrell, D. R. Blake, N. J. Blake, L. Cinquini, M. T. Coffey, L. K. Emmons, R. C. Cohen, R. J. DeYoung, J. E. Dibb, F. L. Eisele, F. M. Flocke, A. Fried, F. E. Grahek, W. B. Grant, J. W. Hair, J. W. Hannigan, B. J. Heikes, B. L. Lefer, R. L. Mauldin, J. L. Moody, R. E. Shetter, J. A. Snow, R. W. Talbot, J. A. Thornton, J. G. Walega, A. J. Weinheimer, B. P. Wert, and A. J. Wimmers (2003), Ozone depletion events observed in the high latitude surface layer during the TOPSE aircraft program, ***J. Geophys. Res., vol. 108***, no. D4, 8356, doi:10.1029/2001JD001507.

Sander, R., R. Vogt, G. W. Harris, and P. J. Crutzen (1997), Modeling the chemistry of ozone, halogen compounds, and hydrocarbons in the Arctic troposphere during spring, ***Tellus, 49B***, 522-532.

Sander, R., J. Burrows and L. Kaleschke (2006), Carbonate precipitation in brine – a potential trigger for tropospheric ozone depletion events, ***Atmos. Chem. Phys., 6***, 4653-4658.

Schröeder, W. H. and J. Munthe (1998), Atmospheric mercury-An overview, ***Atmos. Env., 32***, 809-822.

Schröeder, W. H., K.G. Anlauf, L.A. Barrie, J.Y. Lu, A. Steffen, D.R. Schneeberger, T. Berg (1998), Arctic spring time depletion of mercury, ***Nature, 394***, 331-332.

Simpson, W. R., Alvarez-Aviles, L., Douglas, T. A., Sturm, M., and Dominé, F. (2005), Halogen in the coastal snow pack near Barrow Alaska: Evidence for active bromine air-snow chemistry during springtime, ***Geophys. Res. Lett., 32***, L04811, doi:10.1029/2004GL021748.

Simpson, W. R., R. von Glasow, K. Riedel, P. Anderson, P. Ariya, J. Bottenheim, J. Burrows, L. Carpenter, U. Frieß, M. E. Goodsite, D. Heard, M. Hutterli, H.-W. Jacobi, L. Kaleschke, B. Neff, J. Plane, U. Platt, A. Richter, H. Roscoe, R. Sander, P. Shepson, J. Sodeau, A. Steffen, T. Wagner, E. Wolff (2007a), Halogens and their role in polar boundary-layer ozone depletion, ***Atmos. Chem. Phys., 7***, 4375-4418.

Simpson, W. R., D. Carlson, G. Hoenninger, T. A. Douglas, M. Sturm, D. K. Perovich, and U. Platt (2007b), The Dependence of Arctic Tropospheric Halogen Chemistry on Sea Ice Conditions, ***Atmos. Chem. Phys., 7,*** 621 – 627, doi: 10.1029/2004GL022132.

Sirois, A. and L. A. Barrie (1999), Arctic lower tropospheric aerosol trends and composition at Alert, Canada: 1980-1995, ***J. Geophys. Res, vol. 104,*** No. D9, p. 11,599-11,618.

Steffen, A., W. Schroeder, J. Bottenheim, J. Narayan, J. D. Fuentes (2002), Atmospheric mercury concentrations: measurements and profiles near snow and ice surfaces in the Canadian Arctic during Alert 2000, ***Atmos. Env, 36,*** 2653-2661.

Tang, T. and J.C. McConnell (1996), Autocatalytic release of bromine from Arctic snow pack during polar sunrise, ***Geophys. Res. Lett., 23,*** 2633-2636.

Toom-Sauntry, D. and L. A. Barrie (2002), Chemical composition of snowfall in the high Arctic: 1990-1994, ***Atmos. Env., 36,*** 2683-2693.

Vogt, R., P. J. Crutzen, and R. Sander (1996), A mechanism for halogen release from sea salt aerosol in the romote marine boundary layer, ***Nature, 338,*** 327-330.

Vogt. R., R. Sander, R. von Glasow, and P. Crutzen (1999), Iodine chemistry and its role in halogen activation and ozone loss in the marine boundary layer: a model study, ***J. Atmos. Chem., 32,*** 375-395.

Wagenbach, D., Ducroz, F., Mulvaney, R., Keck, L., Minikin, A., Legrand, M., Hall, J. S., and Wolff, E. W. (1998), Sea-salt aerosol in coastal Antarctic regions, ***J. Geophys. Res., 103*** (D9), 10,961-10,974.

Wagner, T. and U. Platt (1998), Satellite mapping of enhanced BrO concentrations in the troposphere, N***ature, 395,*** 486-490.

Wagner, T., Leue, C., Wenig, M., Pfeilstcker, K., and Platt, U. (2001), Spatial and temporal distribution of enriched boundary layer BrO concentrations measured by the GOME instrument aboard ERS-2, ***J. Geophys. Res., 106*** (D20), 24,225 – 24,235.

Wennberg, P. (1999), Bromine explosion, ***Nature, 397,*** 299-301.

World Health Organization (WHO) (1991), Environmental health criteria 118: inorganic mercury, WHO, Geneva, Switzerland, 168.

World Health Organization (WHO) (1990), Environmental health criteria 101: methylmercury, WHO, Geneva, Switzerland, 144.

World Health Organization (WHO) (1989), Environmental health criteria 86: mercury-environmental aspects, WHO, Geneva, Switzerland, 115.

Woshner, V. M., T. M. O'Hara, G. R. Bratton, and V. R. Beasley (2001), Concentrations and interactions of selected essential and non-essential elements in ringed seals and polar bears of Arctic Alaska, *J. of Wildlife Diseases, 37(4)*, 711-721.

Appendix: Methods

The total amount of Barrow 2004, 2005, and 2007 campaign samples is 136, 425 and 844 respectively. The procedure to sort and analyze all these samples for conductivity and ion content are discussed in sections 1 through 4. Vial cleaning and sampling procedures are discussed in section 5 and 6 respectively. And lastly aerosol particle sampling, instrument description and sample analysis are presented in section 7.

A.1 Conductivity measurements

A.1.1 Samples from 2004

The 2004 campaign main purpose was to study how sea salts are distributed as we move away from the main source, the ocean. We also collected snow stratigraphy, frost flowers and blowing snow. All sampling vials were labeled the same B for Barrow and a number starting with 1. Regardless of type of sample the label remain the same and notes were taken describing what type of sample was collected in a particular vial. To measure conductivity samples were melted and a small aliquot was separated in a different vial.

A.1.2 Samples from 2005

The 2005 campaign was big effort to obtain as many different types of ice reservoir (ion reservoir), study in close proximity the lead (sea ice opening), and learn about ion mobility during melt. Different experiments were design to accomplish our goals. Sampling vials in this campaign had different labels that describe their use and what kind of snow sampling they were going to be used for. Most B2 vials were used to sample surface snow on the sea ice, they are expected to be high in salinity, and therefore their conductivities are expected to be high. BF vials were used to collect from snow-trap trays and tundra surface snow. The BF vials experiment was design to collect freshly deposited snow, we expected their conductivities to be low. BM vials main purpose was to sample water from the melt. Some of the B2, BF and BM samples were used to sample other type of snow or ice or interesting samples. To keep track of the samples they were not re-labeled, but notes and descriptions were taken in the field and later on classification codes were assign to match sampling experiment samples. BS stands for salty samples, so their conductivities were expected to be very high, four times higher than seawater for frost flowers (extremely salty samples).

A.1.2.1 Snow and melt samples

Conductivity measurements on B2, BF, and BM vials were performed at different times to avoid contaminating BF with the salty B2 samples. The day before measuring conductivities approximately 60 samples were taken out of the cold room fridge and melted over a period of 12 hours. During this time any kind of precipitate will go into solution making the melted snow solution homogeneous. We used trays to melt the samples in the vertical position to avoid leaks from loose caps. Around 60 extra vials (same number and kind than melted samples) and let them air dry, old vials can be reused for this part. Cleaning procedures are discussed later. The vials were labeled with the same name as the sample and add 10 mL of water (18.2 MΩ). A clean 10 mL glass pipet was used for this. One mL aliquot was taken from the sample and add it to the 10 mL water vial. By diluting the sample 11 times, the original sample is not contaminated and we also have enough volume to sink the probe to measure the conductivity.

Samples with low volume when melted (less than 10 mL) were separated and dealt with differently, see low volume samples section. The Ion Chromatograph AS40 vials (autosampler vials) require 4 to 5 mLs of sample in order to run for anions and cations we need at least 10 mLs of sample in addition to a few extra mL to measure conductivity and to rinse glassware.

A.1.2.2 Frost flower samples

Prior to sampling we labeled vial and cap and weighted them. The samples were melted for 12 to 24 hours, and from time to time opened the cap and closed it again to allow the air inside equilibrate with the air outside to avoid any changes while the samples were weighted. We wrote down the mass of vial plus sample and with the mass of the empty vial calculate the sample mass (SM).

SM = Vial (with cap) and sample – Empty vial (with cap) (A1)

The sample volume was calculated using the value for water density at room temperature (24.1°C)

$$SV = \frac{SM}{\rho} \tag{A2}$$

Sample volume is SV, SM is sample mass and ρ is water density.

We added 30 mL of water (18.2 MΩ) to each vial. If there was more than 10 mL of melted sample originally then we added 20 mL. The dilution factor for these samples is calculated via this equation,

$$Df = \frac{SV + WV}{SV} \tag{A3}$$

Df is the dilution factor, SV the sample volume and WV added volume of water.

The IC AS40 vials were used to measure conductivities for these samples in order not to contaminate the diluted original sample. Cleaning procedures for the AS40 vials are in the cleaning procedure section of the methods.

A.1.2.3 Low volume sample

The samples that have less than 10 mLs of melted sample were considered to be low volume. If the conductivity was known we diluted the sample to be run in the 500 μL loop. If the conductivity was unknown because there were not even 2 mLs of melted sample we followed these instructions: obtained mass of the vial and sample. Then added 10 mLs of water, after we transferred the sample to a new and clean blue cap vial (labeling new vials with same name as sample). We cleaned the old vial and let it dry, then weighted them and calculate the sample mass, then the sample volume and then the dilution factor as we did for BS samples. These samples were analyzed in the 250 or 500μL injection volume loop.

A.1.2.4 Snow core samples

We melted the samples for 24 hours, and cleaned the same amount of blue cap vials and labeled them same as the sample. Before transferring some of the sample we shacked the bottle with the melted sample, and immediately after, the sample was transferred to a blue cap vial and measured the conductivity, no dilution was made for conductivity measurements. After measuring the conductivity the aliquot used for conductivity was discard and added a new clean aliquot. This new aliquot was now for IC analysis.

A.1.2.5 Kite samples

The samples were melted for 12 hours; different volumes of water were added to the bag with the bottle inside to rinse as good as possible the walls of the bag and bottle. The rinsed water was transferred to a previously weighted blue cap vial. The idea was to obtain a dilution factor as we did for BS and low volume samples.

A.1.3 Samples from 2007

The 2007 campaign objectives were to build a time series data set of snow and aerosol simultaneously, and study the apparent distribution of ions in snow types that represent the Arctic surface. Conductivity measurements were taken random and equally for all types of snow samples. Approximately 100 to 150 samples were melted for a period of 12 to 16 hours. We used AS40 vials to measure the conductivity of each replicate sample to avoid contaminating the original sample. The conductivity values are a guide to know how to analyze for Ion Chromatography (IC). After determine the optimal IC analysis conditions, if dilution was needed for ion analysis the conductivity of the dilution was measured. By measuring conductivity of dilutions we are assure that when conductivity and ion values are compared we are actually comparing the same solution.

A.2 Analysis techniques

A.2.1 Sorting samples for Ion Chromatography analysis

The conductivity values were used to sort samples into different conductivity ranges for the Ion Chromatograph (IC) analysis. The IC column capacity is 50 nanomoles of any ion, pass this value the column saturates and the measurement is compromised. The injection volume dictates how much sample enters the column, the more volume of a highly concentrated sample the easier it is to saturate the column. Thus, different injection volumes were selected to analyze the samples. We used the correlation between conductivity and concentration (Eq. 4) to approximate the maximum and minimum conductivity each injection volume to not overpass 50 nanomoles. In 2004 two injection volumes were used, 250 and 500 μL, to analyzed all the samples. If the sample was high in conductivity we diluted to analyze 250 μL of the sample. In 2005 and 2007 six injection volumes covered the lowest and highest conductivity range for the IC analysis, 10, 25, 62, 150, 250, and 500 μL. If samples had conductivities higher than 625 micro S then dilution was required, we diluted them to be in the range of the 25 micro L loop. Table A1 shows how much of a sample that falls under certain conductivity range.

Table A 1. Injection volume (μL)

Injection volume (μL)	Conductivity range (μS)
10	200 – 625
25	100 – 200
62	38 – 100
150	26 – 38
250	13 – 26
500	< 13

Conductivity and concentration correlation

$$\text{Concentration } (\mu\text{M}) = \text{Conductivity } (\mu\text{S}) * 8 \tag{A4}$$

A.2.2 Ion chromatographer specifications

Samples from 2004 were analyzed in an IC 1500 for anions and in an Atomic Absorption Spectrometer (AA) 3300 for cations (see section 3 for more details on AA). Samples from 2005 and 2007 were analyzed using an IC 2000 for anions and cations.

Table A 2. Ion Chromatography instrument specifications.

Year	Analysis	Column	Suppressor	Eluent generator
2004	Anion	AS17	ASRS ultra II 4 mm	EG40 KOH
	Cation	NA	NA	NA
2005	Anion	AS17	ASRS ultra II 4 mm	EG40 KOH
	Cation	CS12A	CSRS-300 4mm	EGC MSA
2007	Anion	AS17	ASRS ultra II 4 mm	EG40 KOH
	Cation	CS12A	CSRS-300 4mm	EGC MSA

A.2.3 Ion chromatography integration procedure

The integration of the peaks is an important step in obtaining accurate results. Consistency in the integration procedure is key to guarantee that each samples has been treated the same way. For accuracy each samples and standards were also integrated equally. Blanks were run at the beginning and end of each run, we zoomed the scale of one blank and used this scale for each sample to check the baseline. Anomalies in the baseline are detected and if needed peak delimiters are moved to mimic the blank's baseline. The next step was to make sure each peak was label with the correct ion name. Each peak was individually zoomed and quickly went over all samples observing baseline problems or other anomalies. When comparing different analysis days, the slope of each run for each ion was checked to observe if these were similar. The slope is the mathematical relation the instrument uses to quantify each ion. One would expect the slope to be consistent for each ion. At this point the data can be exported to a spreadsheet and a program that processes the samples and matches replicates. Additional testing is needed to approve the integration procedure and find outliers. The charge balance test checks that the anion sum versus the cation sum is in less than 35 % error. The conductivity test checks that the slope of conductivity versus sum of anions is in close proximity to 8. After conducting the charge balance and conductivity tests the outliers are flagged and continue to analyze the data. Normally, the first time the outlier detection tests are used we re-examine each of the outlier's chromatogram for inconsistencies with the integration process, but if nothing is found the samples are considered outliers.

A.2.4 Atomic Absorption cation measurements

Cation analysis in 2004 was carried on using a Flame Atomic Absorption (AA) Spectrometer 3300. The cations analyzed with AA were Na^+, Mg^{2+} and Ca^{2+}. Standards and samples were prepared according to the instruments capacity. Mg^{2+} and Ca^{2+} were analyzed as they were for anions using the IC, but Na^+ needed additional dilutions.

A.3 Standard preparation

Standards were freshly prepared for each IC run, from a cation and anion standard stock solution. The standard stock solutions in 2004 (Table 2) differ from 2005 and 2007 (Table 3), which were prepared to mimic at best sea salt ratios, so Na^+, Cl^- and SO_4^{2-} would have the highest signal and the other ions would have a smaller signal. New standard stock solutions were prepared for each year, one for anions and one for cations. The injection volume indicates how much of a sample can be injected into the column to prevent saturation, since column saturation compromises the efficiency of the quantification process. The following sections contain tables summarizing what standards were used with each injection loop size and the recipe to prepare each standard solution from the stock.

A.3.1 Standard stock solution preparation

Table A 3. Preparation recipe for 2004 standard stock solution.

Ion	***Compound***	***Molecular weight (g/mol)***	***Needed mass (g)***	***Stock solution expected concentration (M)***
F^-	NaF	41.99	0.2624	0.0125
Cl^-	KCl	74.55	0.4659	0.0125
NO_2	$NaNO_2$	69.00	0.1725	0.0050
Br^-	NaBr	102.89	0.2572	0.0050
NO_3^-	$NaNO_3$	84.99	0.5312	0.0125
SO_4^{2-}	$(NH_4)_2SO_4$	132.14	1.6518	0.0250
PO_4^{2-}	Na_2HPO_4	141.96	0.3549	0.0050
Li^+	LiCl	42.39	0.0265	0.00125
Na^+	CH_3COONa	82.03	0.1025	0.00250
K^+	KCl	74.55	0.0466	0.00125
Sr^{2+}	$SrCl_2$•6H2O	266.62	0.0667	0.00050
NH_4^+	NH_4Cl	53.49	0.0334	0.00125
Mg^{2+}	$MgCl_2$•6H2O	203.3	0.1271	0.00125
Ca^{2+}	$CaSO_4$	136.15	0.0851	0.00125

Table A 4. Preparation recipe for 2005 and 2007 standard stock solution.

Ion	***Compound***	***Molecular weight (g/mol)***	***Needed mass (g)***	***Stock solution expected concentration (M)***
Na^+	NaCl	58.44	8.7660	0.150
K^+	KNO^3	101.09	2.0218	0.020
Ca^{2+}	$Ca(NO_3)_2 \bullet 4H_2O$	236.15	4.7230	0.020
NH_4^+	NH_4NO_3	80.04	0.4002	0.005
Mg^{2+}	$MgCl_2 \bullet 6H_2O$	203.3	5.0825	0.025
Cl^-	NaCl	58.46	8.7690	0.150
SO_4^{2-}	$MgSO_4$	120.37	1.8056	0.015
Br^-	NaBr	102.89	0.5145	0.005
F^-	NH_4F	37.04	0.1852	0.005
NO_3^-	NH_4NO_3	80.04	0.4002	0.005
NO_2^-	$NaNO_2$	69.00	0.3450	0.005

A.3.2 2004 standard preparation

Table A 5. Injection volume loop and their corresponding standards for the 2004 IC analysis.

Injection volume loop (μL)	***Standard***
250	A, B, Y, Z
500	A, B, C, Z

Table A 6. Standard name and preparation instructions for 2004 IC and AA analysis.

Standard	***Recipe***
A	1 mL from stock into 500 mL volumetric flask
B	10 mL from A into 25 mL volumetric flask
C	10 mL from B into 25 mL volumetric flask
Y	100 mL from A into 500 mL 10 mL volumetric flask
Z	30 mL from A into 500 mL 10 mL volumetric flask

A.3.3 2005 standard preparation

Table A 7. Injection volume loop and their corresponding standards for the 2005 IC analysis.

Injection volume loop (μL)	***Standard***
10	A, B, C, H, D, K
25	C D, E, F, K, H
62	D, F, G, H, K
150	D, H, I, K
230	D, J, K
500	L, M, N

Table A 8. Standard name and preparation instructions for 2005 IC analysis.

Standard	***Recipe***
A	1 mL from stock + 29 mL of water
B	2 mL from stock into 100 volumetric flask
C	1 mL from stock into 100 mL volumetric flask
D	1 mL from stock into 1000 mL volumetric flask
E	1 mL from stock + 149 mL of water
F	1 mL from stock + 299 mL of water

G	20 mL from E 5 mL of water
H	1 mL from stock into 500 volumetric flask
I	1 mL from stock into 599 mL of water
J	20 mL from H into 10 of water
K	5 mL from H into 25 of water
L	4 mL from F in 16 mL of water
M	2 mL from F in 18 mL of water
N	1 mL from F in 19 mL of water

A.3.4 2007 standard preparation

Table A 9. Injection volume loop and their corresponding standards for the 2005 IC analysis.

Injection volume loop (μL)	***Standard***
10	A, B, C, D, H, O, Q
25	C, E, F, H, D, O, Q
62	G, F, H, D, O, P, Q, R
150	H, J, D, O, Q, R
230	J, P, O, Q, R
500	D, O, P, Q, R

Table A 10. Standard name and preparation instructions for 2005 IC analysis.

Standard	***Recipe***
A	1 mL from stock + 29 mL of water
B	2 mL from stock into 100 volumetric flask
C	1 mL from stock into 100 mL volumetric flask
D	1 mL from stock into 1000 mL volumetric flask
E	1 mL from stock + 149 mL of water
F	1 mL from stock + 299 mL of water
G	20 mL from E 5 mL of water
H	1 mL from stock into 500 volumetric flask
I	1 mL from stock into 599 mL of water
J	20 mL from H into 10 of water
K	5 mL from H into 25 of water

A.4 Vial cleaning procedure

A.4.1 Snow sampling vials cleaning procedure

Cleaners put on free-powder latex gloves and rinse them with 18.2MΩ water, and then paper towel was set aside to dry vials and caps at the end. The vials and caps were separated for cleaning. When vials and caps were new they were filled with 18.2MΩ water, and then shacked the water out three times, this step was repeated three times. When vials and caps were reused an 18.2MΩ water and soap mix was added then scrubbed and rinsed three times shacking the water out three times. At the end vials were set on the paper towel to dry.

A.4.2 Ion Chromatography autosampler vials and caps (AS40)

A pre-cleaned 4000 mL Erlenmeyer was filled with18.2MΩ water and the AS40 vials were sunk in making sure the inside was fully covered with water. The vials were rinsed before adding to the Erlenmeyer. After four hours of soaking the water was changed for new 18.2MΩ water and left soaking for 24 hours. The caps were cleaned the same way as the vials, but in separate containers.

A.5 Sampling procedure

The different campaigns over the three-year study had different objectives, thus different type of samples were collected. Regardless of the sample type there are a few steps to follow that avoided contaminating, and missing samples. When sampling snow samplers approached the site facing the wind, identified a target site and proceeded to put on a Tyvek suit, a facemask and polypropylene gloves. Usually there were two samplers one would be collecting the sample, clean hands, and the other would be assisting clean hands in finding and passing sampling vials, dirty hands. As clean hands collects the sample dirty hands takes notes on sampling vial label, type of snow, site, date, time, and description of surroundings.

A.5.1 Sampling procedure of different types of ice crystals and melt (water)

- Snow sampling: Sampled in a 50 mL polypropylene vial for ions and different sized Teflon bottles for Hg. Used the edge of the vial to scoop the snow inside the vial for ions and scoops to fill Hg bottles.
- Vertical snow sampling: Dug a snow pit and with the edge of the vial scrapped the edge of the pit from bottom to top.
- Frost flower sampling: Most of the time tried to use the vial edge to scoop the crystals into the vial, except when sampling brine, we used a dropper, and for frost flower tips, we used tweezers and transfer to vial.
- Tray sampling: Four pyrex trays were set approximately 1 m above ground on a table. Freshly deposited snow was collected in the trays, and soon after we would sample it.
- Survey samples: We sampled surface and vertical snow in four 100 m lines, every 5 m. Bag sampling consists of approximately 1 cup scoop of snow into a 2 gallon bag for each 100 m line.
- Kite sampling: Filled a 500 mL bottle with liquid nitrogen attached to a pulley system on a kite and lift it to certain altitude. We collected what condensed on the outside of the bottle into a bag. In the lab we melted the sample and transferred to a vial for analysis.
- Snow core: Dug a snow pit, penetrated entire snow pack with a PVC corer, slide a shovel under the corer opening and inverted into the bottle.
- Water: filled a 50 mL polypropylene syringe with melted snow, melted sea ice, or river water and transferred to 50 mL polypropylene vial (same used for snow sampling).

A.5.2 Sample storage and handling

After a day of sampling one sampler would read filled vials label and another sampler would check the name of the sample in the field notebook. Once a sample was checked it was stored in a cooler outside if it was at least -10°C or inside a cold room freezer. At the end of the campaign measurements were taken to ship frozen samples. Rapidly after arriving to the final destination samples were stored in a freezer until analysis time.

A.6 Aerosol particle sampling

A.6.1 Instrument description

A three-stage modified Davis Rotating Universal-size-cut Monitoring (DRUM) impactor was used to study the chemical composition of aerosol particles. Impactors are normally composed of a pump, inlet, cyclone, different sized stages were the particles are collected by impaction, and a motor that rotates the impaction site. The pump provides air suction power of 3 L/min, the inlet receives particles and leads them to the cyclone. The cyclone allows particles smaller than 2.5 microns (depending on the experiment the cyclone limit can change) to pass on to the instrument and discards larger particles. The three-stage impactor sizes used for this experiment were 2.5 – 0.84, 0.84 – 0.30, and 0.30 – 0.12 microns. The modified DRUM used in this study contains all traditional components, but its motor has been modified to rotate depending on a program. Traditional impactors are called continuous DRUM impactors because their motors are always in motion and rotate 1 mm every six hours. The modified DRUM can be programmed to stay stationary in the same impaction site for however long is needed. In this study the modified DRUM was programmed to rotate every six hours 1 cm. In other words each sample is a time integral of six hours and are separated by 1 cm. The separation allows cutting the impaction strip without contaminating the next sample. The impaction strip used was made of Teflon in contradiction to the more traditional Mylar.

A.6.2 Sample analysis

Each Teflon strip had capacity for 16 samples, which equals to four days of sampling. Once the strip was changed for another, the strip was labeled with size particle, impaction starting point, and time and date of collection. Strips were kept with snow samples untill time of analysis, transported in Ziploc bags and away from the sun. At the time of analysis the strip was cut in squares using a pre-cleaned blade. Each square was set inside an AS40 vial (IC autosampler vial) and 2 mL of 18.2 MΩcm water. After assuring that the strip was submerged in the water the samples were sonicated in an ultrasonic bath for 40 minutes. Samples were analyzed using Ion Chromatography in the 500 μL loop.